Folate Binding Protein as a Therapeutic Natural Nanotechnology

by

Rachel L. Wallace

A dissertation submitted in partial fulfillment
of the requirements of the degree of
Doctor of Philosophy
(Chemistry)
in the University of Michigan
2018

Doctoral Committee

Professor Mark M. Banaszak Holl, Co-Chair
Professor Anne J. McNeil, Co-Chair
Professor Bradford Orr
Professor Melanie Sanford

I fill you with Naming.
Be!

◆

Journey before destination.

◆

Hallows, not Horcruxes.

Rachel L. Wallace

rlmerzel@umich.edu

ORCID iD: 0000-0002-0637-3970

for Dee Dee

ACKNOWLEDGEMENTS

First and foremost, I am immeasurably grateful to my advisor, Mark Banaszak Holl. He is both a phenomenal scientist and advisor, and I would not have become the scholar I am today without his guidance and mentorship. As I progressed through my PhD program, he fostered my intellectual development, encouraged involvement in work outside of chemistry, supported my efforts towards a career in science and technology public policy, and always pushed me to reach higher in anything I tried. He has helped me to grow professionally and personally, and I am so thankful to consider him a mentor and colleague.

My dissertation committee has also been a great source of support and guidance throughout graduate school. As a physicist Brad Orr provided valuable insights on all my projects at group meeting every week. He deeply engaged with my research, and I am thankful to have had the opportunity to work closely with him for five years. Anne McNeil has in many ways been a second chemistry advisor for me. Her support and mentorship, both personal and professional, have been a key component of my success here. I am particularly grateful to have had the opportunity to work with her on chemical education projects, which turned out to be a formative part of my graduate school experience. Melanie Sanford has contagious enthusiasm for all things science, and I tried to carry that with me, even after I rotated out of her lab. Her insightful questions always pushed me to situate my research in broader scientific and social contexts. She also encouraged me to reach for those higher impact journals. I am immensely thankful to Brad, Anne, and Melanie for their help, support, and expertise over the last five years.

I have also had the privilege of working with an incredible group of undergraduate and graduate students and post-doctoral fellows. Most notably, Junjie (JJ) Chen and I worked on closely related projects for most of our time in the Banaszak Holl group. He has been a wonderful research partner, and he taught me so much. I definitely could not have done this work without him, especially because I was an inorganic chemist working on a biological chemistry project. He was unwaveringly patient and kind, and I'm grateful for my time working with and

learning from him. Undergraduate students Sarah Boutom, Carolina Frey, and Rachel Garn contributed extensively to the work in this dissertation and brought fresh insights and suggestions to the research effort. I also worked with a number of other undergraduates and graduate student rotators on research not reflected in this thesis. Rotators Taylor Soucy and Violet Sheffey and undergraduates Lauren Purser, Monica Olszewski, and Andrew Wong did fantastic work on the nanoplastics water project. I learned so much from serving as a mentor for all these students, and I am grateful to consider them friends and colleagues.

I am also hugely appreciative of the professional relationships and friendships with my other labmates, both current and former. Isabel Colón-Bernal, Taeyong (Ted) Ahn, Jinhee Kim, Zi Li, Phillip Yang, Rachel Shiffman, Alexis Jones, and Alyssa Travitz help make our lab a wonderful place to work. Our lab is intensely collaborative, and I have learned so much from every person and a wide variety of research subjects (collagen to ACLs to polymers to nanoplastics). It's been a great ride, and I'm thankful for the chance to have worked with everyone.

This body of research would never have been as successful without the scientific work and mentorship of the graduate students who finished their PhDs while I was in the lab. Mallory van Dongen, Casey Dougherty, Sriram Vaidyanathan, and Meagan Cauble built the foundations for my research. Their work was a jumping off point, and I often translated the methods they developed and materials they made to my own research. Beyond the research, however, they were outstanding mentors and colleagues. Each in their own way, they helped me along the twisting path of earning a PhD. I highly value our enduring friendships.

I must give special recognition for those involved in the mouse studies (Chapter 5). Brent Ward helped to plan the experiment, and Brent and Mark Vartanian did all experimental procedures involving the mice (Chapter 5). I have ventured far my inorganic chemistry background, and I definitely could not have gotten to this exciting endpoint without Brent's expertise. Thank you, as well, to MNIMBS for use of their cell culture facilities, with particular recognition to Rahul Rattan and Pam Wong for helping a chemist get her cells growing, healthy, and happy.

Many thanks, as well, to the Chemistry office staff. They have all helped me to get through the sometimes confusing administrative side of graduate school and made the entire process so much easier. In particular, Cornelius Wright and Liz Oxford have been amazing

sources of support and guidance, especially helping me navigate the somewhat unusual academic path I took through my PhD program.

The National Science Foundation played a special role in my graduate education, funding me for three years through a Graduate Research Fellowship.

As I started writing these acknowledgements, it was easy to recognize the contributions and influence of mentors, colleagues, and labmates, but I knew there were so many more people who had helped me through the PhD process. I started making a list, and I was stuck by how many of these people were women – strong, motivated, brilliant, accomplished women who have forged their way in a careers and environments that can be harsh and unwelcoming at times. These women inspired me to become the best scientist and scholar I could and provided endless support, advice, and guidance – both professional and personal – along the way. Many of these women I already mentioned above, but they, along with a number of others, are deserving of further recognition.

Anne McNeil and Melanie Sanford are brilliant scientists and educators and demonstrate tremendous leadership, insight, and compassion every day. Isabel, Jinhee, Mallory, Meagan, Casey, Sarah, Carolina, Rachel S., Rachel G., Alyssa, Lauren, Taylor, Violet, and Monica are amazing young women, and I am so excited that we get to grow together as the next generation of scientists.

I invested a substantial part of my time in graduate school in the Science, Technology, and Public Policy (STPP) Program at the Ford School of Public Policy. While in the STPP program, I had the privilege of learning from an incredible group of women. Shobita Parthasarathy, Joy Rohde, and Kaitlin Raimi introduced me to the complicated role of S&T in society and supported my development into a multidisciplinary scholar. I am particularly grateful to Shobita for the opportunity to do independent research under her mentorship for a semester. The chance to do research in and write for a field so far outside of chemistry both incredibly challenging and rewarding.

Although they are no longer at the University, two colleagues from my chemical education and STPP work have turned into great friends. Michele Nelson gave me a crash course in chemical education research, and we had a great time together over a summer developing a new curriculum. Caroline Walsh guided me through the STPP program and has endless

insightful advice on careers in S&T policy. Both were endless sources of support and advice through graduate school, and I am thankful to continue to have both of them in my life.

Above, I highlighted the incredible women who have influenced and inspired me throughout my graduate work. However, the greatest woman in my life has always been my mom. From being a practicing physician to becoming the first female Chief of Staff at her hospital and the first female President of the California Society of Anesthesiologists, all while raising two children, she has always shown that she can, and will, achieve anything she wants. Growing up, I never questioned my ability to accomplish whatever I wanted personally, academically, or professionally because I had my mom as a model. In all aspects of her life, she showcased her intellect, demonstrated her capacity, fought when necessary, and claimed her place. No one could tell her she was not worthy, she instilled that lesson deeply in me. She's my hero, and I truly would not have gotten to this point without her.

If my mom taught me to fight like a woman, my dad taught me to write. We still strongly, intensely, passionately disagree on the use of adverbs, but innumerable times throughout graduate school I have been grateful for his writing lessons. He always told me that my work, especially what I write down, was my signature – my reputation – and I should always aim to make it perfect. Now, at the end of my PhD, I have come to fully appreciate the connection between writing and this idea. I engage with both the Chemistry and STPP fields primarily through writing. The ability to communicate clearly and effectively is essential because it is how these communities know me and judge my contributions. So, while it was sometimes exceedingly frustrating, I am now incredibly grateful for my dad's insistence that I strive for perfection, especially in writing. He did not just tirelessly push me to achieve these goals, however: he lived these lessons. Through both his practice of medicine and his woodworking, he modeled the importance of critical thinking, patience, consistency, and attention to detail. These are exemplary traits he worked to inspire in me and directly contributed to my success today. (How may adverbs do you want to take out of this paragraph?)

So, to both my parents: thank you for your endless encouragement, support, and love.

Mike, you're still a schmoozer, but at least you're a pretty cool one now. Let's hang out more now that you're in the Midwest, ok?

Lacey: Thanks for all the snuggles and love, you crazy beast. You always seemed to know when I needed it most. I hope you enjoyed all those treats I gave you to keep you quiet while I was writing.

Finally, I could not have gotten through graduate school without my husband, Micah. He has been my greatest source of support throughout these five years. Graduate school has great highs and terrible lows, and Micah has always been my loudest cheerleader and most sympathetic commiserator. And now it's on to the next great adventure together. Wherever you will go, always.

TABLE OF CONTENTS

LIST OF FIGURES

LIST OF TABLES

LIST OF APPENDICES

LIST OF ABBREVIATIONS

aFA	antifolate
AFM	atomic force microscopy
CDF	cumulative density function
COG	cyclooctyne glycolic acid
FA	folic acid
FBP	folate binding protein
G5	generation 5
GPC	gel permeation chromatography
KS	Kolmogorov-Smirnov
MALDI-TOF-MS	matrix-assisted laser desorption ionization time-of-flight
MS	mass spectrometry
MTX	methotrexate
NMR	nuclear magnetic resonance
PAMAM	poly(amidoamine)
PBS	phosphate buffered saline
PEG	poly(ethylene glycol)
Q-Q	quantile-quantile
rp-HPLC	reversed phase-high performance liquid chromatography
SCID	severe combined immunodeficient
SDS-PAGE	sodium dodecyl sulfate polyacrylamide gel electrophoresis
UPLC	ultra performance liquid chromatography
XRD	X-ray diffraction

`

ABSTRACT

Serum proteins interact with small molecules and nanoparticles in blood, resulting in protein coronas. Protein coronas influence the bioidentity of the molecules and nanoparticles, playing critical roles in biotransport, uptake, and fate. Targeted therapeutics are often "tagged" for removal or sequestration before reaching their intended tissues.

The research presented here is focused on characterizing and taking advantage of a particular protein corona – the self-aggregation of serum folate binding protein (FBP). FBP is derived from cellular folate receptors, and both bind strongly to folic acid (FA), as well as the antifolate drug methotrexate (MTX). FA has been explored as a targeting agent because folate receptors are overexpressed on a variety of human cancers. Translation to the clinic of FA-targeted therapeutics has been challenging because the interaction of FBP with these materials has not been fully understood or appreciated: therapies tested *in vivo* are likely to operate by different mechanisms than those predicted by *in vitro* experiments in the absence of soluble FBP.

Using atomic force microscopy (AFM), we characterized the self-aggregation of FBP on a particle-by-particle basis at physiological concentrations. FBP self-aggregates into nanoparticles (forming FBPNP) at blood serum concentrations. We further explored the effect of concentration and ligand on the aggregation process. The introduction, and subsequent binding to FBP, of FA, MTX, or leucovorin (LEUC, a FA rescue agent) disrupted existing FBPNP, in most cases inducing reaggregation into new FBPNP. Healthy concentrations of FA and therapeutically relevant concentrations of LEUC produced FBPNP distributions that were not statistically different. This provided a new hypothesis for the perplexing phenomenon that LEUC must be used for FA rescue because high-dose FA itself provides no therapeutic benefit. FBPNP with therapeutic levels of FA or MTX had similar distributions, both of which were significantly different from LEUC-FBPNP. We postulated the degree of FBP aggregation acts as a signaling mechanism and dictates uptake of ligated species.

We studied FBP aggregation with two FA-poly(amidoamine) (PAMAM) dendrimers and two FA-poly(ethylene glycol) (PEG) conjugates. Fluorescence spectroscopy experiments showed that FA and FA-conjugates induced conformational changes throughout the protein population, even with an excess of FBP. Using AFM, we demonstrated the PAMAM conjugates produced large aggregates at sub-stoichiometric concentrations. PAMAM-FA-FBPNP and FA-FBPNP have different distributions, suggesting that translation of targeted conjugates has been challenging because FBP does not traffic the conjugates like free FA. PEG should be used with caution because it disrupted healthy FBP aggregation, potentially inducing artificial folate deficiency.

Given the challenges associated with conjugated therapies, we sought to leverage FBP itself as a targeted vector. We hypothesized that pre-binding FBP to MTX would decrease toxicity and increase therapeutic efficacy. We tested this hypothesis in a KB xenograft tumor model in mice. Surprisingly, FBP alone inhibited tumor growth as compared to saline control and free MTX. This is the first time this therapeutic effect of FBP has been reported. We postulate the excess unbound FBP resulted in folate starvation of the tumors. The groups treated with MTX and FBP also showed inhibition of tumor growth, but toxicity increased with FBP concentration. It is likely that instead of specifically targeting cancer cells, FBP facilitated widespread uptake of MTX, resulting in systemic toxicity. The substantial reduction observed in tumor volume suggests that FBP alone could be employed as a chemotherapeutic. Future work should be focused on exploring this exciting possibility.

CHAPTER 1. Distributions: The Importance of the Chemist's Molecular View of Biological Materials

Rachel L. Merzel [Wallace], Bradford G. Orr, and Mark M. Banaszak Holl
This chapter was submitted to *Biomacromolecules* as a Perspective.

1.1. Abstract

Characterization of materials with biological applications and assessment of physiological effects of therapeutic interventions are critical for translating research to the clinic and preventing adverse reactions. Analytical techniques typically used to characterize targeted nanomaterials and tissues rely on bulk measurement. Therefore, the resulting data represent an *average* structure of the sample, masking stochastic (randomly generated) distributions that are commonly present. In this *Perspective*, we examine almost 20 years of work our group has done in different fields to characterize and control distributions. We discuss the analytical techniques and statistical methods we use and illustrate how we leverage them in tandem with other bulk techniques. We also discuss the challenges and time investment associated with taking such a detailed view of distributions, as well the risks of not fully appreciating the extent of heterogeneity present in many systems. Through three case studies showcasing our research on conjugated polymers for drug delivery, collagen in bone, and endogenous protein nanoparticles, we discuss how identification and characterization of distributions – a molecular view of the system – was critical for understanding the observed biological effects. In all three cases, data would have been misinterpreted and insights missed if we had only relied upon spatially averaged data. Finally, we discuss how new techniques are starting to bridge the gap between

bulk and molecular level analysis, bringing more opportunity and capacity to the research community to address the challenges of distributions and their roles in biology, chemistry, and the translation of science and engineering to societal challenges.

1.2. Introduction: Characterization of nanomaterials and nanostructures in biology

In this *Perspective*, we consider nearly 20 years of effort in our group to characterize stochastic (randomly occurring) distributions arising from molecular level chemistry in a variety of synthetic and natural systems. As a research team composed primarily of chemists, engineers, and physicists with highly integrated medical collaborators and mentors, our group brings distinct perspectives and expertise to characterizing biological materials and systems. Generally, the extent of heterogeneity and the role material distributions play has not been fully appreciated. Here, we present three case studies in the arenas of targeted drug delivery and tissue analysis illustrating the importance of a molecular view of biomaterials and the specific contributions of our research to these fields. Specifically, we highlight examples of how detailed characterizations – and sometimes intentional removal – of distributions have proven critical to understanding the biological behavior.

1.2.1. Analytical techniques for nanoscale characterization

Most analytical techniques used to characterize nanoscale materials and nanostructures rely on bulk measurement. That is, they average over a much larger length scale than the constitutive molecules or nanomaterials. The resulting data represent an *average* molecular and/or nanoscale structure of the sample. For example, conventional spectroscopic techniques (*e.g.*, NMR, IR, UV-Vis), X-ray diffraction (XRD), and dynamic light scattering (DLS) contain information regarding the distribution of sample with line-widths that are not simply interpreted

and are often convolved with other physical properties. The bulk characterization masks stochastic distributions present within the nanomaterials. If a new targeted nanoscale therapy comprises a stochastic distribution, it is difficult, if not impossible to know which species produced the observed physiological effect. In biological tissues, *e.g.* bone and skin, most characterization techniques hide natural heterogeneity or mask localized changes to micro- and nanostructure as a result of disease or therapeutic intervention because the analysis averages over microns to millimeters or even greater sample dimensions. Precise characterization of nanoscale materials and anatomical changes is critical to developing safe and targeted therapies, as well as understanding their physiological effects.[1]

Molecular level characterization of samples and elucidation of structure is a challenging problem. In the research presented here, we primarily took advantage of two techniques to characterize and/or control distributions: reverse-phase high performance liquid chromatography (rp-HPLC) and atomic force microscopy (AFM). We complemented these methods with other bulk techniques, notably NMR and fluorescence spectroscopy, mass spectrometry, DLS, confocal microscopy, and fluorescence lifetime imaging microscopy (FLIM). We demonstrated that rp-HPLC can be used to separate trailing and branching defects in poly(amidoamine) (PAMAM) dendrimers[2–5] and separate species with different number of hydrophobic ligands (dyes, drugs, targeting agents) attached to the hydrophilic backbone.[6–10] AFM allowed for direct, representative imaging of samples and surfaces with nanometer precision in the x and y directions and sub-nanometer precision vertically.[11–21] Importantly, AFM is a topographic technique, measuring the volume of imaged features along with surface morphology and material properties. Hierarchical features from the nanometer to micron scale can be characterized, and no

staining is required for contrast.[15] The large number of individually characterized nanostructures in each AFM image enables robust statistical analysis.

Researchers also turn to XRD because it can provide high resolution (sub-angstrom) information with structural information down to the molecular level. However, these values are calculated from combined measurements of a large sample set of molecules throughout the bulk material – microns to millimeters in the crystal. Crystal structures obtained by XRD represent a spatial average and tend to treat molecular differences as "disorder", masking heterogeneity in the sample. Conversely, AFM typically produces images with slightly lower resolution but provides particle-by-particle measurements. This molecular level analysis is critical for assessing distributions in biological materials and relating changes in distributions to activity.

In our research, we use molecular level and bulk techniques together to build greater scientific understanding. We take advantage of image processing software – particle counting, alignment mapping, etc. – to process large data sets with thousands of structures. We also use conventional cellular biology techniques such as confocal microscopy and flow cytometry to probe the biological implications of distributions. In sum, we make the case here for the investment in a molecular level analysis of biological materials and the importance of understanding the interplay between structural variation and function.

1.2.2. Three cases for a molecular view of biological materials

In the rest of this *Perspective*, we present three broad research studies illustrating the role distributions play in assessing biological materials and outcomes. The first section focuses on multivalent polymers as drug delivery vectors, specifically the challenges associated with heterogeneity resulting from sequential stochastic conjugations. The second section discusses inherent heterogeneity in tissue and changes to the hierarchical structure of collagen as functions

of disease and drug treatment. In the third section we return to drug delivery and combine our analyses of distributions in artificial and natural materials. We highlight our latest research on serum proteins and the role they play in trafficking and bioidentity of their ligands. Analysis of distributions of serum protein nanoparticles (aggregated protein) as functions of concentration and ligand yielded novel hypotheses on the relationship between protein aggregation and activity. This was particularly important for understanding the role of serum proteins in the trafficking of the multivalent polymers discussed in the first section. We emphasize how the success of this work depended on applying lessons on conjugation heterogeneity and collagen characterization from the first two research cases. We translated our understanding of material distributions derived from laboratory synthesis processes and inherently present in natural materials, as well as our expertise in AFM and image analysis, to exploring the relationship between structure, function, and activity in protein nanoparticles. In all three cases we demonstrate how key conclusions insights and conclusions would have been missed if we had only used techniques that measure over larger scales than the molecules or nanostructures in the biological materials

1.3. Distributions in targeted nanoparticles

1.3.1. History and motivation

History and motivation. Over almost 20 years, our group and close collaborators have invested substantial research effort towards developing targeted therapeutics on a generation 5 (G5) PAMAM dendrimer scaffold.[6–9,22–34] In the mid-2000s, our colleagues developed a targeted dendrimer cancer therapeutic that demonstrated significant toxicity to tumor cells *in vitro*.[30] The targeted dendrimer was cleared for Phase I clinical trials. However, sufficient quantities for a clinical trial (kilograms) could not be manufactured consistently, and the trial never moved

forward. Much of our work since that time has been aimed at trying to understand the challenges in scientific understanding, material processing and scale-up, and clinical translation that arise when a small number of ligands is conjugated to a comparatively large number of attachment sites.[2–10] Note that G5 PAMAM has a theoretical 128 attachment sites (purified G5 PAMAM monomer – discussed below – has an average of 93 attachment sites).[4]

In general, nanomaterials (particles, polymers, metals, micelles, etc.) have been a popular focus of research in biomedical applications, including targeted therapy, imaging, and diagnostics.[35] The ability to attach multiple copies of ligands allows for enhanced multivalent targeting and increased drug payloads. The size of the materials enables them to escape renal filtration and facilitates longer blood circulation times, increasing the chances they will reach the target tissues[36,37] (G5 PAMAM is approximately 5 nm in diameter). The enhanced permeability and retention (EPR) effect in leaky tumor vasculature is widely believed to contribute to increased therapeutic efficacy. These attractive advantages have continued to make multivalent nanomaterials a popular area of biomedical research.[26,35,38–48]

1.3.2. Heterogeneity in conjugated nanomaterials

Translation to the clinic of targeted multivalent nanomaterials has been difficult. Targeted nanomaterials that perform well *in vitro* often cannot be formulated on large scales or exhibit unexpected side effects and toxicity when tested *in vivo*. We postulate that many of these adverse effects arise from highly heterogenous mixtures resulting from multiple ligand conjugations.[10] Here, we provide brief context to highlight the scope of the challenge in creating homogenous conjugated nanomaterials, but a full accounting of these synthetic and characterization efforts is not the focus of this *Perspective*. Our group has already published extensively on this work, as well as our research on characterizing, controlling, and eliminating heterogeneous distributions

in this Journal[10,49] and others.[2–8,11,12] Here, we highlight a case in which we demonstrated *in vitro* the importance of explicit consideration of distributions in biological nanomaterials.[9]

The arithmetic mean is the most commonly used parameter for characterizing the number of (functional) ligands on a nanomaterial. Usually this value is determined by bulk characterization such as NMR spectroscopy or gel permeation chromatography (GPC). The mean value fails to convey that the sample actually contains material with a distribution in the number of conjugated ligands. The conjugate distribution is binomial if the attachment of ligands is identical and independent of previous binding events. If the mean number of conjugated ligands is small (*e.g.*, three drugs or four targeting agents) and the ratio of reacted sites to total initial number of sites is low compared to the number of attachment sites (*e.g.*, 128 in a G5 PAMAM dendrimer), the distribution is Poissonian, not Gaussian.[50,51] Characterization of nanomaterials subjected to sequential conjugations (*e.g.*, a targeting agent and then a drug) is more complicated still because the distributions are multiplicative.[2,3,10]

Consider a PAMAM dendrimer conjugate with a mean of four FA and five MTX. Figure 1.1a shows the distribution of species if only four FA or five MTX were conjugated to the dendrimer. Figure 1.1b demonstrates the multiplicative effect

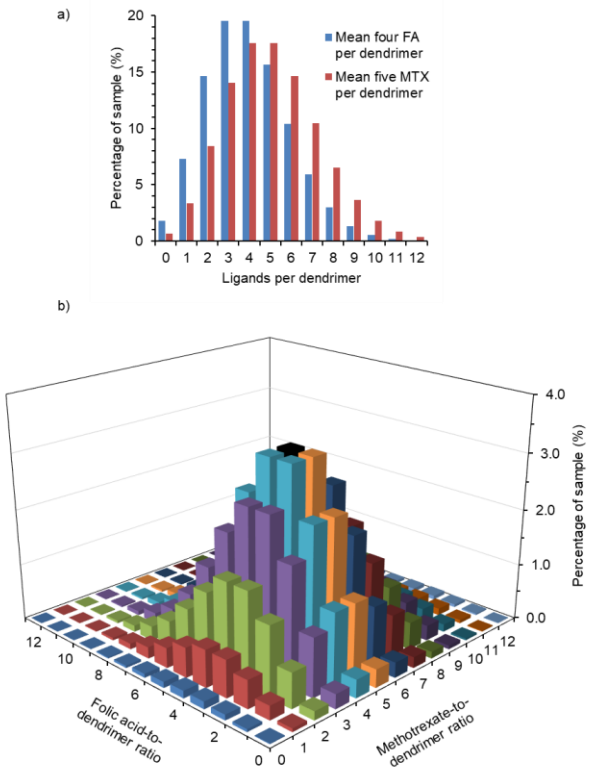

Figure 1.1. a) Poisson distributions of stochastic mixtures of dendrimers with an average of four or five ligands. b) Distribution of species resulting from sequential conjugation of averages of four then five ligands. The chart represents the product of the two distributions. The black bar indicates the nominal material with four FA and five MTX.

of combining two Poisson distributions resulting from stochastic reaction conditions. At most, 3-4% of the doubly conjugated sample material contains 4 FA and 5 MTX ligands. This does not take into account differences in reactivity between the ligands, site-blocking effects with increasing number of ligands conjugated, or autocatalysis of the conjugation process. All these factors can increase the heterogeneity of the system and further decrease the concentration of the mean average material. In many cases, the nominal "average" material may comprise less than one percent of the sample. As a result, it is difficult, if not impossible, to accurately assess the nanomaterial's properties and activity, which is particularly important in biological applications. If these samples are tested for their therapeutic properties *in vitro* or *in vivo*, one or many of the species present may contribute to observed effects. Sample heterogeneity greatly complicates research on the mechanisms of action and side effects, as well as efforts to reproduce results and translate multivalent nanomaterials to the clinic.

Heterogeneity in the scaffold itself is another factor to be considered. Our group has invested significant effort in characterizing and removing trailing generations and branching defects from commercial G5 PAMAM (Figure 1.2a).[4,5] Our standard operating procedure is to purify commercially purchased PAMAM to G5 monomer

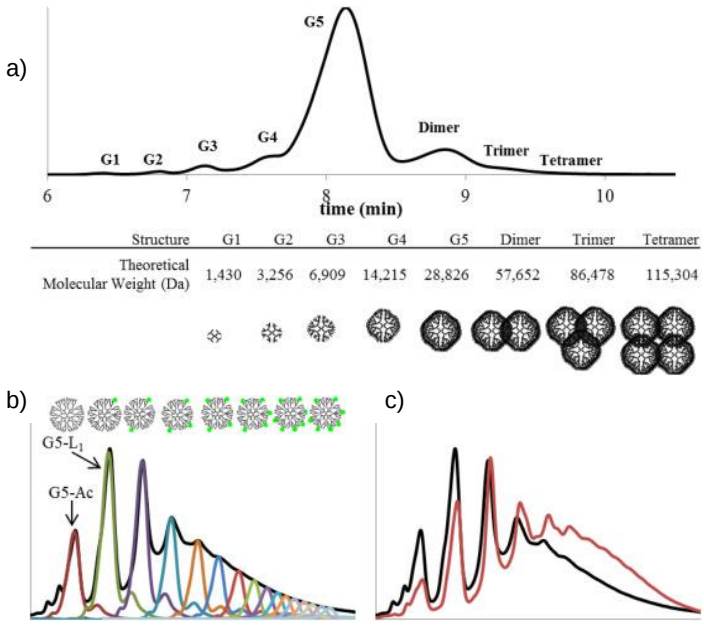

Figure 1.2. Ultra performance liquid chromatography (UPLC) chromatograms at 210 nm. a) As-received G5 dendrimer indicates the presence of trailing generation impurities as well as aggregtation defects. b) as-received acetylated G5 PAMAM (G5-Ac, red trace) contains high weight impurities with no ligand that co-elute with G5 monomers containing one ligand (G5-L1, green trace) in a conjugated sample (black trace). c) Conjugation to an rp-HPLC purified G5 monomer sample (red trace) has narrowed peak width and improved peak resolution compared to the as-received conjugation (black trace). Adapted and reprinted with permission from *Polymer* **2013**, *54*, 4126-4133. © 2013 Elsevier Ltd.

before using it in conjugation reactions. If we do not take this extra step, shifts induced on the rp-HPLC column by each hydrophobic ligand will not be larger than the peak width of the mass distribution of the dendrimer (Figure 1.2b,c and Figure 1.3).[4,5,10] Even with G5 PAMAM monomer, techniques such as MALDI-TOF-MS are of limited use because the mass shift is much narrower than the dendrimer mass distribution itself and the shot noise in the mass spectrometry measurement is approximately the same as the ligand mass.

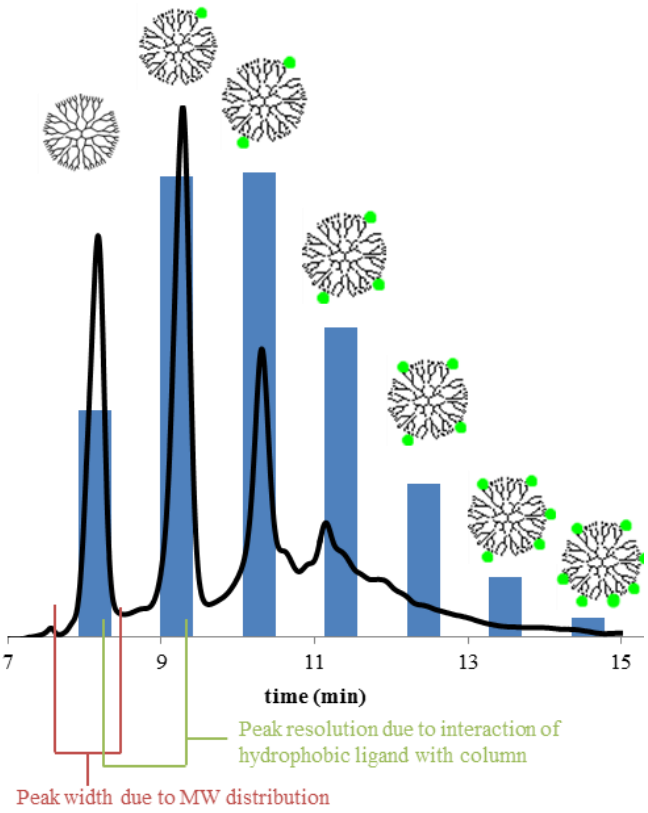

Figure 1.3. HPLC chromatogram of an average conjugate overlaid with the predicted distribution for an average of two ligands-per-particle. Figure adapted and reprinted with permission of *Biomacromolecules* **2014**, *15*, 3215-3234. © 2014 American Chemical Society.

This brief background on nanomaterial-ligand distributions illustrates the scope of the challenge in designing targeted therapeutic, exclusive to issues such as toxicity and biodegradability. In this context, the next subsection discusses work from our group in which we demonstrated that the number of ligands determines outcome *in vitro*, highlighting the critical need for appreciation and consideration of heterogeneous distributions.

1.3.3. Cellular uptake and fluorescence change with dye-dendrimer ratio.

(Highlighting results from *Bioconjugate Chem.* **2015**, *26*, 304–315.)[9]

This study was designed to examine the differences in activity between dendrimers with precise numbers of dyes and stochastic mixtures of material. In particular, we wanted to assess

the implications of using fluorescence to assess cellular uptake and localization. Understanding the interaction between the dendrimer and dye and their response to cellular uptake is critical because the dendrimers are used as vectors for oligonucleotides, antibacterial agents and drugs.[45,48,52–54] Fluorescent dyes are often attached to assess uptake and examine localization within the cells.[55]

We prepared three categories of G5 PAMAM dendrimers conjugated to TAMRA dyes: 1) dendrimers with precisely one to four dyes attached; 2) dendrimers with five or more dyes attached; and 3) dendrimer containing a Poisson distribution of dye with an arithmetic mean of 1.5 (Scheme 1). This last material consisted of mixture of dendrimers with 0, 1, 2, 3, 4, and 5 dyes at 22%, 34%, 25%, 13%, 5% and 1%, respectively. The solution fluorescence properties (intensity and lifetime) of the free dye and each of the six conjugates were examined, in aqueous solutions and biologically relevant control solutions (*e.g.*, cell lysate, with albumin, and in blood serum). We demonstrated that intensity increased and fluorescence lifetime decreased with increasing numbers of dyes (n), but these relationships were not linear. Confocal microscopy experiments showed that cellular uptake of the conjugates varied as function of n. It was necessary to apply correction factors determined from the solution experiments to accurately quantify the extent of uptake. The raw mean fluorescence intensities suggested that uptake decreased with $n \geq 2$. However, once the corrections were applied, the data showed that cells took up more dendrimers with $n \geq 2$ than n=1 material – the opposite trend of what the raw data indicated. The *in vitro* fluorescence properties of the stochastic material (n=1.5_{avg}) is more complicated. Biodistribution can be affected by hydrophobicity, and material with different numbers of ligands can be "separated," or fractionated, through interactions with biomolecules.[56–59] Accurate determination of uptake would require knowing the number of

conjugated dyes per dendrimer (or hydrophobic ligands per polymer more generally), the fluorescent properties of the conjugates, and which species would be preferentially taken up. Application of the corrections showed that the mean fluorescence data for the stochastic mixtures had errors of at least 3- to 5-fold. Relative brightness in confocal microscopy fluorescence images cannot be relied upon to interpret cellular uptake without knowledge of the number of dyes per dendrimer. Caution is necessary when quantifying uptake of stochastic mixtures using mean fluorescence data.

Scheme 1.1. Synthesis, Isolation, and Characterization of G5-NH2-TAMRAn (*n* = 0, 1, 2, 3, 4, 5+, 1.5avg) samples

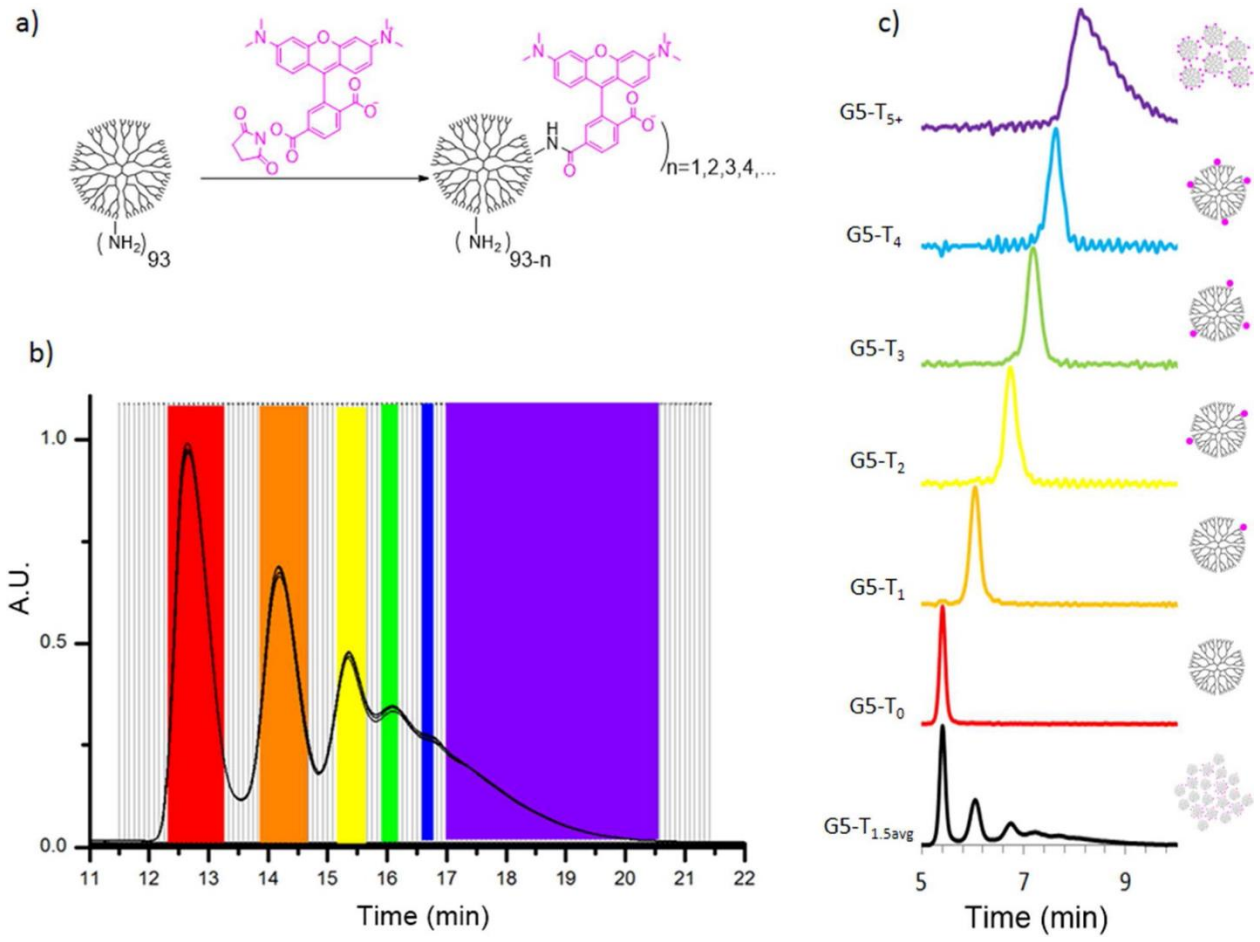

a) Stochastic conjugation of TAMRA to G5 PAMAM dendrimer. b) Isolation of G5-NH_2-$TAMRA_n$ employing semi-preparative rp-HPLC. c) Reinjection of combined fractions on analytical rp-UPLC to determine purity. *n* = 1.5_{avg} (black), 0 (red), 1 (orange), 2 (yellow), 3 (green), 4 (blue), and 5+ (purple). Reprinted with permission from *Bioconjugate Chem.* **2015**, *26*, 304-315.

FLIM experiments further emphasize this point. FLIM measurements are generally insensitive to changes in intensity but do depend on environmental conditions such as pH, ion concentration, and interactions with biomolecules.[60] We postulated that changes in lifetime due to microenvironment would allow for investigation of internal cellular structures and would be small compared to differences in lifetime resulting from variation in the dye to dendrimer ratio. We measured fluorescence lifetime both in cells (Figure 1.4a-h) and in biologically relevant control environments. In both cases, we found that changes in lifetime were of similar magnitude whether the dye ratio was held constant or the environment was held constant. The *n*=1 and *n*=5+ dendrimers had the longest lifetimes in cells, a phenomenon which was duplicated in control

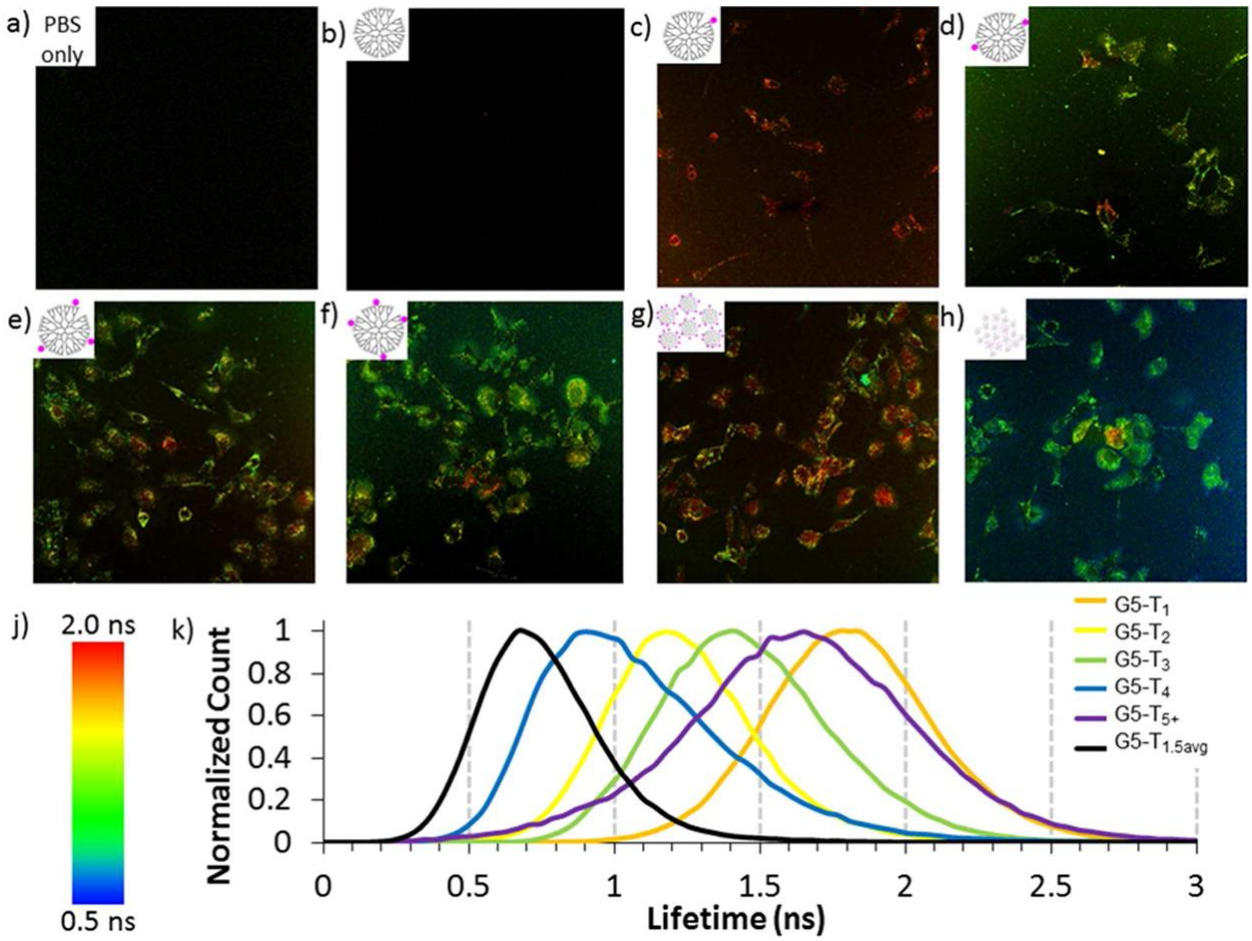

Figure 1.4. FLIM images of HEK293A cells incubated for 3 h with (a) PBS only, (b) G5-NH_2, (c) G5-NH_2-$TAMRA_1$, (d) G5-NH_2-$TAMRA_2$, (e) G5-NH_2-$TAMRA_3$, (f) G5-NH_2-$TAMRA_4$, (g) G5-NH_2-$TAMRA_{5+}$, and (h) G5-NH_2-$TAMRA_{1.5avg}$. (j) Color code for FLIM images. (k) Histograms of fluorescence lifetimes for FLIM images. Images were obtained with a 40× oil immersion objective. Reprinted and adapted with permission from *Bioconjugate Chem.* **2015**, *26*, 304-315.

solutions (Figure 1.4j). Surprisingly, the n=1.5$_{avg}$ mixture had the lowest lifetime and did not show any of the high lifetime components observed in the other high lifetime materials, even though 34% of the stochastic mixture comprised n=1 dendrimer. These data show that lifetime alone cannot be used to interpret biological microenvironments if the precise number of dyes per dendrimer is not known, a situation made even more complicated if the sample has been biologically fractionated.

Overall, these results illustrate the complications associated with testing stochastic mixtures of conjugated polymers for targeted therapy or for probing intracellular structure. The fluorescence properties alone obtained from stochastic mixtures are not reliable measures of uptake or localization in a cell. Differences in the distribution from batch to batch may also change observed outcomes. Appreciation of the challenges imposed by stochastic mixtures is critical for developing new therapies, understanding their biological effects and mechanisms of action, and facilitating their translation into the clinic.

1.4. Distributions in collagen structure

In the first case study, we discussed distributions in artificial materials (multivalent polymer conjugates) generated for biological applications. This second case illustrates the inherent nature of material distribution in tissue, specifically collagen in bone. Our knowledge of statistical methods for studying distributions from our work on multivalent polymer conjugates translated to our research on tissue, but we also developed new methods for characterizing distributions of natural nanostructures and microstructures imaged by AFM.

Type I collagen is the most abundant protein in the body, and therefore, detailed understanding of collagen structure is critical for assessing the effectiveness and impact of a wide variety of diseases and treatments.[61–65] Our group has studied naturally occurring

distributions over multiple levels of the hierarchical nature of collagen (Figure 1.5). The work presented here summarizes our efforts characterize distributions of repeating nanoscale features resulting from the packing of collagen molecules and microstructure and alignment of collagen fibers. We explore the relationship between changes to collagen nanostructure and microstructure as a function of bone type, diseases (osteoporosis induced by estrogen depletion), and treatment. We emphasize how macroscopic analysis methods fail to detect changes in collagen architecture that contribute to the inherent heterogeneity in collagenous tissue.

1.4.1. A brief introduction to collagen

Type I collagen forms the structural scaffold bones, dentin, skin, and tendon.[61–65] As illustrated in Figure 1.5, type I collagen assembles into hierarchical structures, forming microfibrils, fibrils, fibers or bundles, and tissues.[14–19,64,66–76] Various models have been proposed for fibril assembly and the origin of *D*-spacing. In 1963, the Hodge Petruska model depicted the collagen molecules parallel to each other but staggered, resulting in a repeating gap/overlap pattern that gave rise to the single 67 nm *D*-spacing value.[66] According to the Orgel model for fibril assembly, five microfibrils (each composed of three collagen molecules twisted in an α-helix) are packed quasi-hexagonally in the equatorial plane and supertwisted axially.[67] This is a 3D model for fibril assembly based on XRD studies.

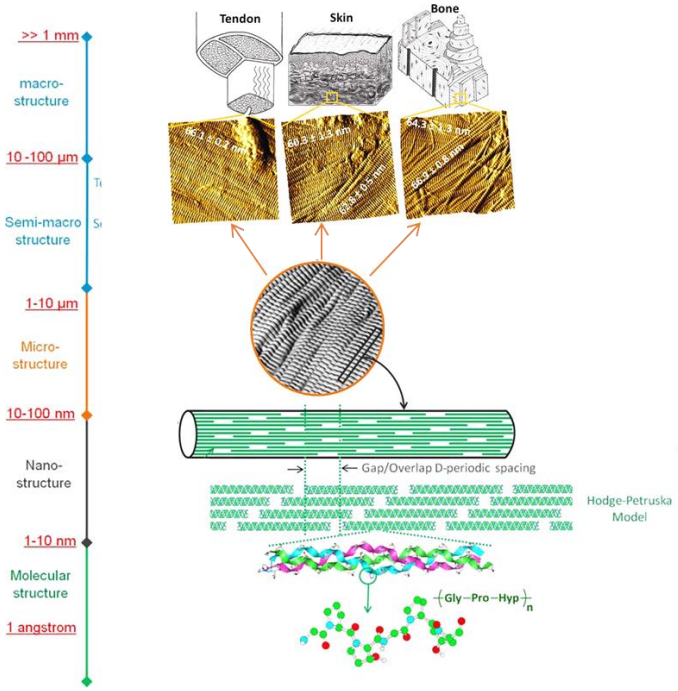

Figure 1.5. Hierarchical structure of collagen structures in tendon, skin, and bone. The AFM images show the *D*-spacing resulting from the parallel staggered alignment of the collagen microfibirls. Adapted and reprinted with permission from *ACS Nano* **2012**, *6*, 9503-9514. © 2012 American Chemical Society.

Both the Hodge Petruska and Orgel models require a single value for the D-spacing of type I collagen, which is commonly reported as 67 nm from XRD, EM, or computational models of the collagen molecule. Each of these techniques provide an average representation of the structure.

Conversely, our group has focused on a fibril-by-fibril approach to collagen analysis. Using AFM, we acquired images across heterogenous tissue surfaces (bone, skin, tendon, and tail from sheep, rats, rabbits, and monkeys) to obtain a representative data sets containing thousands of fibrils.[13–20] We then quantified the *D*-spacing on a fibril-by-fibril basis using two dimensional fast Fourier transform (2D FFT) analysis. The inclusion of thousands of fibrils allowed for statistically robust analyses. We have demonstrated non-Gaussian distributions in collagen nanomorphology, with *D*-spacing measured from 59 nm to 75 nm.[13–20] We found that, in general, there is very little variation in *D*-spacings within bundles (groups of aligned fibrils) but large variations between bundles.[18] Existing models of collagen structure cannot explain these *D*-spacing distributions, but a recent study documented changes in collagen structure at all levels of hierarchy, including *D*-spacing, as a function of disease.[65] Nevertheless, the formation and assembly of collagen fibrils affect the properties of the tissue. Research is still ongoing to understanding the physiological processes, mechanical stresses, and diseases that affect the distributions of *D*-spacings in tissues.

1.4.2. Fibril-by-fibril and multimicron approaches

(Highlighting results from *BoneKEy Rep.* **2015**, *4*, 697[20] and *Bone Reports* **2016**, *5*, 243–251.[21])

In more recent work, we have developed methods for hand-coding the alignment of collagen fibrils. (Figure 1.6).[20] We documented surface heterogeneity and changes in collagen microstructure that would not be reflected in average values incorporating measurements from many fibrils over a larger area of the tissue surface.

Here, we highlight a case in which microstructures changed as a function of disease – estrogen depletion modeling osteoporosis – and treatment with three different drugs. In sum, the study involved analyzing a total of 5,673 fibrils from 84 rabbits split into seven treatment groups.[20,21] After ovariectomy-induced estrogen depletion, the osteoporosis drugs were given to the rabbits as a preventive, not as treatment. Note that all the imaging and analysis was carried out blind to the identity of the samples. Microstructures in the images were hand-coded as bundles if 3-15 fibrils aligned in the same direction and were associated with one another and sheets if more than 20 fibrils aligned in the same direction and continuous with surrounding bone. Together, bundles and sheets were considered to contain *parallel* fibrils and non-aligned fibrils were *oblique* (Figure 1.6). This coding scheme captured at least 95% of all the measured fibrils.

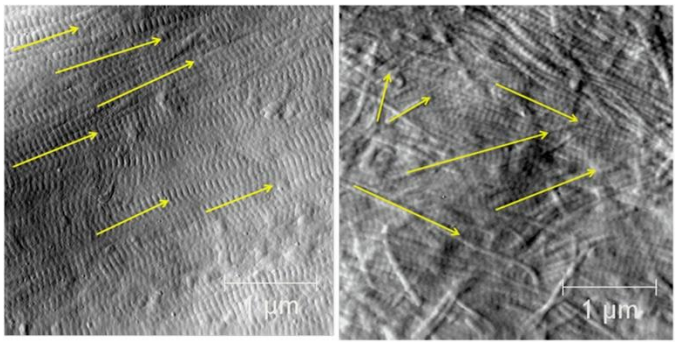

Figure 1.6. AFM images illustrating Parallel and Oblique regions of Type I collagen fibrils. a) *Parallel* region showing multiple aligned fibrils (yellow arrows); b) *Oblique* region showing multiple fibrils with varying alignment (yellow arrows). Adapted and reprinted with permission from BoneKEy Reports **2015**, *4*, 697.

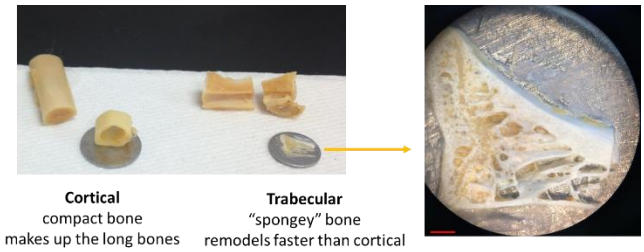

Figure 1.7. Examples of cortical and trabecular bone. Images courtesy of Meagan Cauble.

Importantly, changes to collagen microstructures were observed in cortical bone (compact bone that makes up the long bones, *e.g.*, femur) but not in trabecular bone ("spongey" bone that remodels faster than cortical bone, *e.g.*, the interior of vertebrae) (Figure 1.7). In the control cortical bone, estrogen depletion caused a statistically significant change in the proportions of *parallel* and *oblique* fibrils: incidence of *parallel* fibrils decreased and *oblique*

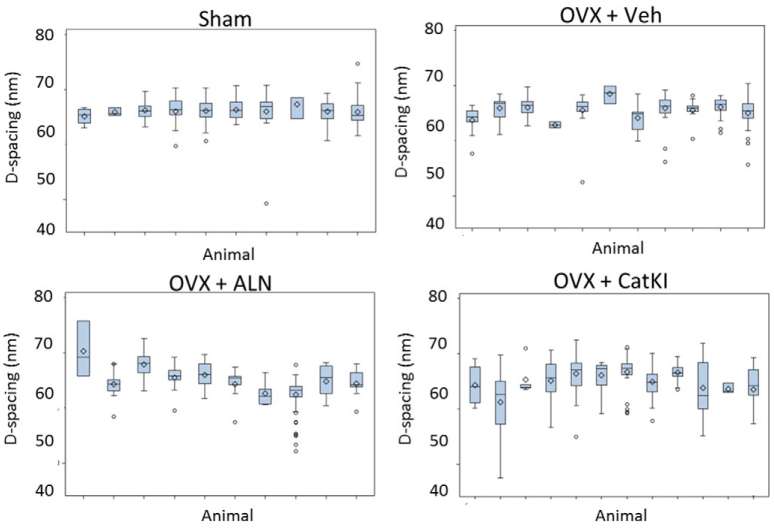

Figure 1.8. Boxplots of the D-spacing distribution of the collagen fibrils located in trabecular bundles obtained for sham, OVX+Vehicle (VEH), OVX+ALN, and OVX+CatKI groups. There are significant differences in the degree of animal-to-animal variability across treatments in trabecular bone (p=0.02, likelihood ratio Chi square test). The animal-to-animal variance for the OVX+Veh. Treatment was marginally significant (p=0.074). Both drug treatments introduced significant animal-to-animal variability in the bundle D-spacing (p b 0.01). Reprinted and adapted with permission from *Bone Reports* **2016**, *5*, 243-251. ©2016 The Authors.

fibrils increased. In the treated animals, the two drugs currently in the clinic partially prevented this change, while the experimental drug fully prevented it.

In both trabecular and cortical bone, the mean *D*-spacing value and the overall *D*-spacing distributions did not change with treatment. In bundles, no signification differences existed between the groups (Figure 1.8). However, treatment induced significant animal-to-animal variability in bundle *D*-spacing in *trabecular* bone. That is, the *D*-spacing means and distributions in trabecular bone remained the same, but *D*-spacings in trabecular bundles were different from animal-to-animal. The control rabbits displayed zero variability (including incorporation of a random effect for the animal) in their bundle distributions, ovariectomized rabbits had non-significant animal-to-animal variability, and the two treatment groups both had significant variability. The phenomenon was not observed in cortical bone. As trabecular bone is responsible for bone growth and remodeling, changes to trabecular collagen structure is of consequence.

More generally, these results provide important insight on the range of reactions to therapies. The differences in response and outcome will likely be even more pronounced in more genetically diverse populations, *e.g.*, humans. These trends would have been missed if

employing techniques that only capture the arithmetic mean of *D*-spacing values average of microns to millimeters (such as XRD) – all values would have been the same and no information regarding the drug effects would have been obtained.

Given the time and labor investment necessary for hand-coding fibril alignment, but we sought ways to speed up and streamline the process. With collaborators, we developed an auto-correlation approach to recognize patterns and quantitatively assess the degree of fibril alignment (Figure 1.9).[21] The full image level analysis (Figure 1.9) generates vector fields that mathematically approximate collagen fibril alignment. These vector fields were used to compute an information-theoretic entropy value: a fibril alignment parameter (FAP). We applied this approach to assessing fibril alignment in cortical and trabecular bone in estrogen depleted and treated animals. FAP distributions showed trabecular fibril alignment shifting towards cortical FAP distributions after ovariectomy. In cortical bone, estrogen depletion affected the formation of bundles and sheets. The three drugs examined affected alignment in cortical and trabecular bone differently. In one case, the drug moved FAP distributions in opposite directions in cortical and trabecular bone. The ability to quickly obtain fibril alignment information across a multimicron scale is important. Together *D*-spacing analysis, hand coding of microstructures, and the FAP distributions provide data on multiple levels of the collagen hierarchical structures, which is critical for understanding and treating disease.

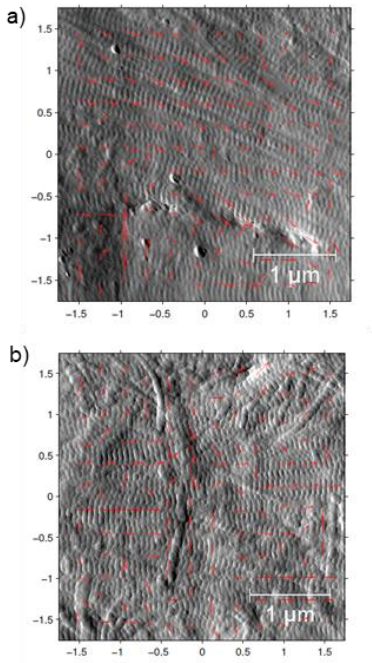

Figure 1.9. AFM images of collagen, with arrows showing local alignment of collagen patches. The alignment was determined using an autocorrelation-based method. The arrow lengths are scaled to show the degree of alignment. a) Collagen with a substantial concentration of *parallel* fibrils. b) Collagen with a with a substantial concentration of *oblique* fibrils. Reprinted and adapted with permission from *Bone Reports* **2016**, *5*, 243-251. ©2016 The Authors.

1.4.3. Implications for treatment of bone diseases

The research summarized in this section demonstrates the importance of studying distributions in multiple levels of the hierarchical structure in bone and other tissues. We emphasize how characterization of collagen structure distributions by AFM and image analysis should inform research on disease mechanisms and treatments. Because collagen is so abundant in the body, greater scientific understanding of the relationship between changes in multiple levels of collagen hierarchical structure and observed physiological outcomes would streamline the development of new therapies for a wide variety of diseases. Research efforts should be focused on creating methods of accelerating molecular and fibril level analysis while ensuring sampling is representative of the heterogenous tissue surface.

1.5. Distributions in natural nanoparticles

The previous two sections focused on characterizations of material distributions resulting from a laboratory synthesis, tissue biosynthesis, and tissue disease and drug treatment. Our more recent efforts combined aspects of this previous work on synthetic and natural materials: we investigated the relationship between distribution and function in intentionally created and controlled nanoparticles made of endogenous serum proteins. This research applies the analytical methods and statistical expertise our group has developed through our earlier research, described above. Specifically, we leveraged our experience making and characterizing dendrimer conjugates with precise ligand ratios and translated the AFM imaging and statistical methods developed in our collagen research to study distributions in the protein nanoparticles. Our overarching goal was to understand the role serum folate binding protein (FBP) plays in folic acid (FA) and antifolate (aFA) drug trafficking. We also hypothesized that the protein itself could be used as a targeted vector, eliminating many of the challenges associated with stochastic

or precisely-defined conjugated polymers. Our conclusions highlight the need of a molecular approach to nanoparticle characterization in biological systems and the importance of employing complementary analytical methods.

1.5.1. Folate binding protein nanoparticles

(Highlighting results from *Chin. Chem. Lett.* **2015**, *26*, 426-430[77] and *Nanoscale* **2017**, *9*, 2603-2615.)[11]

The structure and function of serum FBP have been extensively detailed by ourselves[11–13,49,77] and others.[78–93] For the purposes of this *Perspective*, it is important to note that FBP is derived from membrane bound folate receptors (FRs) and plays a critical role in the complex, multi-protein process of cellular uptake of FA and in embryonic development.[90–100] FRs bind strongly to FA (nanomolar dissociation constant) and are overexpressed on many types of human cancers because rapidly dividing cancer cells require high levels of FA for DNA synthesis.[101–104] As a result, researchers, including ourselves as described in the ligand conjugation section above, have extensively explored FA as a targeting ligand.[105,106,99,100,107–111,27,49,11,6,22] Many of these conjugated targeted drug delivery agents suffer from the same heterogenous distributions discussed above, but upon injection they also interact with serum FBP before ever reaching the target cells. FA and the antifolate (aFA) drug methotrexate (MTX) have the same binding affinity for serum FBP as they do for FRs.[104] Additionally, the binding of FA or MTX to FBP triggers FBP aggregation and protein corona formation.[11–13,49] Protein coronas often define biological identity, so the trafficking, uptake, and therapeutic efficacy of these materials are dictated by FBP before they reach the targeted tumor cells.[112–118] FA-targeted therapies *in vivo* are likely to operate by different mechanisms than those predicted by *in vitro* experiments in the absence of soluble FBP, complicating interpretation of results and clinical translation.

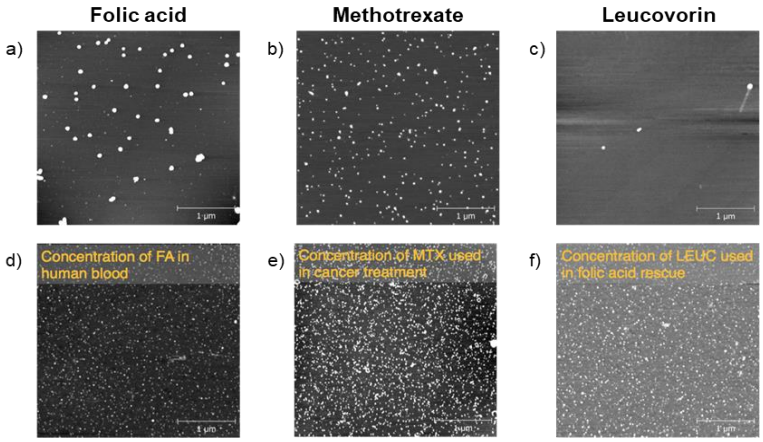

Figure 1.10. AFM images of FBP nanoparticles with folic acid, methotrexate, or leucovorin. a-c) FBP and ligand present at 2 nM. d) FA at 20 nM, FBP at 2 nM. e) MTX at 1,000 nM, FBP at 2 nM. f) LEUC at 1,000 nM, FBP at 2 nM

Our first goal was to develop a better understanding of the interactions between FBP and small molecules (FA and aFAs). Earlier studies of serum FBP were limited by the detection limits of the bulk analytical techniques use such as DLS, GPC, IR spectroscopy.[78–86] Conversely, our attempts to use techniques like DLS were inhibited by the nanomolar protein concentrations required to reflect biological concentrations, the low scattering cross section of the nanoparticles, and biases towards detecting larger particle aggregates. Instead, we characterized FBP aggregation on a particle-by-particle basis using AFM (Figure 1.10).[11] This enabled investigation of FBP aggregation at physiologically and therapeutically relevant concentrations. In many ways, our approach was very similar to the fibril-by-fibril analysis with collagen, and many of the same image analysis techniques and statistical methods were used. The large number of particles imaged allowed for statistically robust analyses of the volume distributions. With hundreds to thousands of FBP nanoparticles (FBPNP) analyzed in each image, examining the distribution of particle volumes (as opposed to primarily relying on the mean volumes) proved critical in developing novel hypotheses on the biotrafficking of FA, MTX, and leucovorin (LEUC, a vitamer of FA).

We showed that at physiological blood serum concentrations of FBP (2 nM), unligated FBP aggregates into nanoparticles comprised of approximately 6-8 proteins. Interestingly, this agreed well with the reported 8-mer crystal structure of FR-α from which the majority of serum

FBP is derived.[103] When FA was added to FBP at concentrations equivalent to FA deficiency in human adults, FBP aggregated into a bimodal distribution: nanoparticles of approximately four FBP and 600 FBP (Figure 10a). The non-uniform volume distribution of FBPNP at low FA concentrations is consistent with previously reported FA-induced apo-holo FBP aggregation.[80] The change in FBP volume distribution compared to healthy levels of FA suggest altered trafficking, biodistribution, and uptake processes that may be associated with symptoms of folate deficiency. Low concentrations of MTX resulted in larger nanoparticles (approximately 30 FBP), and low levels of LEUC completely inhibited aggregation (Figure 10b,c). When the concentration was increased to physiologically healthy or therapeutically relevant levels of FA, MTX, or LEUC the FBPNP volume distribution became more monodisperse with 6-8 FBP per nanoparticle (Figure 10d-f), again the same as the number of proteins crystal structure.

Most surprisingly, our analyses of FBPNP volume distributions presented new hypotheses on the trafficking of LEUC and why it can be used as a FA rescue agent. Following treatment with MTX, LEUC is administered to mitigate toxicity caused by inhibition of FA activity. FA will not provide therapeutic benefit – LEUC must be used instead. The reason for this and the mechanism of action of LEUC has not been not well understood. Most investigations of LEUC have focused at the cellular level, not considering the role of intravenous FBP.

Examination of the FBPNP volume distributions showed that FBPNP in the presence of high (therapeutic) doses of FBP was nearly identical to FBPNP containing therapeutic doses of MTX (Figure 1.11). The body would likely traffic both sets of FBPNP through the same biological pathways,[119,120] preventing FA from acting as a rescue agent, especially because FA and MTX are believed to enter cells via different uptake pathways, potentially triggered by the

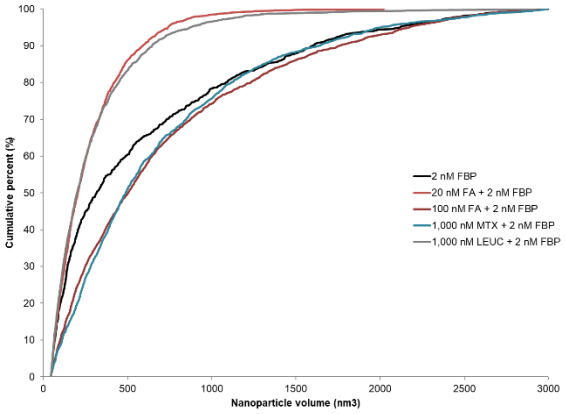

Figure 1.11. Cumulative density function (CDF) plots of selected the volumes FA-, MTX-, and LEUC-containing FBP nanoparticles. The similarity of the nanoparticle volume distributions was assessed using K–S statistics. The K–S testing showed the volume distributions of FBP nanoparticles formed from 20 nM FA + 2 nM FBP and 1000 nM LEUC + 2 nM FBP are not statistically different ($p = 0.310$). All other nanoparticle volume distributions were shown to be statistically different when evaluated with the K–S test. We hypothesize LEUC is effective as a folic acid rescue agent because the FBP nanoparticles formed at therapeutic concentrations of LEUC have the same volume distribution as the nanoparticles formed at healthy FA concentrations (20 nM).

FBP aggregation state. Conversely, FBPNP with high doses of LEUC and physiological levels of FA had volume distributions that were not statistically different. This suggests LEUC is trafficked to cells through the same pathways as FA and can facilitate FA rescue by bypassing the MTX uptake pathway. These results provided the first hypothesis on the perplexing observation that FA itself cannot provide a therapeutic FA rescue benefit, requiring LEUC to be used instead. Had we only relied upon bulk measurements and mean size values in the data analysis, these connections likely would have been missed. The possible role of FBP particle size is particular interesting in light of binary gate "lock and key" or "switch" analogies often employed when developing biological models of action. If particulate size is a factor in determining uptake rates, this suggests the analogy of a fuzzy logic gate is more appropriate for this case as opposed to a binary logic gate.

1.5.2. Conjugation dependent interactions with folate binding protein

(Highlighting results from *Biomacromolecules* **2016**, *17*, 922-927[49] and *Bioconjugate Chem.* **2017**, *28*, 2350-2360.[12])

Here, we bring this *Perspective* full circle to where we started with targeted polymer conjugate and illustrate how we applied lessons from all the research we have highlighted to this point. As we discussed above in detail, sample heterogeneity has plagued the translation into the

clinic of FA-targeted polymer therapeutics.[2–10] Our particle-by-particle work on the interactions between small molecule (FA, MTX, and LEUC) with FBP[11,77] (as well as previous research with FA-conjugates and FBP[6,11,22,27,49,110,111]) informed our guiding hypothesis that the identity of the conjugate itself could dictate the interaction with serum proteins, notably FBP. The combination of conjugation heterogeneity and unnatural serum protein aggregation processes likely leads to unexpected biological outcomes and failure in clinical translation efforts. The AFM and image analysis methods originally developed for our investigations of natural collagen distributions again proved critical in assessing FBP nanoparticle distributions. In contrast to our small molecule-FBP and collagen work, however, we used molecular level approaches in combination with solution fluorescence spectroscopy. The results discussed below demonstrate the risk in interpreting molecular interactions and structural information from only bulk techniques reporting averaged measurements. FBPNP distributions were dictated by both the chemical identity of the polymer scaffold and the conjugation method, but fluorescence spectroscopy experiments partially masked nuances in these results. The role both factors play in protein corona formation and ultimate fate of the targeted conjugate is often under appreciated.

Following a similar approach as we used on our studies of small molecule-FBP interactions, we directed our efforts towards characterizing the FA-conjugate-FBP interactions. We compared four FA-polymer conjugates: 1) $G5_{Ac}$-COG-$FA_{1.0}$; 2) $G5_{Ac}$-$FA_{4(avg);}$ and 3) poly(ethylene glycol)-FA (PEG-FA) of two different polymer chain lengths (Figure 1.12). The first – $G5_{Ac}$-$FA_{4(avg)}$ was a stochastic mixture with a mean of four FA conjugated to the dendrimer (Figure 1.12a). Based on the Poisson distribution, approximately 20% of the samples had four FA conjugated (Figure 1.12b). The second conjugate, $G5_{Ac}$-COG-$FA_{1.0}$ had precisely one FA conjugated through a cyclooctyne glycolic acid-amino acid linker (Figure 1.12b). This

conjugate was synthesized and isolated by rp-HPLC methods similar to those described above.[6–9] The PEG-FA conjugates (Figure 1.12d) were commercially available. Chain lengths of 2 kDa and 30 kDA were used in this study. NMR spectroscopy was used to quantify the concentration of active FA-conjugated material (PEG_{2kDa}-FA ~25%; PEG_{30kDa}-FA ~15%).

Tryptophan fluorescence quenching experiments – carried out in solution at protein concentrations an order of magnitude higher than physiological levels (58 nM *vs.* 2 nM) – indicated that free FA and $G5_{Ac}$-$FA_{4(avg)}$ induced similar changes in FBP conformation upon binding (Figure 1.13). This effect was observed whether the conjugate was added to an excess of FBP (Figure 1.13a) or FBP was added to an excess of (Figure 1.13b). The data also showed that

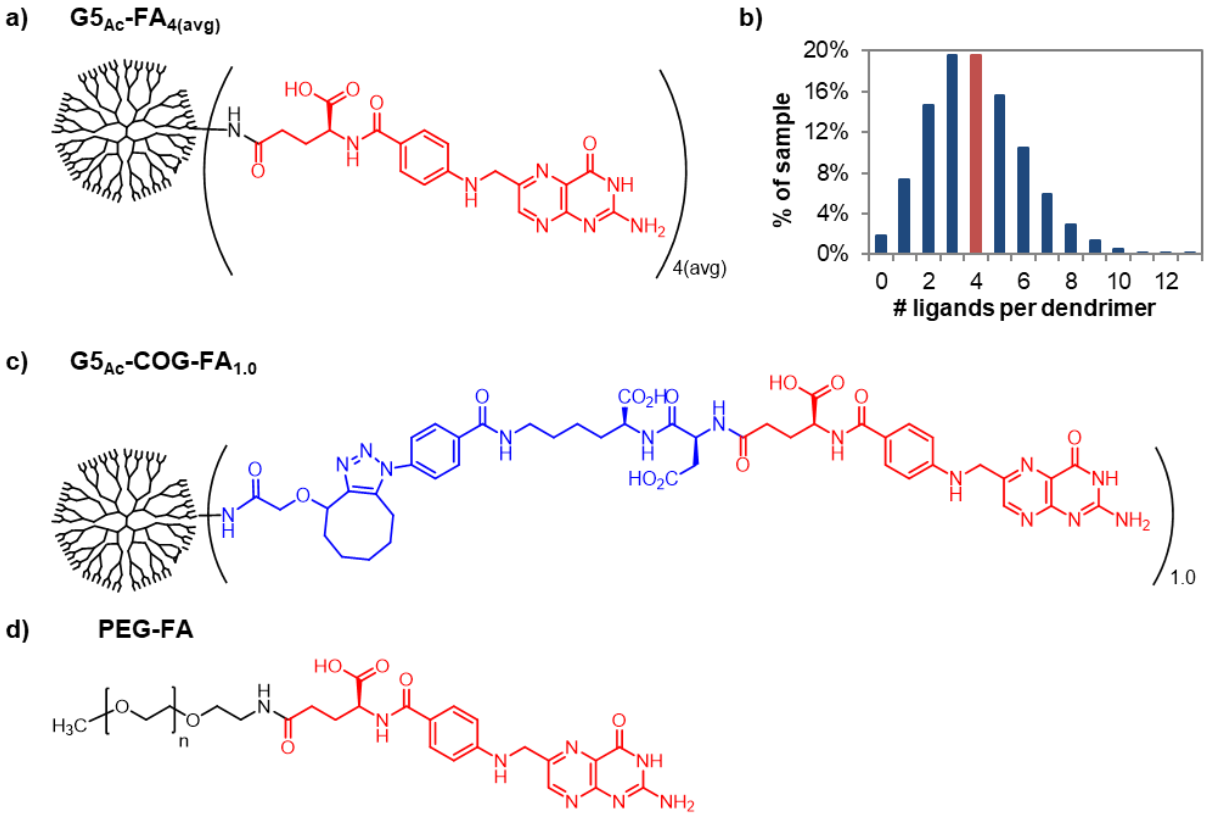

Figure 1.12. Representations of polymer-conjugate materials. For the PAMAM dendrimers, all terminal amines are acetylated following ligand conjugation. a) Folic acid (FA, red) conjugated directly to G5 PAMAM (black), producing $G5_{Ac}$-$FA_{4(avg)}$; b) Distribution resulting from a stochastic conjugation with an average of 4 ligands and 93 arms; c) FA (red) conjugated to G5 PAMAM (black) via a cyclooctyne glycolic acid (COG)-amino acid linker (blue), producing $G5_{Ac}$-COG-$FA_{1.0}$; d) FA (red) conjugated to poly(ethylene glycol) (black). Adapted and reprinted with permission from *Bioconjugate Chem.* **2017**, *28*, 2350-2360.

any amount of FA (free or conjugated) was sufficient to induce conformational changes and subsequent fluorescence quenching throughout the entire protein population. $G5_{Ac}$-COG-$FA_{1.0}$ resulted in significantly larger protein conformational changes, even in substoichiometric amounts of the conjugate. It bound essentially irreversibly to FBP and could not be displaced from the binding pocket by large excesses of free FA.[49] These data agreed with previous experiments demonstrating the same binding effect to surface-anchored FBP.[6] The PEG conjugates resulted in very little fluorescence quenching, likely due to the long polymer chain blocking access to the binding pocket.[49,12]

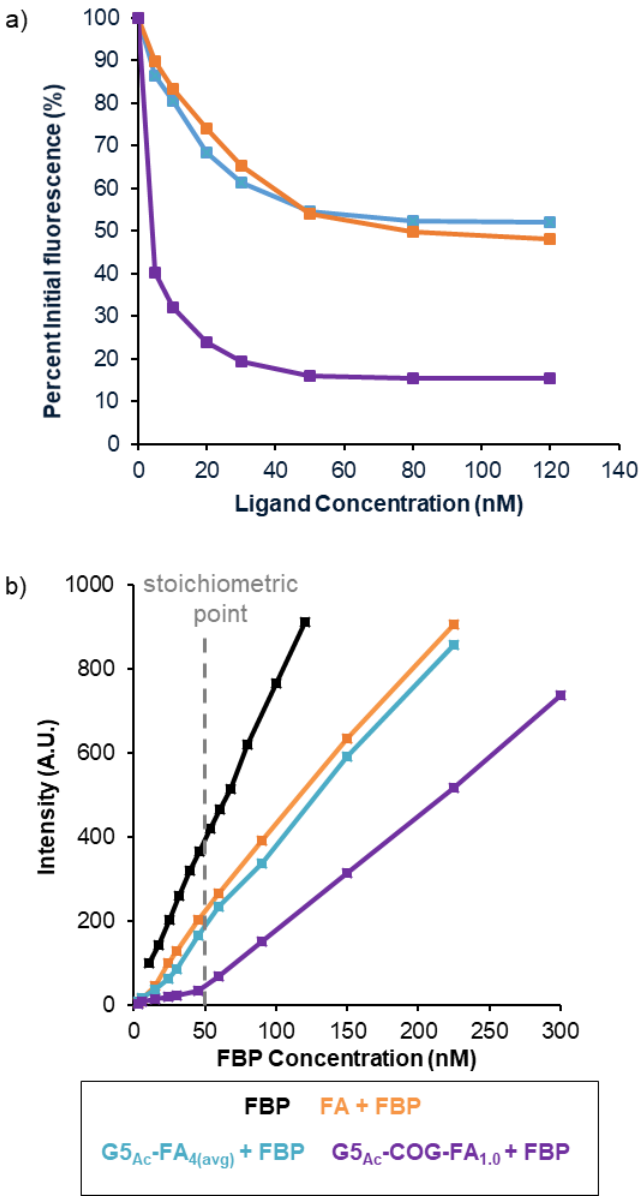

Figure 1.13. a) Tryptophan fluorescence quenching upon addition of free FA or FA conjugate to FBP. FBP concentration was 58 nM. Note the strong fluorescence quenching at approximately 0.1 equivalents of $G5_{Ac}$-COG-$FA_{1.0}$. b) Titration of FBP into FA (50 nM) and $G5_{Ac}$-FA polymer conjugates (50 nM). FA materials produced conformational changes throughout the protein population. For both experiments, excitation = 280 nm, emission = 342 nm; pH = 7.4 (1x PBS). Panel (b) reprinted and adapted with permission from *Bioconjugate Chem*. **2017**, *28*, 2350-2360.

Particle-by-particle analysis by AFM revealed important distinctions in the conjugate-protein interactions. The fluorescence data indicated free FA and $G5_{Ac}$-$FA_{4(avg)}$ had similar binding interactions with FBPNP, but the FBPNP volume distributions were significantly different. FBPNP containing

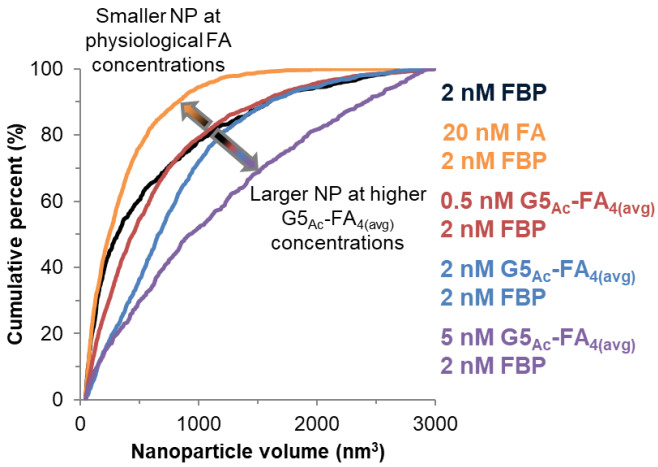

Figure 1.14. Cumulative density function (CDF) plots of the measured volume distributions of 2 nM FBP, 20 nM FA + 2 nM FBP, and $G5_{Ac}$-$FA_{4(avg)}$ + FBP nanoparticles. The similarity of the nanoparticle volume distributions was assessed using K−S statistics, which showed all nanoparticle volume distributions to be statistically different. Analysis of the volume distributions indicated that FBP nanoparticle size increases with increasing $G5_{Ac}$-$FA_{4(avg)}$ concentration. Reprinted and adapted with permission from *Bioconjugate Chem*. **2017**, *28*, 2350-2360.

free FA were smaller than unligated FBPNP (Figure 1.14). Conversely, upon binding to $G5_{Ac}$-$FA_{4(avg)}$, FBP rearranged into substantially larger nanoparticles. Consistent with the fluorescence data, $G5_{Ac}$-COG-$FA_{1.0}$ resulted in very large aggregates with each conjugate inducing conformational changes and aggregation in more than one protein (Figure 1.15). This agrees will with our fluorescence data in Figure 13 demonstrating even with an excess of FBP, $G5_{Ac}$-COG-$FA_{1.0}$ induced conformational changes throughout the protein population, resulting in fluorescence quenching. We postulate the long COG linker facilitates the strong binding interaction and FBP conformational changes, a phenomenon which we cover extensively elsewhere. PEG conjugates of all chain lengths disrupted FBP aggregation and no nanoparticles were observed.

In combination, these results illustrate both the risk of relying solely on bulk techniques to characterize these systems and the challenges of translating FA-targeted therapies into the clinic. The underlying assumption of FA-targeted therapies is that they are trafficked in the body like FA. That is, they should work because they go to cells and tissues with enhanced uptake of FA. The fluorescence spectroscopy data alone suggested that $G5_{Ac}$-$FA_{4(avg)}$ would likely have been a good candidate for a targeted therapeutic because they induced the same degree of conformational change in FBP. However, as shown in Figure 14, the opposite trends in

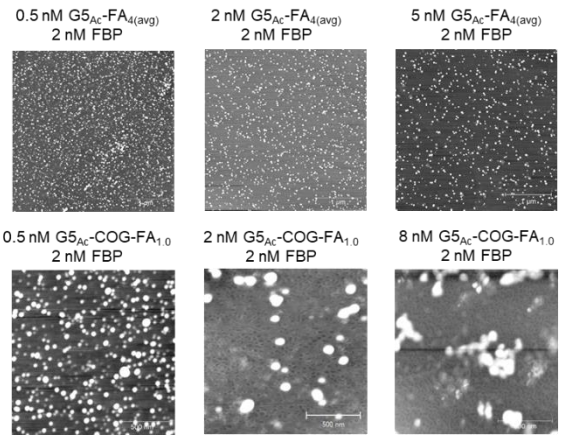

Figure 1.15. AFM images demonstrating the differences in aggregation when FBP is exposed to $G5_{Ac}$-$FA_{4(avg)}$ and $G5_{Ac}$-COG-$FA_{1.0}$. Images reprinted with permission from *Bioconjugate Chem*. **2017**, *28*, 2350-2360.

nanoparticle size upon ligand binding make it likely free FA and $G5_{Ac}$-$FA_{4(avg)}$ would not follow the same trafficking and uptake pathways. Along the same lines, the very large aggregates with $G5_{Ac}$-COG-$FA_{1.0}$ would be expected to exhibit different behavior *in vivo*. In contrast to the dendrimer conjugates, the AFM data showed no nanoparticles were present in samples containing PEG. The fluorescence spectroscopy data suggested that a weaker binding interaction between PEG-FA and FBP, but that alone does not demonstrate the extent of disruption in the system. PEG is the most common polymer in biomedical applications and is used to inhibit the formation of deleterious protein coronas on targeted conjugates.[116,121] It is therefore not surprising that PEG disrupted already existing FBPNP. PEG-containing FA-targeted conjugates likely would not follow the biotrafficking pathways of FA, and the inclusion of the polymer in rationally designed targeted vectors warrants consideration.

1.5.3. Implications for targeted drug delivery

Protein aggregation is often considered to be an indication of disease or disfunction, such as β-amyloid formation associated with Alzheimer's disease.[122] However, decade's worth of FBP aggregation data, including ours, indicate that FBP aggregation is a healthy and natural process and that understanding the changes in particle aggregate distribution as a function of changes in conditions is critical to understanding and controlling function.[11,78–86] FBP plays a central role in cellular uptake of FA and is essential for healthy embryonic development. In this

context, we hypothesized that pre-binding MTX to FBP before injecting it would enhance targeting of tumor cells and decrease off-target uptake. We carried out an *in vivo* experiment treating mice bearing xenograft tumors with MTX pre-bound to FBP.[123] Surprisingly, FBP alone was observed to dramatically inhibit tumor growth as compared to saline control and free MTX. In this case, there is no need to include a toxic chemotherapeutic such as MTX. This suggests that solely by manipulating the concentration level of endogenous FPB, a wide range of tumor types could be treated. We hypothesize the excess unbound FBP resulted in folate starvation of the tumors. The groups treated with MTX and FBP also showed inhibition of tumor growth, but toxicity increased with FBP concentration. It is likely that instead of specifically targeting the cancer cells, FBP facilitated widespread uptake of MTX, resulting in systemic toxicity. Future studies will investigate the therapeutic efficacy of FBP over a wide range of concentrations, as well as exploring how FBP-induced folate starvation could be synergistic with other therapies. This promising research on using an endogenous protein alone without a toxic small molecule is a completely novel approach in this field.

As demonstrated through the research presented here, heterogeneity and serum protein interactions have proven to be two significant obstacles to clinical translation or targeted therapeutics. Researchers may turn more towards protein-based therapies to mitigate the challenges, in addition to avoiding problems of immunogenicity and biodegradability. Protein carriers also mitigate manufacturing, immunogenicity, and biodegradability problems associated with synthetic drug delivery vectors. One of the powerful achievements in drug delivery over the last decade is Abraxane, an albumin-bound form of paclitaxel.[124–128] Researchers recently reported a cancer vaccine using albumin as a carrier showing great promise in *in vivo* trials.[129] Many more albumin-based approaches are currently in clinical trials. Taking advantage of

natural and health protein aggregation processes may indeed provide a key to avoiding the challenges of heterogeneous distributions in synthetic and natural drug delivery materials.

1.6. Conclusions and future outlook

In this *Perspective* we examined almost two decades of our research team's work to characterize heterogeneous distributions in multivalent polymers, collagen hierarchical structure, and serum protein nanoparticles. By tracing through the history of our work, we illustrated how our most recent work on protein nanoparticles leveraged all our collaborative knowledge and expertise on distributions. We showed how our methods were widely applicable and translated between research projects characterizing distributions created in both synthetic materials and inherently present in natural tissues. In each of the research cases, we emphasized how our unique molecular level analytical and statistical approaches were critical for interpreting data, understanding biological results, and facilitating development of new insights and hypotheses that would be missed through bulk measurements. As a set, the examples and discussion included here are intended to make a convincing case for the importance of a molecular level view of biological materials. We encourage investment in the development of methods to expand scientific understanding of the interplay between molecular level distributions and structural variation and function.

Relatively new techniques are starting to bridge the gap between bulk analytical methods and molecular level analysis. For example, combined AFM and IR spectroscopy allows for IR spectra to be acquired with as high as approximately 10 nm lateral resolution (Figure 1.16). In our current research efforts, we are employing AFM-IR to examine changes in mineral-collagen ratio throughout bone as a function of disease and treatment; identify microdamage that leads to failure in anterior cruciate ligaments; investigate uptake of nanoplastics into mussels; study the

chemical composition of atmospheric particles; and characterize the composition of a variety of composite polymers. As techniques that enable nanoscale, molecular, or chemical identity level characterization (*e.g.*, AFM-IR, AFM-mass spectrometry, and single particle tracking) become more widely available, the broader research community will have more capacity to address the challenges of heterogeneity and distributions presented here.

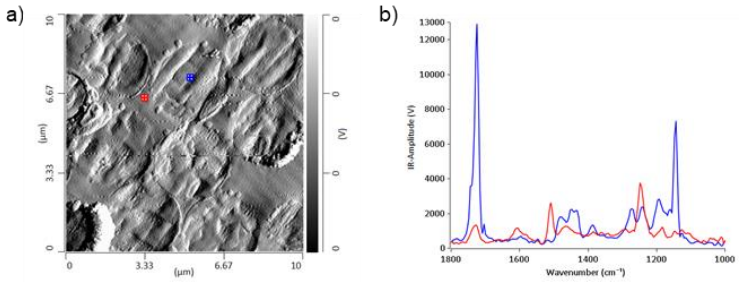

Figure 1.16. Example of AFM-IR, with a) a deflection image and b) IR spectra acquired at locations indicated by the squares on the image. The blue spectrum clearly shows the signals from poly(methyl methacrylate) beads (the circles) as compared to the epoxy (red trace). Acquired on a nanoIR2 from Anasys Instruments.

1.7. References

(1) Chen, J.; Ahn, T.; Colón-Bernal, I. D.; Kim, J.; Banaszak Holl, M. M. The Relationship of Collagen Structural and Compositional Heterogeneity to Tissue Mechanical Properties: A Chemical Perspective. *ACS Nano* **2017**, *11* (11), 10665–10671.

(2) Mullen, D. G.; Fang, M.; Desai, A.; Baker, J. R.; Orr, B. G.; Banaszak Holl, M. M. A Quantitative Assessment of Nanoparticle−Ligand Distributions: Implications for Targeted Drug and Imaging Delivery in Dendrimer Conjugates. *ACS Nano* **2010**, *4* (2), 657–670.

(3) Mullen, D. G.; Banaszak Holl, M. M. Heterogeneous Ligand–Nanoparticle Distributions: A Major Obstacle to Scientific Understanding and Commercial Translation. *Acc. Chem. Res.* **2011**, *44* (11), 1135–1145.

(4) van Dongen, M. A.; Desai, A.; Orr, B. G.; Baker, J. R.; Banaszak Holl, M. M.; Baker Jr, J. R.; Banaszak Holl, M. M. Quantitative Analysis of Generation and Branch Defects in G5 Poly(amidoamine) Dendrimer. *Polymer.* **2013**, *54* (16), 4126–4133.

(5) Mullen, D. G.; Desai, A.; van Dongen, M. A.; Barash, M.; Baker, J. R.; Banaszak Holl, M. M. Best Practices for Purification and Characterization of PAMAM Dendrimer. *Macromolecules* **2012**, *45* (12), 5316–5320.

(6) van Dongen, M. A.; Silpe, J. E.; Dougherty, C. A.; Kanduluru, A. K.; Choi, S. K.; Orr, B. G.; Low, P. S.; Banaszak Holl, M. M. Avidity Mechanism of Dendrimer–Folic Acid Conjugates. *Mol. Pharm.* **2014**, *11* (5), 1696–1706.

(7) van Dongen, M. A.; Rattan, R.; Silpe, J.; Dougherty, C.; Michmerhuizen, N. L.; Van

Winkle, M.; Huang, B.; Choi, S. K.; Sinniah, K.; Orr, B. G.; et al. Poly(amidoamine) Dendrimer–Methotrexate Conjugates: The Mechanism of Interaction with Folate Binding Protein. *Mol. Pharm.* **2014**, *11* (11), 4049–4058.

(8) Dougherty, C. A.; Furgal, J. C.; van Dongen, M. A.; Goodson, T.; Banaszak Holl, M. M.; Manono, J.; DiMaggio, S. Isolation and Characterization of Precise Dye/Dendrimer Ratios. *Chem. – A Eur. J.* **2014**, *20* (16), 4638–4645.

(9) Dougherty, C. A.; Vaidyanathan, S.; Orr, B. G.; Banaszak Holl, M. M. Fluorophore:Dendrimer Ratio Impacts Cellular Uptake and Intracellular Fluorescence Lifetime. *Bioconjug. Chem.* **2015**, *26* (2), 304–315.

(10) van Dongen, M. A.; Dougherty, C. A.; Banaszak Holl, M. M. Multivalent Polymers for Drug Delivery and Imaging: The Challenges of Conjugation. *Biomacromolecules* **2014**, *15* (9), 3215–3234.

(11) Merzel, R. L.; Boutom, S. M.; Chen, J.; Frey, C.; Shedden, K.; Marsh, E. N. G.; Banaszak Holl, M. M. Folate Binding Protein: Therapeutic Natural Nanotechnology for Folic Acid, Methotrexate, and Leucovorin. *Nanoscale* **2017**, *9* (7), 2603–2615.

(12) Merzel, R. L.; Frey, C.; Chen, J.; Garn, R.; van Dongen, M.; Dougherty, C. A.; Kandaluru, A. K.; Low, P. S.; Marsh, E. N. G.; Banaszak Holl, M. M. Conjugation Dependent Interaction of Folic Acid with Folate Binding Protein. *Bioconjug. Chem.* **2017**, *28* (9), 2350–2360.

(13) Chen, J.; Klem, S.; Jones, A. K.; Orr, B.; Banaszak Holl, M. M. Folate-Binding Protein Self-Aggregation Drives Agglomeration of Folic Acid Targeted Iron Oxide Nanoparticles. *Bioconjug. Chem.* **2017**, *28* (1), 81–87.

(14) Erickson, B.; Fang, M.; Wallace, J. M.; Orr, B. G.; Les, C. M.; Banaszak Holl, M. M. Nanoscale Structure of Type I Collagen Fibrils: Quantitative Measurement of D-Spacing. *Biotechnol. J.* **2013**, *8* (1), 117–126.

(15) Wallace, J. M.; Chen, Q.; Fang, M.; Erickson, B.; Orr, B. G.; Banaszak Holl, M. M. Type I Collagen Exists as a Distribution of Nanoscale Morphologies in Teeth, Bones, and Tendons. *Langmuir* **2010**, *26* (10), 7349–7354.

(16) Wallace, J. M.; Erickson, B.; Les, C. M.; Orr, B. G.; Banaszak Holl, M. M. Distribution of Type I Collagen Morphologies in Bone: Relation to Estrogen Depletion. *Bone* **2010**, *46* (5), 1349–1354.

(17) Fang, M.; Liroff, K. G.; Turner, A. S.; Les, C. M.; Orr, B. G.; Holl, M. M. B. Estrogen Depletion Results in Nanoscale Morphology Changes in Dermal Collagen. *J. Invest. Dermatol.* **2012**, *132* (7), 1791–1797.

(18) Fang, M.; Goldstein, E. L.; Turner, A. S.; Les, C. M.; Orr, B. G.; Fisher, G. J.; Welch, K. B.; Rothman, E. D.; Banaszak Holl, M. M. Type I Collagen D-Spacing in Fibril Bundles of Dermis, Tendon, and Bone: Bridging between Nano- and Micro-Level Tissue

Hierarchy. *ACS Nano* **2012**, *6* (11), 9503–9514.

(19) Fang, M.; Holl, M. M. B. Variation in Type I Collagen Fibril Nanomorphology: The Significance and Origin. *Bonekey Rep.* **2013**, *2*.

(20) Cauble, M. A.; Rothman, E.; Welch, K.; Fang, M.; Duong, L. T.; Pennypacker, B. L.; Orr, B. G.; Banaszak-Holl, M. M. Alteration of Type I Collagen Microstructure Induced by Estrogen Depletion Can Be Prevented with Drug Treatment. *Bonekey Rep.* **2015**, *4*, 697.

(21) Cauble, M. A.; Muckley, M. J.; Fang, M.; Fessler, J. A.; Welch, K.; Rothman, E. D.; Orr, B. G.; Duong, L. T.; Holl, M. M. B. Estrogen Depletion and Drug Treatment Alter the Microstructure of Type I Collagen in Bone. *Bone Reports* **2016**, *5*, 243–251.

(22) Mullen, D. G.; McNerny, D. Q.; Desai, A.; Cheng, X.; DiMaggio, S. C.; Kotlyar, A.; Zhong, Y.; Qin, S.; Kelly, C. V; Thomas, T. P.; et al. Design, Synthesis, and Biological Functionality of a Dendrimer-Based Modular Drug Delivery Platform. *Bioconjug. Chem.* **2011**, *22* (4), 679–689.

(23) Landmark, K. J.; DiMaggio, S.; Ward, J.; Kelly, C.; Vogt, S.; Hong, S.; Kotlyar, A.; Myc, A.; Thomas, T. P.; Penner-Hahn, J. E.; et al. Synthesis, Characterization, and in Vitro Testing of Superparamagnetic Iron Oxide Nanoparticles Targeted Using Folic Acid-Conjugated Dendrimers. *ACS Nano* **2008**, *2* (4), 773–783.

(24) Majoros, I. J.; Myc, A.; Thomas, T.; Mehta, C. B.; Baker, J. R. PAMAM Dendrimer-Based Multifunctional Conjugate for Cancer Therapy: Synthesis, Characterization, and Functionality. *Biomacromolecules* **2006**, *7* (2), 572–579.

(25) Li, M.-H.; Choi, S. K.; Thomas, T. P.; Desai, A.; Lee, K.-H.; Kotlyar, A.; Banaszak Holl, M. M.; Baker Jr, J. R. Dendrimer-Based Multivalent Methotrexates as Dual Acting Nanoconjugates for Cancer Cell Targeting. *Eur. J. Med. Chem.* **2012**, *47*, 560–572.

(26) Baker, J. R. Why I Believe Nanoparticles Are Crucial as a Carrier for Targeted Drug Delivery. *WIREs. Nanomed. Nanobiotechnol.* **2013**, *5* (5), 423–429.

(27) Ward, B. B.; Dunham, T.; Majoros, I. J.; Baker, J. R. Targeted Dendrimer Chemotherapy in an Animal Model for Head and Neck Squamous Cell Carcinoma. *J. Oral Maxillofac. Surg.* **2011**, *69* (9), 2452–2459.

(28) Quintana, A.; Raczka, E.; Piehler, L.; Lee, I.; Myc, A.; Majoros, I.; Patri, A. K.; Thomas, T.; Mulé, J.; Baker, J. R. Design and Function of a Dendrimer-Based Therapeutic Nanodevice Targeted to Tumor Cells through the Folate Receptor. *Pharm. Res.* **2002**, *19* (9), 1310–1316.

(29) Majoros, I. J.; Thomas, T. P.; Mehta, C. B.; Baker, J. R. Poly(amidoamine) Dendrimer-Based Multifunctional Engineered Nanodevice for Cancer Therapy. *J. Med. Chem.* **2005**, *48* (19), 5892–5899.

(30) Kukowska-Latallo, J. F.; Candido, K. A.; Cao, Z.; Nigavekar, S. S.; Majoros, I. J.;

Thomas, T. P.; Balogh, L. P.; Khan, M. K.; Baker, J. R. Nanoparticle Targeting of Anticancer Drug Improves Therapeutic Response in Animal Model of Human Epithelial Cancer. *Cancer Res.* **2005**, *65* (12).

(31) Betley, T. A.; Hessler, J. A.; Mecke, A.; Banaszak Holl, M. M.; Orr, B. G.; Uppuluri, S.; Tomalia, D. A.; Baker, J. R. Tapping Mode Atomic Force Microscopy Investigation of Poly(amidoamine) Core−Shell Tecto(dendrimers) Using Carbon Nanoprobes. *Langmuir* **2002**, *18* (8), 3127–3133.

(32) Betley, T. A.; Banaszak Holl, M. M.; Orr, B. G.; Swanson, D. R.; Tomalia, D. A.; Baker, J. R. Tapping Mode Atomic Force Microscopy Investigation of Poly(amidoamine) Dendrimers: Effects of Substrate and pH on Dendrimer Deformation. *Langmuir* **2001**, *17* (9), 2768–2773.

(33) Baker, J. R.; Quintana, A.; Piehler, L.; Banazak-Holl, M.; Tomalia, D.; Raczka, E. The Synthesis and Testing of Anti-Cancer Therapeutic Nanodevices. *Biomed. Microdevices* **2001**, *3* (1), 61–69.

(34) Hong, S.; Bielinska, A. U.; Mecke, A.; Keszler, B.; Beals, J. L.; Shi, X.; Balogh, L.; Orr, B. G.; Baker, J. R.; Banaszak Holl, M. M. Interaction of Poly(amidoamine) Dendrimers with Supported Lipid Bilayers and Cells: Hole Formation and the Relation to Transport. *Bioconjug. Chem.* **2004**, *15* (4), 774–782.

(35) Peer, D.; Karp, J. M.; Hong, S.; Farokhzad, O. C.; Margalit, R.; Langer, R. Nanocarriers as an Emerging Platform for Cancer Therapy. *Nat Nano* **2007**, *2* (12), 751–760.

(36) Fang, J.; Nakamura, H.; Maeda, H. The EPR Effect: Unique Features of Tumor Blood Vessels for Drug Delivery, Factors Involved, and Limitations and Augmentation of the Effect. *Adv. Drug Deliv. Rev.* **2011**, *63* (3), 136–151.

(37) Greish, K. Enhanced Permeability and Retention (EPR) Effect for Anticancer Nanomedicine Drug Targeting. In *Cancer Nanotechnology*; Grobmyer, S. R., Moudgil, B. M., Eds.; Humana Press, 2010; Vol. 624, pp 25–37.

(38) Pasut, G.; Veronese, F. M. Polymer-Drug Conjugation, Recent Achievements and General Strategies. *Progress in Polymer Science (Oxford)*. Pergamon August 1, 2007, pp 933–961.

(39) Duncan, R.; Gaspar, R. Nanomedicine(s) under the Microscope. *Mol. Pharm.* **2011**, *8* (6), 2101–2141.

(40) Duncan, R.; Richardson, S. C. W. Endocytosis and Intracellular Trafficking as Gateways for Nanomedicine Delivery: Opportunities and Challenges. *Mol. Pharm.* **2012**, *9* (9), 2380–2402.

(41) Svenson, S. Theranostics: Are We There Yet? *Molecular Pharmaceutics*. American Chemical Society March 4, 2013, pp 848–856.

(42) van der Meel, R.; Vehmeijer, L. J. C.; Kok, R. J.; Storm, G.; van Gaal, E. V. B. Ligand-

Targeted Particulate Nanomedicines Undergoing Clinical Evaluation: Current Status. *Adv. Drug Deliv. Rev.* **2013**, *65* (10), 1284–1298.

(43) Röglin, L.; Lempens, E. H. M.; Meijer, E. W. A Synthetic "tour de Force": Well-Defined Multivalent and Multimodal Dendritic Structures for Biomedical Applications. *Angewandte Chemie - International Edition*. WILEY-VCH Verlag January 3, 2011, pp 102–112.

(44) Kelkar, S. S.; Reineke, T. M. Theranostics: Combining Imaging and Therapy. *Bioconjug. Chem.* **2011**, *22* (10), 1879–1903.

(45) Lee, C. C.; MacKay, J. A.; Fréchet, J. M. J. J.; Szoka, F. C. Designing Dendrimers for Biological Applications. *Nat. Biotechnol.* **2005**, *23* (12), 1517–1526.

(46) Boas, U.; Heegaard, P. M. H. Dendrimers in Drug Research. *Chem. Soc. Rev.* **2004**, *33* (1), 43.

(47) Temming, K.; Schiffelers, R. M.; Molema, G.; Kok, R. J. RGD-Based Strategies for Selective Delivery of Therapeutics and Imaging Agents to the Tumour Vasculature. *Drug Resist. Updat.* **2005**, *8* (6), 381–402.

(48) Haag, R.; Kratz, F. Polymer Therapeutics: Concepts and Applications. *Angew. Chemie Int. Ed.* **2006**, *45* (8), 1198–1215.

(49) Chen, J.; van Dongen, M. A.; Merzel, R. L.; Dougherty, C. A.; Orr, B. G.; Kanduluru, A. K.; Low, P. S.; Marsh, E. N. G.; Banaszak Holl, M. M. Substrate-Triggered Exosite Binding: Synergistic Dendrimer/Folic Acid Action for Achieving Specific, Tight-Binding to Folate Binding Protein. *Biomacromolecules* **2016**, *17* (3), 922–927.

(50) Hakem, I. F.; Leech, A. M.; Johnson, J. D.; Donahue, S. J.; Walker, J. P.; Bockstaller, M. R. Understanding Ligand Distributions in Modified Particle and Particlelike Systems. *J. Am. Chem. Soc.* **2010**, *132* (46), 16593–16598.

(51) Hakem, I. F.; Leech, A. M.; Bohn, J.; Walker, J. P.; Bockstaller, M. R. Analysis of Heterogeneity in Nonspecific PEGylation Reactions of Biomolecules. *Biopolymers* **2013**, *99* (7), 427–435.

(52) Larson, N.; Ghandehari, H. Polymeric Conjugates for Drug Delivery. *Chemistry of Materials*. American Chemical Society March 13, 2012, pp 840–853.

(53) Mintzer, M. A.; Simanek, E. E. Nonviral Vectors for Gene Delivery. *Chemical Reviews*. American Chemical Society February 11, 2009, pp 259–302.

(54) Mintzer, M. A.; Grinstaff, M. W. Biomedical Applications of Dendrimers: A Tutorial. *Chem. Soc. Rev.* **2011**, *40* (1), 173–190.

(55) Chen, M.; Yin, M. Design and Development of Fluorescent Nanostructures for Bioimaging. *Progress in Polymer Science*. Pergamon February 1, 2014, pp 365–395.

(56) Pansare, V. J.; Hejazi, S.; Faenza, W. J.; Prud'homme, R. K. Review of Long-Wavelength Optical and NIR Imaging Materials: Contrast Agents, Fluorophores, and Multifunctional Nano Carriers. *Chem. Mater.* **2012**, *24* (5), 812–827.

(57) He, C.; Hu, Y.; Yin, L.; Tang, C.; Yin, C. Effects of Particle Size and Surface Charge on Cellular Uptake and Biodistribution of Polymeric Nanoparticles. *Biomaterials* **2010**, *31* (13), 3657–3666.

(58) Philipp Seib, F.; Jones, A. T.; Duncan, R. Establishment of Subcellular Fractionation Techniques to Monitor the Intracellular Fate of Polymer Therapeutics I. Differential Centrifugation Fractionation B16F10 Cells and Use to Study the Intracellular Fate of HPMA Copolymer–doxorubicin. *J. Drug Target.* **2006**, *14* (6), 375–390.

(59) Yang, Y.; Sunoqrot, S.; Stowell, C.; Ji, J.; Lee, C.-W.; Kim, J. W.; Khan, S. A.; Hong, S. Effect of Size, Surface Charge, and Hydrophobicity of Poly(amidoamine) Dendrimers on Their Skin Penetration. *Biomacromolecules* **2012**, *13* (7), 2154–2162.

(60) Chen, L. C.; Lloyd, W. R.; Chang, C. W.; Sud, D.; Mycek, M. A. Fluorescence Lifetime Imaging Microscopy for Quantitative Biological Imaging. *Methods Cell Biol.* **2013**, *114*, 457–488.

(61) Ottani, V.; Martini, D.; Franchi, M.; Ruggeri, A.; Raspanti, M. Hierarchical Structures in Fibrillar Collagens. *Micron* **2002**, *33* (7–8), 587–596.

(62) Kadler, K. E.; Baldock, C.; Bella, J.; Boot-Handford, R. P. Collagen at a Glance. *Journal of cell science*. The Company of Biologists Ltd June 15, 2007, pp 1955–1958.

(63) Kadler, K. E.; Holmes, D. F.; Trotter, J. A.; Chapman, J. A. Collagen Fibril Formation. *Biochem. J.* **1996**, *316* (1), 1–11.

(64) Hulmes, D. J. S. Building Collagen Molecules, Fibrils, and Suprafibrillar Structures. In *Journal of Structural Biology*; Academic Press, 2002; Vol. 137, pp 2–10.

(65) Li, T.; Chang, S. W.; Rodriguez-Florez, N.; Buehler, M. J.; Shefelbine, S.; Dao, M.; Zeng, K. Studies of Chain Substitution Caused Sub-Fibril Level Differences in Stiffness and Ultrastructure of Wildtype and Oim/oim Collagen Fibers Using Multifrequency-AFM and Molecular Modeling. *Biomaterials* **2016**, *107*, 15–22.

(66) Hodge, A. J.; Petruska, J. A. *Recent Studies with the Electron Microscope on Ordered Aggregates of the Tropocollagen Molecule*; Academic Press: New York, 1963.

(67) Orgel, J. P. R. O.; Irving, T. C.; Miller, A.; Wess, T. J. Microfibrillar Structure of Type I Collagen in Situ. *Proc. Natl. Acad. Sci.* **2006**, *103* (24), 9001–9005.

(68) Miller, A.; Wray, J. S. Molecular Packing in Collagen. *Nature* **1971**, *230* (5294), 437–439.

(69) Hulmes, D. J. S.; Miller, A. Quasi-Hexagonal Molecular Packing in Collagen Fibrils [34]. *Nature*. Nature Publishing Group December 20, 1979, pp 878–880.

(70) Fraser, R. D. B.; MacRae, T. P.; Miller, A.; Suzuki, E. Molecular Conformation and Packing in Collagen Fibrils. *J. Mol. Biol.* **1983**, *167* (2), 497–521.

(71) Fraser, R. D. B.; MacRae, T. P.; Miller, A. Molecular Packing in Type I Collagen Fibrils. *J. Mol. Biol.* **1987**, *193* (1), 115–125.

(72) Trus, B. L.; Piez, K. A. Compressed Microfibril Models of the Native Collagen Fibril. *Nature* **1980**, *286* (5770), 300–301.

(73) Traub, W.; Piez, K. A. The Chemistry and Structure of Collagen. *Adv. Protein Chem.* **1971**, *25* (C), 243–352.

(74) Piez, K. A.; Trus, B. L. A New Model for Packing of Type-I Collagen Molecules in the Native Fibril. *Biosci. Rep.* **1981**, *1* (10), 801–810.

(75) Brodsky, B.; Eikenberry, E. F. [5] Characterization of Fibrous Forms of Collagen. *Methods Enzymol.* **1982**, *82*, 127–174.

(76) Hulmes, D. J.; Wess, T. J.; Prockop, D. J.; Fratzl, P. Radial Packing, Order, and Disorder in Collagen Fibrils. *Biophys. J.* **1995**, *68* (5), 1661–1670.

(77) Merzel, R. L.; Chen, J.-J.; Marsh, E. N. G.; Holl, M. M. B. Folate Binding protein—Outlook for Drug Delivery Applications. *Chinese Chem. Lett.* **2015**, *26* (4), 426–430.

(78) Pedersen, T.; Svendsen, I.; Hansen, S.; Holm, J.; Lyngbye, J. Aggregation of a Folate-Binding Protein from Cow's Milk. *Carlsberg Res. Commun.* **1980**, *45* (2), 161–166.

(79) Hansen, S. I.; Holm, J.; Lyngbye, J.; Pedersen, T. G.; Svendsen, I. Dependence of Aggregation and Ligand Affinity on the Concentration of the Folate-Binding Protein from Cow's Milk. *Arch. Biochem. Biophys.* **1983**, *226* (2), 636–642.

(80) Holm, J.; Schou, C.; Babol, L. N.; Lawaetz, A. J.; Bruun, S. W.; Hansen, M. Z.; Hansen, S. I. The Interrelationship between Ligand Binding and Self-Association of the Folate Binding Protein. The Role of Detergent?tryptophan Interaction. *Biochim. Biophys. Acta - Gen. Subj.* **2011**, *1810* (12), 1330–1339.

(81) Holm, J.; Lawaetz, A. J.; Hansen, S. I. Ligand Binding Induces a Sharp Decrease in Hydrophobicity of Folate Binding Protein Assessed by 1-Anilinonaphthalene-8-Sulphonate Which Suppresses Self-Association of the Hydrophobic Apo-Protein. *Biochem. Biophys. Res. Commun.* **2012**, *425* (1), 19–24.

(82) Christensen, U.; Holm, J.; Hansen, S. I. Stopped-Flow Kinetic Studies of the Interaction of Bovine Folate Binding Protein (FBP) and Folate. *Biosci. Rep.* **2006**, *26* (4), 291–299.

(83) Kaarsholm, N. C.; Kolstrup, A.-M.; Danielsen, S. E.; Holm, J.; Hansen, S. I. Ligand-Induced Conformation Change in Folate-Binding Protein. *Biochem. J.* **1993**, *292* (3), 921–925.

(84) Holm, J.; Babol, L. N.; Markova, N.; Lawaetz, A. J.; Hansen, S. I. The Interrelationship between Ligand Binding and Thermal Unfolding of the Folate Binding Protein. The Role of Self-Association and pH. *Biochim. Biophys. Acta - Proteins Proteomics* **2014**, *1844* (3), 512–519.

(85) Bruun, S. W.; Holm, J.; Hansen, S. I.; Jacobsen, S. Application of Near-Infrared and Fourier Transform Infrared Spectroscopy in the Characterization of Ligand-Induced Conformation Changes in Folate Binding Protein Purified from Bovine Milk: Influence of Buffer Type and pH. *Appl. Spectrosc.* **2006**, *60* (7), 737–746.

(86) Bruun, S. W.; Holm, J.; Hansen, S. I.; Andersen, C. M.; Norgaard, L.; Nørgaard, L. A Chemometric Analysis of Ligand-Induced Changes in Intrinsic Fluorescence of Folate Binding Protein Indicates a Link between Altered Conformational Structure and Physico-Chemical Characteristics. *Appl. Spectrosc.* **2009**, *63* (12), 1315–1322.

(87) Kur, E.; Mecklenburg, N.; Cabrera, R. M.; Willnow, T. E.; Hammes, A. LRP2 Mediates Folate Uptake in the Developing Neural Tube. *J. Cell Sci.* **2014**, *127* (10), 2261–2268.

(88) Birn, H.; Zhai, X. Y.; Holm, J.; Hansen, S. I.; Jacobsen, C.; Christensen, E. I.; Moestrup, S. K. Megalin Binds and Mediates Cellular Internalization of Folate Binding Protein. *FEBS J.* **2005**, *272* (17), 4423–4430.

(89) Christensen, E. I.; Birn, H. Megalin and Cubilin: Multifunctional Endocytic Receptors. *Nat. Rev. Mol. Cell Biol.* **2002**, *3* (4), 258–268.

(90) Rothberg, K. G.; Ying, Y. S.; Kolhouse, J. F.; Kamen, B. A.; Anderson, R. G. The Glycophospholipid-Linked Folate Receptor Internalizes Folate without Entering the Clathrin-Coated Pit Endocytic Pathway. *J. Cell Biol.* **1990**, *110* (3).

(91) Rothberg, K. G.; Ying, Y. S.; Kamen, B. A.; Anderson, R. G. Cholesterol Controls the Clustering of the Glycophospholipid-Anchored Membrane Receptor for 5-Methyltetrahydrofolate. *J. Cell Biol.* **1990**, *111* (6).

(92) Smart, E. J.; Mineo, C.; Anderson, R. G. W. Clustered Folate Receptors Deliver 5-Methyltetrahydrofolate to Cytoplasm of MA104 Cells. *J. Cell Biol.* **1996**, *134* (5), 1169–1177.

(93) Moradi, E.; Vllasaliu, D.; Garnett, M.; Falcone, F.; Stolnik, S. Ligand Density and Clustering Effects on Endocytosis of Folate Modified Nanoparticles. *RSC Adv.* **2012**, *2* (7), 3025.

(94) Weitman, S. D.; Weinberg, A. G.; Coney, L. R.; Zurawski, V. R.; Jennings, D. S.; Kamen, B. A. Cellular Localization of the Folate Receptor: Potential Role in Drug Toxicity and Folate Homeostasis. *Cancer Res.* **1992**, *52* (23), 6708–6711.

(95) Campbell, I. G.; Jones, T. A.; Foulkes, W. D.; Trowsdale, J. Folate-Binding Protein Is a Marker for Ovarian Cancer Folate-Binding Protein Is a Marker for Ovarian Cancer. *CANCER Res.* **1991**, *51* (33), 5329–5338.

(96) Weitman, S. D.; Lark, R. H.; Coney, L. R.; Fort, D. W.; Frasca, V.; Zurawski, V. R.; Kamen, B. A. Distribution of the Folate Receptor GP38 in Normal and Malignant Cell Lines and Tissues. *Cancer Res.* **1992**, *52* (12), 3396–3401.

(97) Ross, J. F.; Chaudhuri, P. K.; Ratnam, M. Differential Regulation of Folate Receptor Isoforms in Normal and Malignant Tissues in Vivo and in Established Cell Lines. Physiologic and Clinical Implications. *Cancer* **1994**, *73* (9), 2432–2443.

(98) Bandara, N. A.; Hansen, M. J.; Low, P. S. Effect of Receptor Occupancy on Folate Receptor Internalization. *Mol. Pharm.* **2014**, *11* (3), 1007–1013.

(99) Sega, E.; Low, P. Tumor Detection Using Folate Receptor-Targeted Imaging Agents. *Cancer Metastasis Rev.* **2008**, *27* (4), 655–664.

(100) Hilgenbrink, A. R.; Low, P. S. Folate Receptor-Mediated Drug Targeting: From Therapeutics to Diagnostics. *J. Pharm. Sci.* **2005**, *94* (10), 2135–2146.

(101) Bailey, L. B.; Gregory, J. F. Folate Metabolism and Requirements. *J. Nutr.* **1999**, *129* (4), 779–782.

(102) Kompis, I. M.; Islam, K.; Then, R. L. DNA and RNA Synthesis: Antifolates. *Chemical Reviews*. American Chemical Society 2005, pp 593–620.

(103) Chen, C.; Ke, J.; Zhou, X. E.; Yi, W.; Brunzelle, J. S.; Li, J.; Yong, E.-L.; Xu, H. E.; Melcher, K. Structural Basis for Molecular Recognition of Folic Acid by Folate Receptors. *Nature* **2013**, *500* (7463), 486–489.

(104) Wibowo, A. S.; Singh, M.; Reeder, K. M.; Carter, J. J.; Kovach, A. R.; Meng, W.; Ratnam, M.; Zhang, F.; Dann, C. E. Structures of Human Folate Receptors Reveal Biological Trafficking States and Diversity in Folate and Antifolate Recognition. *Proc. Natl. Acad. Sci.* **2013**, *110* (38), 15180–15188.

(105) Low, P. S.; Henne, W. A.; Doorneweerd, D. D. Discovery and Development of Folic-Acid-Based Receptor Targeting for Imaging and Therapy of Cancer and Inflammatory Diseases. *Acc. Chem. Res.* **2008**, *41* (1), 120–129.

(106) Low, P. S.; Kularatne, S. A. Folate-Targeted Therapeutic and Imaging Agents for Cancer. *Curr. Opin. Chem. Biol.* **2009**, *13* (3), 256–262.

(107) Leamon, C. P.; Reddy, J. A. Folate-Targeted Chemotherapy. *Adv. Drug Deliv. Rev.* **2004**, *56* (8), 1127–1141.

(108) Assaraf, Y. G.; Leamon, C. P.; Reddy, J. A. The Folate Receptor as a Rational Therapeutic Target for Personalized Cancer Treatment. *Drug Resistance Updates*. 2014.

(109) Sudimack, J.; Lee, R. J. Targeted Drug Delivery via the Folate Receptor. *Adv. Drug Deliv. Rev.* **2000**, *41* (2), 147–162.

(110) Wu, Y.; Guo, R.; Wen, S.; Shen, M.; Zhu, M.; Wang, J.; Shi, X. Folic Acid-Modified Laponite Nanodisks for Targeted Anticancer Drug Delivery. *J. Mater. Chem. B Mater. Biol. Med.* **2014**, *2* (42), 7410–7418.

(111) Hu, Y.; Wang, R.; Wang, S.; Ding, L.; Li, J.; Luo, Y.; Wang, X.; Shen, M.; Shi, X. Multifunctional Fe_3O_4 @ Au Core/shell Nanostars: A Unique Platform for Multimode Imaging and Photothermal Therapy of Tumors. *Sci. Rep.* **2016**, *6* (February), 28325.

(112) Cedervall, T.; Lynch, I.; Lindman, S.; Berggård, T.; Thulin, E.; Nilsson, H.; Dawson, K. A.; Linse, S. Understanding the Nanoparticle-Protein Corona Using Methods to Quantify Exchange Rates and Affinities of Proteins for Nanoparticles. *Proc. Natl. Acad. Sci. U. S. A.* **2007**, *104* (7), 2050–2055.

(113) Lynch, I.; Cedervall, T.; Lundqvist, M.; Cabaleiro-Lago, C.; Linse, S.; Dawson, K. A. The Nanoparticle–protein Complex as a Biological Entity; a Complex Fluids and Surface Science Challenge for the 21st Century. *Adv. Colloid Interface Sci.* **2007**, *134*, 167–174.

(114) Salvati, A.; Åberg, C.; Dawson, K. A.; Monopoli, M. P.; Åberg, C.; Salvati, A.; Dawson, K. A.; Aberg, C.; Salvati, A.; Dawson, K. A. Biomolecular Coronas Provide the Biological Identity of Nanosized Materials. *Nat. Nanotechnol.* **2012**, *7* (12), 779–786.

(115) Aggarwal, P.; Hall, J. B.; McLeland, C. B.; Dobrovolskaia, M. A.; McNeil, S. E. Nanoparticle Interaction with Plasma Proteins as It Relates to Particle Biodistribution, Biocompatibility and Therapeutic Efficacy. *Adv. Drug Deliv. Rev.* **2009**, *61* (6), 428–437.

(116) Owens III, D. E.; Peppas, N. A. Opsonization, Biodistribution, and Pharmacokinetics of Polymeric Nanoparticles. *Int. J. Pharm.* **2006**, *307* (1), 93–102.

(117) Walczyk, D.; Bombelli, F. B.; Monopoli, M. P.; Lynch, I.; Dawson, K. A. What the Cell "sees" in Bionanoscience. *J. Am. Chem. Soc.* **2010**, *132* (16), 5761–5768.

(118) Lynch, I.; Dawson, K. A. Protein-Nanoparticle Interactions. *Nano Today* **2008**, *3* (1–2), 40–47.

(119) Antony, A. C. Folate Receptors. *Annu. Rev. Nutr.* **1996**, *16* (1), 501–521.

(120) Matherly, L. H.; Hou, Z.; Deng, Y. Human Reduced Folate Carrier: Translation of Basic Biology to Cancer Etiology and Therapy. *Cancer Metastasis Rev.* **2007**, *26* (1), 111–128.

(121) Otsuka, H.; Nagasaki, Y.; Kataoka, K. PEGylated Nanoparticles for Biological and Pharmaceutical Applications. *Adv. Drug Deliv. Rev.* **2003**, *55* (3), 403–419.

(122) Chiti, F.; Dobson, C. M. Amyloid Formation by Globular Proteins under Native Conditions. *Nat. Chem. Biol.* **2009**, *5* (1), 15–22.

(123) Merzel, R. L.; Chen, J.; Frey, C.; Jones, Alexis, K.; Vartanian, M.; Ward, B. B.; Banaszak Holl, M. M. Folate Binding Protein Inhibits Tumor Growth. *Submitted*.

(124) Kratz, F.; Elsadek, B. Clinical Impact of Serum Proteins on Drug Delivery. *J. Control. Release* **2012**, *161* (2), 429–445.

(125) Elsadek, B.; Kratz, F. Impact of Albumin on Drug Delivery — New Applications on the Horizon. *J. Control. Release* **2012**, *157* (1), 4–28.

(126) Kratz, F. Albumin as a Drug Carrier: Design of Prodrugs, Drug Conjugates and Nanoparticles. *J. Control. Release* **2008**, *132* (3), 171–183.

(127) Merlot, A. M.; Kalinowski, D. S.; Richardson, D. R. Unraveling the Mysteries of Serum Albumin - More than Just a Serum Protein. *Front. Physiol.* **2014**, *5*, 1–7.

(128) Larsen, M. T.; Kuhlmann, M.; Hvam, M. L.; Howard, K. A. Albumin-Based Drug Delivery: Harnessing Nature to Cure Disease. *Mol. Cell. Ther.* **2016**, *4*, 3.

(129) Zhu, G.; Lynn, G. M.; Jacobson, O.; Chen, K.; Liu, Y.; Zhang, H.; Ma, Y.; Zhang, F.; Tian, R.; Ni, Q.; et al. Albumin/vaccine Nanocomplexes That Assemble in Vivo for Combination Cancer Immunotherapy. *Nat. Commun.* **2017**, *8* (1), 1954.

CHAPTER 2. Folate Binding Protein – Outlook for Drug Delivery Application

Reproduced with permission from:
Rachel L. Merzel [Wallace], Junjie Chen, E. Neil G. Marsh, and Mark M. Banaszak Holl
Chinese Chemical Letters **2015**, *26*, 426-430.

2.1. Abstract

Serum proteins represent an important class of drug and imaging agent delivery vectors. In this mini-review, key advantages of using serum proteins are discussed, followed by the particular advantages and challenges associated with employing soluble folate binding protein. In particular, approaches employing drugs that target folate metabolism are reviewed. Additionally, the slow-onset, tight-binding interaction of folate with folate binding protein and the relationship to a natural oligomerization mechanism is discussed. These unique aspects of folate binding protein suggest interesting applications for the protein as a vector for further drug and imaging agent development.

2.2. Introduction

In the body, drugs are transported in the blood where they can encounter over 100,000 proteins. The vast majority of these proteins are albumin (55%) and immunoglobulins (38%), such as IgG, IgA, and IgM, with smaller amounts of lipoproteins and transferrin.[1] All drugs or drug delivery scaffolds come into contact with these proteins, and the complexes formed often dominate the observed pharmacokinetics and biodistribution. These protein–drug interactions

have long played a significant role in small molecule drug design and are now recognized to greatly complicate the development of new drug delivery scaffolds in the field of nanomedicine.[2] One solution to this challenge is the judicious selection of an endogenous serum protein as the delivery scaffold for a given drug, imaging agent, or theranostic combining therapy and imaging.[3] Of the serum proteins, albumin has garnered the most attention and resulted in clinical applications.[4–6] There are currently seven clinically approved drugs or imaging agents employing the albumin scaffold, with applications including the treatment of metastatic breast cancer (Abraxane1) and diabetes (Levemir®, Victoza®) and imaging of cardiovascular and cerebral circulation (^{99m}Tc-Albures, Vasovist®) and lymph nodes (^{99m}Tc-Nanocol). Albumin is currently being explored for a variety of other applications, including theranostics [7,8]. Transferrin has also been explored for drug and imaging agent delivery; however, transferrin-based systems have yet to reach the clinic.[9] Both albumin (66.5 kDa) and transferrin (78 kDa) have molecular weights above the renal clearance threshold, contributing to long circulation times. Both proteins accumulate in malignant and inflamed tissue due to the enhanced permeation and retention (EPR) effect and internalize into cells via receptor specific endocytosis processes. These favorable properties, and the successes noted above, have prompted extensive research into both of these proteins, with over 4,000 papers published to date.

Despite these successes, the toxicity of small molecule cancer therapeutics remains a significant challenge. Off-target dosing (uptake of the cancer therapeutic by healthy cells as well as the tumor cells) leads to a wide range of side effects, sometimes necessitating sub-optimal dosing, which can lead to worse outcomes for patients. To address this problem, researchers have worked to develop targeted therapeutics that deliver drug to tumor cells while avoiding healthy cells. Folic acid (FA) is a widely studied targeting ligand for both molecular and nanoscale

cancer therapies because folate receptors (FRs) are overexpressed on the surfaces of the cancer cell membranes[10,11] Folate is necessary for thymidine biosynthesis, and hence for de-novo DNA biosynthesis, and so rapidly dividing cancer cells increase the concentration of FRs on plasma membrane surfaces. To date, seven FA-targeted cancer therapeutics have advanced to clinical trials, but none have progressed to full clinical development. Even with targeted drug delivery agents, dose-limiting toxicity due to uptake by healthy cells remains a problem. Additionally, the expression of FRs on the surfaces of tumor cells is highly variable both from individual to individual and within a given cancer type. The folate metabolic pathway is also the target for inhibitors of dihydrofolate reductase (DHFR).[12–15] Clinically approved DHFR-inhibitor drugs are used to treat a variety of cancers and autoimmune diseases (methotrexate, pemetrexed), bacterial infections (trimetrexate, piritrexim), and malaria (pyrimethamine).

Can the substantial advantages of employing an endogenous serum protein for drug delivery be combined with drugs designed to target and inhibit the folate metabolic pathway? This minireview discusses recent advances in the understanding of soluble folate binding protein (FBP) and possible applications of this protein for drug delivery. First, we review the structure and hypothesized functions for FBP, including possible roles in folate metabolism. The approaches for isolation of the protein are also discussed. Second, we examine recent data regarding the detailed binding mechanism of FBP with FA, FA-conjugates, and antifolate (aFA)-conjugates. Third, we discuss the outlook for folate binding protein as a transport agent for therapeutics and imaging agents, including advantages and challenges of this approach.

2.3. The structure, function, and isolation of folate binding protein

Folate binding protein (FBP) is a 30 kDa glycoprotein containing 222 amino acids present in 1–2 nmol/L concentrations in human serum and other body fluids and 100 nmol/L

concentrations in milk.[16–20] The functions of FBP in the body are not well understood, but it has been hypothesized to regulate the trafficking and homeostasis of folate, protect against folate degradation, and shield against bacterial utilization of folate. FBP is closely related to two isoforms of membrane-bound FRs: FRa and FR-b, both of which are connected to plasma cell membranes via glycosylphosphatidylinositol (GPI) anchors.[17,21] A third isoform, FR-g, is a secreted protein and lacks the signal for modification with a GPI anchor. Soluble FBP inherently lacks a GPI modification. X-ray crystal structures of the FA-bound protein were recently reported (Figure 2.1).[14,15] FBP is obtained on the gram scale by purification of whey protein.[20,22–26], although engineered proteins have been expressed in Chinese Hamster Ovary (CHO) cells.[14]

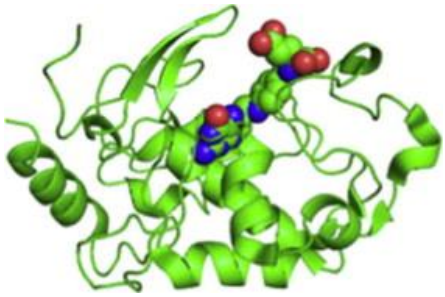

Figure 2.1. The X-ray structure of folate receptor α with folic acid in the binding site.

Glycosylation of the protein is not required for the FA-binding activity of soluble FBP.[27–29] The quaternary structure of FBP changes as a function of FA-binding, consistent with a slow-onset, tight-binding interaction. At micromolar concentrations, the binding of FA to FBP also induces a self-assembly/aggregation process that has been examined *in vitro*.[30,31] Interestingly, the aggregation of FR-a in the cell membrane has been shown to be an integral part of FA-binding and cellular internalization.[32,33] Recently, it was discovered that FBP internalizes into cells via a megalin-mediated endocytosis pathway,[34] suggesting the possibility of megalin playing a direct role in folate metabolism. This observation is particularly interesting for the use of FBP in chemotherapeutic targeting.

2.4. The binding mechanism of folic acid to folate binding protein

Folic acid binds to FBP via a slow-onset, tight-binding mechanism (Equation 1).[35] The initial FBP interaction with folic acid is followed by a reorganization of the protein structure, leading to the observed nanomolar FA–FBP binding constant. The induction of structural change in the FBP upon binding FA is characterized by quenching of the inherent tryptophan fluorescence in FBP [30,36]. The change in structure is hypothesized to lead to reduction of the number hydrophobic residues on the protein surface, resulting in a FA-ligand induced aggregation of the protein.[37,38]

$$\text{FA} + \text{FBP} \underset{k_{-1}}{\overset{k_1}{\rightleftharpoons}} \text{FA—FBP} \underset{k_{-2}}{\overset{k_2}{\rightleftharpoons}} \text{FA—FBP}^* \qquad \text{Equation 1}$$

At pH 7.4, the degree of aggregation (*n*) is dependent on FBP concentration. As measured by gel-filtration, at concentrations of 1–10 nmol/L, FBP–FA is monomeric, whereas a tetramer $(FBP–FA)_4$ and a nonamer $(FBP–FA)_9$, were observed for concentrations of 1.0 mmol/L and 10 mmol/L, respectively. Ultracentrifugation experiments indicated that oligomers as high as $(FBP–FA)_{30}$ were present for 100 mmol/L solutions of FBP. High performance liquid chromatography (HPLC) and sodium dodecyl sulfate-poly(acrylamide) gel electrophoresis (SDS–PAGE) both indicate the formation of three new species upon FA binding to FBP.[39] The HPLC studies are particularly interesting as they provide a ready method for quantifying the relative amounts of each species present in solution. More work is needed to understand how these three species relate to tetramers, nonamers, and other species reported in the fluorescence, gel-filtration, and ultracentrifugation studies. These data indicate that a monomer structure is anticipated to be the dominant form of the protein in most biological tissues where the FBP concentration is 1–2 nmol/L; however, these reported oligomerization properties may play an important role in the binding and aggregation of FR-a in the cell membrane prior to internalization. A stopped-flow

kinetic study examined the relative binding strengths of folic acid to FBP and to albumin.[36] This comparison is of particular interest since albumin has a concentration of 0.6–0.7 mmol/L in blood, or a factor 500,000 more concentrated than FBP. FBP binds FA tightly with a K_d < 1.3 nmol/L, whereas albumin exhibits much weaker binding with a K_d of 21 2.1 mmol/L. For human plasma, this indicates that FBP will be fully bound by folate, with the remaining 7– 30 nmol/L of folate present more weakly associated with albumin. The values of K_d suggest that about 3% of folate in human serum will be present in free form. Lowering the pH from 7.4 to the more acidic values commonly found in endosomes activates deoligomerization of the FBP and release of the bound FA.

2.5. The binding mechanism of folic acid conjugates to folate binding protein

There has been a substantial amount of interest in using FA-conjugates for targeted drug and imaging agent delivery[10,11,40–50] and for targeted polymer vectors.[51–55] Based on the FBP and albumin concentrations present in human serum,[36] FA-conjugates employed at a micromolar concentration would be expected to interact extensively with albumin as well as to saturate all available soluble FBP. The rate of binding to FBP already present in serum would be determined by the k_{off} of existing bound FA and the production of new FBP. This suggests that both FBP and albumin could play useful roles in biodistribution of FA-conjugates; however, this aspect of their *in vivo* delivery has been poorly explored to date. Generally, it has been presumed that small molecule conjugates will bind with equal or lesser affinity to FBP (or FR-α) as compared to FA. HPLC and SDS–PAGE assessment of the interaction of FBP with FA-conjugates of generation 5 poly(amidoamine) (G5 PAMAM) dendrimer indicated the formation of complexes and that these complexes were stable to the addition of further free of FA.[39] It has been a goal to design polymer conjugates that have increased avidity for membrane bound FR-α due to

multivalent binding,[52] and surface-bound FBP has been used to model FR-α.[53,56] The surface plasmon resonance (SPR) technique used to quantify binding in many of these studies detected an increase in binding with the number of FA attached to the polymer, as well as evidence of a tightly bound fraction that did not desorb over ~5–10 min of the experiment. This behavior was attributed to multivalency, with increasing numbers of FA giving greater avidity. Unfortunately, SPR, which is only sensitive to changes in surface mass, is unable to detect the changes in protein structure that occur during a slow-onset, tight-binding mechanism. Subsequent studies employing G5 PAMAM dendrimer containing just one FA per polymer particle exhibited the same irreversible binding to the FBP that had been ascribed to 2–4 FA conjugated to a single dendrimer multivalently binding to 2–4 FBP.[57] In addition, it was demonstrated that the increase in binding constant was proportional to total FA concentration. These data led to a closer analysis of the work of Holm, Hansen *et al.* and the assignment of a slow-onset, tight binding mechanism for the interaction of FA-conjugates of G5 PAMAM with FBP, as illustrated in Figure 2.2. SPR binding studies of methotrexate-conjugates of G5 PAMAM monomer and dimer species were also consistent with this binding mechanism.[58] Additional experiments are needed to fully explore the nature of the polymer structure, molecular weight, and topological constraints associated with these FBP interactions. Namely, this type of binding can only be achieved if the polymer does not bind to FBP prior to the binding of FA; however, following FA-binding and the rearrangement of the protein surface, it must be

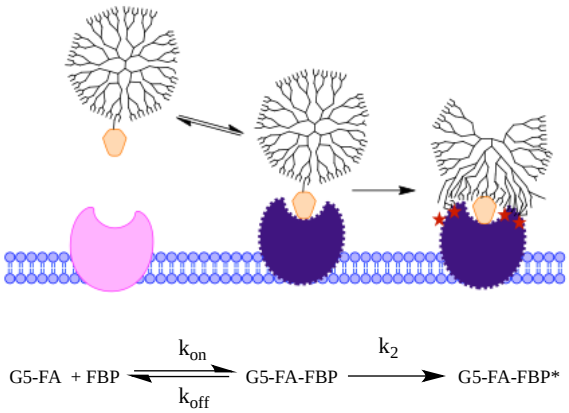

favorable for a network of van der Waals interactions to form between the polymer and the protein.

2.6. Outlook for folate binding protein as a transport agent for therapeutics and imaging agents: Advantages and challenges

Serum binding proteins offer an important vector for the transport of drugs and imaging agents.[3] Albumin has the advantages of being the most common serum protein (0.6–0.7 mmol/L) and is promiscuous in terms of binding to a wide range of hydrophobic molecules.[3–6]. It is also large enough at 66.5 kDa to avoid renal clearance. By way of contrast, FBP is present at just 1–2 nmol/L in blood and at 30 kDa is cleared by the kidney; however, these differences offer an interesting opportunity to engineer FBP for drug delivery. First, if longer circulation times are desired, the natural oligomerization mechanism of FBP provides an opportunity to form dimer, tetramers, or larger species that will be above the renal threshold for clearance. Can the degree of oligomerization be controlled by the binding strength between FBP and the FA-conjugate? The interaction with FBP provides a pathway to avoid renal clearance for a wide variety of FA-conjugated materials. Indeed, such an oligomerization process may already be occurring *in vivo*. Second, the much lower plasma concentration of FBP may be coupled to a more specific, and more active, endocytosis mechanism than the pathway(s) employed by albumin. The recent discovery of a megalin-mediated endocytosis pathway for FBP [34] is very promising, as this could provide a route for the uptake of the FBP/FA-conjugate complexes. Again, it is possible such a pathway is already followed *in vivo* by FA-conjugates and/or that additional studies could further develop this mechanism as an important approach to selective uptake. Third, FBP, as part of the folic acid metabolic pathway, is mechanistically linked to a highly successful class of drugs, namely the aFAs, which include methotrexate, pemetrexed, raltitrexed, trimetrexate, and pyrimethamine (Figure 2.3).[12,59] By developing methods to strongly bind aFA-conjugates to FBP

prior to injection into the bloodstream, it may be possible to increase the specificity of targeting of the antifolate drug as a chemotherapeutic agent. Like albumin, FBP oligomers should passively target the tumor *via* the EPR effect.[3] Then, up-regulated megalin receptors, which have been observed in the T-47D and MCF-7 breast cancer lines[60] and in prostate cancer tissue,[61] can play a role in active uptake of the FBP. It has already been demonstrated that megalin up-regulation can be employed for targeted delivery using apolipoproteins.[60] Based on these literature reports, targeting of prostate and breast cancer using FBP appears to be a particularly promising area to explore.

In addition to cancer applications, antifolates have also been employed for control of malaria. Indeed, proguanil and pyrimethamine were the drugs of choice prior to development of widespread resistance to this therapy.[62,63] Toxicity and efficacy concerns with the artemisinin-based combination therapies have caused pyrimethamine-based therapy to remain the best option for intermittent preventative treatment for pregnant women and infants. The high-level of expression of megalin in the infant intestine suggests that FBP-based vectors may be a generally effective approach to drug delivery. Pre-binding the drug to FBP may assist in both uptake and subsequent transport of the drug.

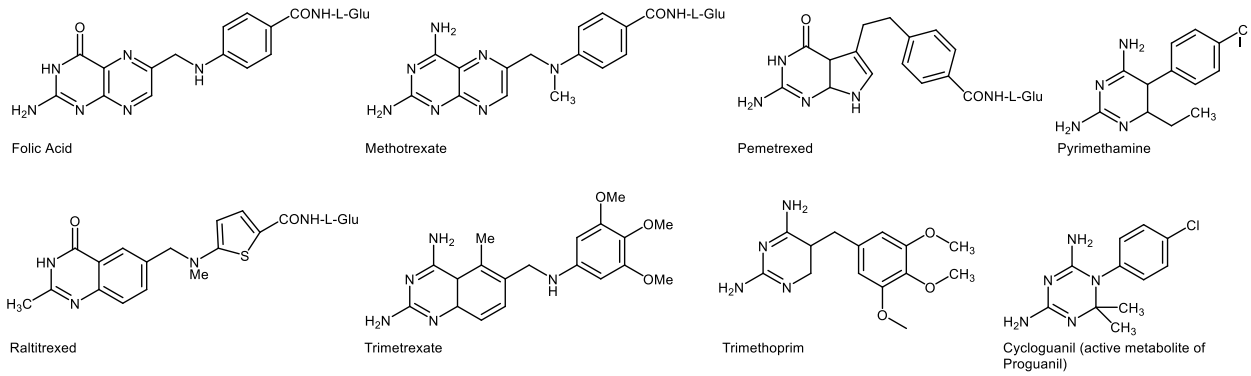

Figure 2.2. The structures of folic acid and a variety of antifolates

2.7. Summary

Serum binding proteins show exceptional promise for drug and imaging agent delivery applications,[3] and numerous successful therapeutics based on albumin are currently in the clinic.[4–6] FBP, another serum protein, is of particular interest because of its role in folate metabolism and the natural oligomerization process that occurs when FA binds to FBP. The FA–FBP interaction has been shown to proceed through a slow-onset, tight-binding mechanism leading to changes in the quaternary structure of the protein. In addition, the pH dependence of both FA-binding and oligomerization contribute to a natural release mechanism for materials inside the cell. These three facets of this protein's behavior offer a powerful set of tools for designing the next generation drug and imaging agent delivery materials.

2.8. References

1. Shen, Y.; Jacobs, J. M.; Camp, D. G.; Fang, R.; Moore, R. J.; Smith, R. D.; Xiao, W.; Davis, R., W.; Tompkins, R. G. Ultra-High-Efficiency Strong Cation Exchange LC/RPLC/MS/MS for High Dynamic Range Characterization of the Human Plasma Proteome. *Anal. Chem.* **2004**, *76*, 1134-1144.

2. Lynch, I.; Dawson, K. A. Protein-Nanoparticle Interactions. *NanoToday* **2008**, *3*, 40-47.

3. Kratz, F.; Elsadek, B. Clinical impact of serum proteins on drug delivery. *J. Controlled Release* **2012**, *161*, 429-445.

4. Merlot, A. M.; Kalinowski, D. S.; Richardson, D. R. Unraveling the mysteries of serum albumin - more than just a serum protein. *Frontiers in Physiology* **2014**, *5*, 1-7.

5. Elsadek, B.; Kratz, F. Impact of albumin on drug delivery - New applications on the horizon. *Journal of Controlled Release* **2012**, *157*, 4-28.

6. Kratz, F. Albumin as a drug carrier: Design of prodrugs, drug conjugates and nanoparticles. *Journal of Controlled Release* **2008**, *132*, 171-183.

7. Chen, Q.; Liang, C.; Wang, X.; He, J. K.; Li, Y. G.; Liu, Z. An albumin-based theranostic nano-agent for dual-modal imaging guided photothermal therapy to inhibit lymphatic metastasis of cancer post surgery. *Biomaterials* **2014**, *35*, 9355-9362.

8. Chen, Q.; Wang, C.; Zhan, Z. X.; He, W. W.; Cheng, Z. P.; Li, Y. Y.; Liu, Z. Near-infrared dye bound albumin with separated imaging and therapy wavelength channels for imaging-guided photothermal therapy. *Biomaterials* **2014**, *35*, 8206-8214.

9. Luck, A. N.; Mason, A. B. Structure and dynamics of drug carriers and their interaction with cellular receptors: Focus on serum transferrin. *Adv. Drug Delivery Rev.* **2013**, *65*, 1012-1019.

10. Leamon, C. P. Folate-targeted drug strategies for the treatment of cancer. *Current Opinion in Investigational Drugs* **2008**, *9*, 1277-1286.

11. Low, P. S.; Henne, W. A.; Doorneweerd, D. D. Discovery and development of folic-acid-based receptor targeting for Imaging and therapy of cancer and inflammatory diseases. *Acc. Chem. Res.* **2008**, *41*, 120-129.

12. Kompis, I. M.; Islam, K.; Then, R. L. DNA and RNA synthesis: Antifolates. *Chem. Rev.* **2005**, *105*, 593-620.

13. Sharma, M.; Chauhan, P. M. S. Dihydrofolate reductase as a therapeutic target for infectious diseases: opportunities and challenges. *Future Medicinal Chemistry* **2012**, *4*, 1335-1365.

14. Wibowo, A. S.; Singh, M.; Reeder, K. M.; Carter, J. J.; Kovach, A. R.; Meng, W. Y.; Ratnam, M.; Zhang, F. M.; Dann, C. E. Structures of human folate receptors reveal biological trafficking states and diversity in folate and antifolate recognition. *Proc. Natl. Acad. Sci. USA* **2013**, *110*, 15180-15188.

15. Chen, C.; Ke, J.; Zhou, X. E.; Yi, W.; Brunzelle, J. S.; Li, J.; Young, E.-L.; Xu, H. E.; Melcher, K. Structural basis for molecular recognition of folic acid by folate receptors. *Nature* **2013**, *500*, 486-490.

16. Ghitis, J. Folate Binding in Milk. *Am. J. Clin. Nutr.* **1967**, *20*, 1-4.

17. Hoier-Madsen, M.; Holm, J.; Hansen, S. I. alpha isoforms of soluble and membrane-linked folate-binding protein in human blood. *Bioscience Reports* **2008**, *28*, 153-160.

18. Antony, A. C. Folate receptors. *Annual Review of Nutrition* **1996**, *16*, 501-521.

19. Henderson, G. B. Folate Binding Proteins. *Annu. Rev. Nutr.* **1990**, *10*.

20. Holm, J.; Babol, L. N.; Markova, N.; Lawaetz, A. J.; Hansen, S. I. The interrelationship between ligand binding and thermal unfolding of the folate binding protein. The role of self-association and pH. *Biochimica Et Biophysica Acta-Proteins and Proteomics* **2014**, *1844*, 512-519.

21. Kamen, B. A.: Folate Receptors and Therapeutic Applications. In *Targeted Drug Strategies for Cancer and Inflammation*; Jackman, A. L., Leamon, C. P., Eds.; Springer, 2011.

22. Nygren-Babol, L.; Jagerstad, M. Folate-Binding Protein in Milk: A Review of Biochemistry, Physiology, and Analytical Methods. *Critical Reviews in Food Science and Nutrition* **2012**, *52*, 410-425.

23. Grossowicz, N. Purification and properties of the folate-binding protein. *Methods Enzymol.* **1980**, *66*.

24. Treloar, T.; Grieve, P. A.; Nixon, P. F. One-step Affinity Purification of Folate-Binding Protein, a minor whey protein. *Aust. J. Dairy Tech.* **2000**, *59*, 96.

25. Svendsen, I.; Martin, B.; Pedersen, T. G.; Hansen, S. I.; Holm, J.; Lyngbye, J. Isolation And Characterization Of The Folate-Binding Protein From Cows Milk. *Carlsberg Research Communications* **1979**, *44*, 89-99.

26. Svendsen, I. B.; Hansen, S. I.; Holm, J.; Lyngbye, J. The Complete Amino-Acid-Sequence Of The Folate-Binding Protein From Cows Milk. *Carlsberg Research Communications* **1984**, *49*, 123-131.

27. Roberts, S. J.; Petropavlovskaja, M.; Chung, K. N.; Knight, C. B.; Elwood, P. C. Role of individual N-linked glycosylation sites in the function and intracellular transport of the human alpha folate receptor. *Archives of Biochemistry and Biophysics* **1998**, *351*, 227-235.

28. Ratnam, M.; Marquardt, H.; Duhring, J. L.; Freisheim, J. H. Homologous membrane folate binding-proteins in human-placenta - cloning and sequence of a cDNA. *Biochemistry* **1989**, *28*, 8249-8254.

29. Luhrs, C. A. The Role Of Glycosylation In The Biosynthesis And Acquisition Of Ligand-Binding Activity Of The Folate-Binding Protein In Cultured Kb Cells. *Blood* **1991**, *77*, 1171-1180.

30. Bruun, S. W.; Holm, J.; Hansen, S. I.; Andersen, C. M.; Norgaard, L. A Chemometric Analysis of Ligand-Induced Changes in Intrinsic Fluorescence of Folate Binding Protein Indicates a Link Between Altered Conformational Structure and Physico-Chemical Characteristics. *Appl. Spectrosc.* **2009**, *63*, 1315-1322.

31. Holm, J.; Lawaetz, A. J.; Hansen, S. I. Ligand binding induces a sharp decrease in hydrophobicity of folate binding protein assessed by 1-anilinonaphthalene-8-sulphonate which suppresses self-association of the hydrophobic apo-protein. *Biochem. Biophys. Res. Commun.* **2012**, *425*, 19-24.

32. Smart, E. J.; Mineo, C.; Anderson, R. G. W. Clustered folate receptors deliver 5-methyltetrahydrofolate to cytoplasm of MA104 cells. *Journal of Cell Biology* **1996**, *134*, 1169-1177.

33. Moradi, E.; Vllasaliu, D.; Garnett, M.; Falcone, F.; Stolnik, S. Ligand density and clustering effects on endocytosis of folate modified nanoparticles. *RSC Adv.* **2012**, *2*, 3025-3033.

34. Birn, H.; Zhai, X. Y.; Holm, J.; Hansen, S. I.; Jacobsen, C.; Christensen, E. I.; Moestrup, S. K. Megalin binds and mediates cellular internalization of folate binding protein. *Febs Journal* **2005**, *272*, 4423-4430.

35. Sculley, M. J.; Morrison, J. F.; Cleland, W. W. Slow-binding inhibition: The general case. *Biochim. Biophys. Acta* **1996**, *1298*, 78-86.

36. Christensen, U.; Holm, J.; Hansen, S. I. Stopped-flow kinetic studies of the interaction of bovine folate binding protein (FBP) and folate. *Bioscience Reports* **2006**, *26*, 291-299.

37. Hansen, S. I.; Holm, J.; Lyngbye, J.; Pedersen, T. G.; Svendsen, I. Dependence Of Aggregation And Ligand Affinity On The Concentration Of The Folate-Binding Protein From Cows Milk. *Arch. Biochem. Biophys.* **1983**, *226*, 636-642.

38. Pedersen, T. G.; Svendsen, I. B.; Hansen, S. I.; Holm, J.; Lyngbye, J. Aggregation Of A Folate-Binding Protein From Cows Milk. *Carlsberg Res. Comm.* **1980**, *45*, 161-166.

39. Shi, X.; Bi, X.; Ganser, T. R.; Hong, S.; Myc, L. A.; Desai, A.; Banaszak Holl, M. M.; Baker, J. R. HPLC Analysis of functionalized poly(amidoamine) dendrimers and the interaction between a folate-dendrimer conjugate and folate binding protein. *The Analyst* **2006**, *131*, 842-848.

40. Kelderhouse, L. E.; Chelvam, V.; Wayua, C.; Mahalingam, S.; Poh, S.; Kularatne, S. A.; Low, P. S. Development of Tumor-Targeted Near Infrared Probes for Fluorescence Guided Surgery. *Bioconjugate Chem.* **2013**, *24*, 1075-1080.

41. van Dam, G. M.; Themelis, G.; Crane, L. M. A.; Harlaar, N. J.; Pleijhuis, R. G.; Kelder, W.; Sarantopoulos, A.; de Jong, J. S.; Arts, H. J. G.; van der Zee, A. G. J.; Bart, J.; Low, P. S.; Ntziachristos, V. Intraoperative tumor-specific fluorescence imaging in ovarian cancer by folate receptor-alpha targeting: first in-human results. *Nature Medicine* **2011**, *17*, 1315-U1202.

42. Kennedy, M. D.; Jallad, K. N.; Thompson, D. H.; Ben-Amotz, D.; Low, P. S. Optical imaging of metastatic tumors using a folate-targeted fluorescent probe. *Journal of Biomedical Optics* **2003**, *8*, 636-641.

43. Low, P. S.; Kularatne, S. A. Folate-targeted therapeutic and imaging agents for cancer. *Curr. Opin. Chem. Bio.* **2009**, *13*, 256-262.

44. Chen, Q.; Li, K. A.; Wen, S. H.; Liu, H.; Peng, C.; Cai, H. D.; Shen, M. W.; Zhang, G. X.; Shi, X. Y. Targeted CT/MR dual mode imaging of tumors using multifunctional dendrimer-entrapped gold nanoparticles. *Biomaterials* **2013**, *34*, 5200-5209.

45. Li, J. C.; Zheng, L. F.; Cai, H. D.; Sun, W. J.; Shen, M. W.; Zhang, G. X.; Shi, X. Y. Polyethyleneimine-mediated synthesis of folic acid-targeted iron oxide nanoparticles for in vivo tumor MR imaging. *Biomaterials* **2013**, *34*, 8382-8392.

46. Wang, Y.; Guo, R.; Cao, X.; Shen, M.; Shi, X. Encapsulation of 2-methoxyestradiol within multifunctional poly(amidoamine) dendrimers for targeted cancer therapy. *Biomaterials* **2011**, *2011*, 3322-3329.

47. Chen, P.; Qin, J.; Zhou, B.; Chen, Q.; Shen, M.; Zhu, M.; Lu, X.; Shi, X. Targeted tumor CT imaging using folic acid-modified PEGylated dendrimer-entrapped gold nanoparticles. *Polym. Chem.* **2013**, *4*, 4412-4424.

48. Lui, H.; Xu, Y.; Wen, S.; Q., C.; Zheng, L.; Shen, M.; Zhao, J.; Zhang, G.; Shi, X. Targeted Tumor Computed Tomagraphy Imaging Using Low-Generation Dendrimer-Stabilized Gold Nanoparticles. *Chem. Eur. J.* **2013**, *19*, 6409-6416.

49. Wen, S.; Liu, H.; Cai, H.; Shen, M.; Shi, X. Targeted and pH-Responsive Delivery of Doxorubicin to Cancer Cells Using Multifunctional Dendrimer-Modified Multi-Walled Carbon Nanotubes. *Adv. Healthcare Mater.* **2013**, *2*, 1267-1276.

50. Liang, X. H.; Sun, Y.; Liu, L. S.; Zhao, Y. Y.; Hu, X. Y.; Fan, J. Regioselective synthesis and initial evaluation of a folate receptor targeted rhaponticin prodrug. *Chin. Chem. Lett.* **2012**, *23*, 1133-1136.

51. Gabizon, A.; Horowitz, A. T.; Goren, D.; Tzemach, D.; Mandelbaum-Shavit, F.; Qazen, M. M.; Zalipsky, S. Targeting folate receptor with folate linked to extremities of poly(ethylene glycol)-grafted liposomes: In vitro studies. *Bioconjugate Chem.* **1999**, *10*, 289-298.

52. Kukowska-Latallo, J. F.; Candido, K. A.; Cao, Z. Y.; Nigavekar, S. S.; Majoros, I. J.; Thomas, T. P.; Balogh, L. P.; Khan, M. K.; Baker, J. R. Nanoparticle targeting of anticancer drug improves therapeutic response in animal model of human epithelial cancer. *Cancer Res.* **2005**, *65*, 5317-5324.

53. Silpe, J. E.; Sumit, M.; Thomas, T. P.; Huang, B.; Kotlyar, A.; van Dongen, M.; Banaszak Holl, M. M.; Orr, B. G.; Choi, S. K. Avidity Modulation of Folated-Targeted Multivalent Dendrimers for Evaluating Biophysical Models of Cancer Targeting Nanoparticles. *ACS Chem. Biol.* **2013**, *8*, 2063-2071.

54. Zhang, Y.; Xu, M.-Y.; Jiang, T.-K.; Huang, W.-Z.; Wu, J.-Y. Low generational polyamidoamine dendrimers to enhance the solubiity of folic acid: a "dendritic effect" investigation. *Chin. Chem. Lett.* **2014**, *25*, 815-818.

55. Sunoqrot, S.; Bugno, J.; Lantvit, D.; Burdette, J.E.; Hong, S.; Prolonged blood circulation and enhanced tumor accumulation of folate-targeted dendrimer-polymer hybrid nanoparticles. *J. Controlled Release* **2014**, *191*, 115-122.

56. Hong, S.; Leroueil, P. R.; Majoros, I.; Orr, B. G.; Baker, J. R.; Banaszak Holl, M. M. The Binding Avidity of a Nanoparticle-Based Multivalent Targeted Drug Delivery Platform. *Chemistry and Biology* **2007**, *14*, 107-115.

57. van Dongen, M. A.; Silpe, J. E.; Dougherty, C. A.; Kanduluru, A. K.; Choi, S. K.; Orr, B. G.; Low, P. S.; Banaszak Holl, M. M. Avidity Mechanism of Dendrimer-Folic Acid Conjugates. *Molec. Pharm.* **2014**, *11*, 1696-1706.

58. van Dongen, M. A.; Rattan, R.; Silpe, J. E.; Dougherty, C. A.; Michmerhuizen, N.; Van Winkle, M.; Huang, B.; Choi, S. K.; Sinniah, K.; Orr, B. G.; Banaszak Holl, M. M.

Poly(amidoamine) Dendrimer-Methotrexate Conjugates: The Mechanism of Interaction with Folate Binding Protein. *Mol. Pharmaceutics* **2014**, *11*, 4049-4058.

59. McGuire, J. J. Anticancer Antifolates: Current Status and Future Directions. *Curr. Pharm. Design* **2003**, *9*, 2593-2613.

60. Xue, H. Y.; Wong, H. L. Targeting megalin to enhance delivery of anti-clusterin small-interfering RNA nanomedicine to chemo-treated breast cancer. *Eur. J. Pharm. Biopharm.* **2012**, *81*, 24-32.

61. Holt, S. K.; Karyadi, D. M.; Kwon, E. M.; Stanford, J. L.; Nelson, P. S.; Ostrander, E. A. Association of Megalin genetic polymorphisms with prostate cancer risk and prognosis. *Clinical Cancer Research* **2008**, *14*, 3823-3831.

62. Muller, I. B.; Hyde, J. E. Antimalarial drugs: modes of action and mechanisms of parasite resistance. *Future Microbiology* **2010**, *5*, 1857-1873.

63. Schlitzer, M. Malaria chemotherapeutics part 1: History of antimalarial drug development, currently used therapeutics, and drugs in clinical development. *ChemMedChem* **2007**, *2*, 944-986.

CHAPTER 3. Folate Binding Protein: Therapeutic Natural Nanotechnology for Folic Acid, Leucovorin, and Methotrexate

Reproduced with permission of The Royal Society of Chemistry from:
Rachel L. Merzel [Wallace], Sarah M. Boutom, Junjie Chen, Carolina Frey, Kerby Shedden, E. Neil G. Marsh, and Mark M. Banaszak Holl
Nanoscale **2017**, *9*, 2603-2615.

3.1. Introduction

Serum proteins are known to interact with small molecules and nanoparticles in blood and therefore play a critical role in the transport, cellular uptake, and efficacy of both small molecule and nanoparticle drugs.[1,2] Human blood serum has over 100,000 proteins, which makes predicting the interactions between serum proteins and drugs, and the resulting biological effects, a challenging task. In many cases, drug delivery researchers try to shield small molecule, nanoparticle, or protein-based drugs from serum proteins using a poly(ethylene glycol) (PEG) shell in order to avoid the formation of protein coronas that have a deleterious effect on the biodistribution and efficacy of the drug.[3,4] However, in this study, we have sought to exploit and understand the interaction of a particular serum protein, folate binding protein (FBP), with folic acid (vitamin B9 and cancer targeting agent). We have also explored the interactions of FBP with methotrexate (an antifolate drug) and leucovorin (a vitamer of folic acid) (Figure 3.1). Our results have implications for dosing schedules and new drug development.[5]

Generally, the aggregation of proteins is associated with disease – the most commonly cited example of this is amyloid-β deposits linked with Alzheimer's disease.[6] Recently, however, we have probed the formation of natural protein nanoparticles that are likely involved in transporting small molecules in the blood stream of healthy individuals. We have demonstrated that folate binding protein (FBP) exhibits concentration- and ligand-dependent aggregation into nanoparticles at human blood serum concentrations.

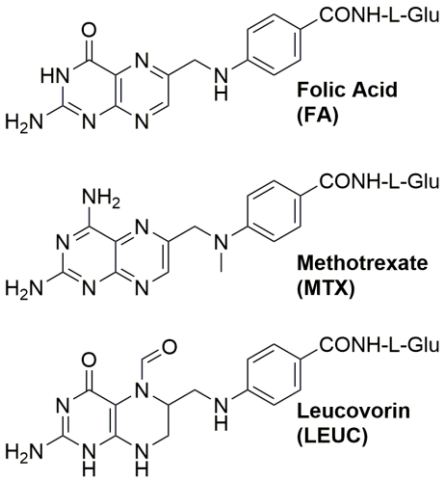

Figure 3.1. The structures of folic acid (FA, vitamin B9), methotrexate (MTX), and leucovorin (LEUC). MTX is used for the treatment of cancer and rheumatoid arthritis. LEUC is administered for "folic acid rescue" after cancer treatment with MTX in order to reduce adverse events in patients due to the severe toxicity of the drug.

FBP is particularly interesting because it has been hypothesized to regulate the trafficking and homeostasis of folic acid (FA), protect against FA degradation, and shield against bacterial utilization of FA.[7–11] FA binds very strongly to FBP with a nanomolar dissociation constant, which is postulated to be critical for cellular uptake because FA is not synthesized by animals but must be obtained in the diet.[12–17] FA, is required for the synthesis of DNA and plays a key role in neural tube development and brain function in fetuses and infants.[18–20] Quickly dividing cancer cells require large amounts of FA for DNA synthesis, and as a result, the cancer cells display upregulation of folate receptors (FRs) on their outer cell membranes. As such, FA has been extensively used as a targeting ligand for drugs and imaging agents.[12,16,17] This strategy of making FA-drug and FA-dye conjugates has had demonstrated success in vitro, but none of these systems have successfully advanced through clinical trials.

Beyond FA-targeted drug delivery systems, FBP is of further interest because the protein is known to bind to members of the antifolate (aFA) class of drugs, which have applications in

the treatment of cancer, inflammation, malaria, and bacterial infection. For this study, we focus on the aFA methotrexate (MTX), along with the vitamer leucovorin (LEUC, folinic acid). MTX is an FA antagonist and exerts its anti-proliferative effects by competitively inhibiting dihydrofolate reductase (DHFR), thereby blocking purine, thymidine, and some amino acid synthesis.[21,22] LEUC is used as a folic acid rescue agent following treatment with MTX. The importance of DHFR inhibition has led many MTX pharmacology studies to focus at the cellular level; however, MTX delivery to the cancer cell is a critical step in achieving an effective therapeutic index. This drug is given systemically (intravenously or intramuscularly) and distributes through the body via the blood, encountering FBP, which we argue has profound implications on transport and delivery. None of the FA-targeted or aFA therapies mentioned above have exploited the aggregation properties of FBP discussed here, and more generally, the research community has paid relatively little attention to the role of FBP in the transport and uptake of these targeted systems, with the notable exceptions of Birn *et al.* and Kur *et al.* (*vide infra*).[23,24]

FBP is a ∼30 kDa glycoprotein present at 1–2 nM concentrations in human serum and other body fluids and 100 nM concentrations in milk.[7–9,25,26] FBP is believed to be derived from two isoforms of membrane-bound folate receptors (FR-α and FR-β) that have undergone cleavage of the glycosylphosphatidylinositol (GPI) tails anchoring the receptors in the plasma membrane.[26,27] A third isoform, FR-γ, is a secreted protein and lacks the signal for modification with a GPI anchor. Bovine FBP (bFBP)[28] and human FBP (hFBP) have >80% homology, including 100% homology for the 21 key residues making up the FA binding site[19,29] and have been found to exhibit similar aggregation phenomena to those we describe in this paper.[9–11,30–34] For this work, we have employed the more accessible bFBP.

The previous FBP aggregation studies have explored the interaction of FBP with FA and aFAs in the nanomolar to micromolar concentration range. These efforts clearly demonstrate the self-aggregating characteristics of FBP, as well as the ligand-dependent aggregation. In particular, it has been recently noted that the aggregates formed are quite stable,[9] suggesting they could play an important role in biological FA transport. However, the results of these studies were difficult to apply to understanding the challenges for the delivery of aFA drugs and FA-targeted therapeutics since they are mostly performed at concentrations (~0.2–10 μM, and sometimes higher) substantially above the physiologically relevant concentrations of FBP (0.2–2 nM). We chose to re-examine the self-aggregation and ligand-induced aggregation of FBP in the 0.2–100 nM concentration range. In this study we used atomic force microscopy (AFM) to characterize the folate binding protein nanoparticles (FBPNP) on a particle-by-particle basis and to obtain a direct measure of particle size distribution. Our attempts to use lightscattering at these physiological concentrations were complicated by the low scattering cross-sections of the small particles and the technique's strong signal bias to large particle sizes. Generally, we found that FA, LEUC, and MTX interact with FBP to form nanoparticles composed of ~4–15 proteins (n ~ 4–15, n = number of proteins in each FBPNP) with volumes of ~300–800 nm^3 (radii ~ 3–6 nm). However, FBPNP size distributions vary dramatically, and importantly, with changing ligand concentrations. We also observed self-aggregation of apo-FBP at physiological concentrations.

3.2. Results and discussion

Nanoparticles of FBP, FA–FBP, MTX–FBP, and LEUC–FBP formed in 1× PBS were examined by AFM as function of FBP concentration and ligand : FBP ratio. We were particularly interested in both the self- and ligand-induced aggregation of FBP over the physiological protein concentration range of 0.2–100 nM. In brief, samples were prepared using

10 to 20 nM stock solutions of FBP and the ligand of choice. For example, a 1:1 ratio FBP:FA sample was created by adding 20 μL of 20 nM FBP to 160 μL of PBS, then adding 20 μL of 20 nM FA, resulting in a clear, colorless solution. The FA–FBP nanoparticles were captured by spin-coating at 3,000 RPM 20 μL of the FBPNP solution onto a freshly cleaved mica surface. We have previously found this to be a useful method for isolating nanoparticles from solution and avoiding aggregation associated with concentrating solutions or drying samples.[35,36] After spin-coating, the mica surface was washed to remove the buffer salt. AFM imaging was performed in tapping mode. The volumes of the FBPNP were extracted directly from the AFM data. We estimated the number of FBP in each particle by calculating the volume of one FBP using a density of 1.1 $cm^3\ g^{-1}$. Assuming a spherical aggregate in solution, the detected volume of each FBPNP was used to extrapolate the radius of each particle.

3.2.1. Concentration dependence of FBP nanoparticle formation at physiological pH and salt concentrations

Using AFM, we studied the concentration-dependent aggregation of FBP in 1× PBS over the protein concentration range of 0.2–100 nM (Table 3.1, Figure 3.2, Figure 3.3, S3.1 and S3.2†). In the distribution of nanoparticle volumes, the most commonly occurring species (mode) was a single FBP (calculated volume: 45 nm^3), representing 10% and 18% of the total

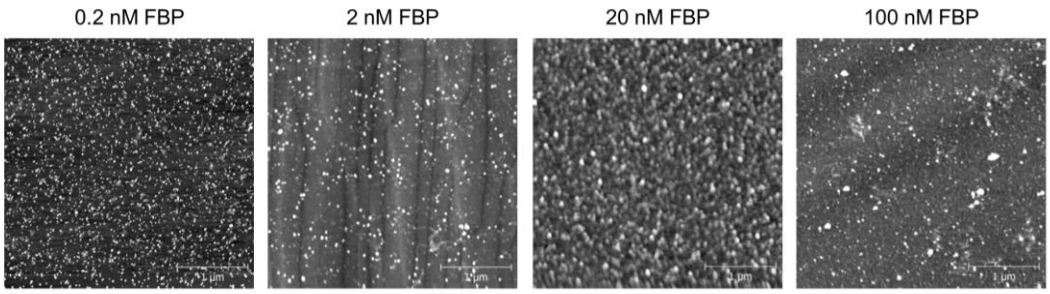

Figure 3.2. AFM images of FBP nanoparticles formed in 1× PBS over a range of protein concentrations, including the physiological concentrations in tissue and blood (0.2–2 nM) and the concentration in human breast milk (100 nM). FBP nanoparticles were captured by spin-coating solutions containing the nanoparticles onto freshly-cleaved mica. Statistical data and the degree of aggregation of the particles are shown in Table 3.1. Histograms of the volume distribution of 2 nM FBP are provided in Figure 3.3. Plots and statistical analysis of the 0.2 nM FBP nanoparticle distribution are provided in Figure A.1.

particles measured for 0.2 nM and 2 nM solutions, respectively. In both cases the particle distribution formed a long tail to higher volumes. At 2 nM FBP, which is the physiological concentration of FBP in human blood, we characterized FBPNP with a mean volume of 605 nm^3 (n ~ 13, radius = 4.6 nm). In this sample, ~3% of particles had a volume of 13 ± 1 proteins. At 0.2 nM FBP, which is more representative of some tissue concentrations, we observed FBPNP in which the mean volume was 565 nm^3 (*n* ~ 13, radius = 4.7 nm); ~5% of particles had a volume of 13 ± 1 proteins. Comparing the 0.2 nM and 2 nM FBP, 90% of the particles formed at 0.2 nM are slightly smaller than those present at 2 nM (Figure A.1b). For the largest 10% of the particles, the FBPNP volumes in the two samples are the same. At 20 nM FBP and 100 nM FBP, we observed extensive aggregation into FBPNP of similar sizes as the samples at lower concentrations. However, these more concentrated solutions resulted in multilayers of particles on mica surface, making it impossible to obtain accurate volume measurements for individual nanoparticles.

Table 3.1. Summary of mean, median, and mode of FBP nanoparticle volumes formed over a range of concentrations of FBP in 1× PBS. Particle volumes and distributions were determined by analyzing AFM images of FBP nanoparticles captured by spin-coating the solutions onto freshlycleaved mica

	FBP Conc. [nM]	Particle count	Mean Volume [nm^3] (Mean Radius) [nm]	Mean # FBP per particle (*n*)	Volume Median [nm^3]	Volume Mode [nm^3]
Folate binding protein	0.2	1928	565 ± 557 (4.7 ± 1.5)	13	371	72
	2	738	605 ± 1160 (4.6 ± 1.8)	13	316	58
	20	Multilayers of overlapping particles → accurate volume measurements could not be generated				
	100					

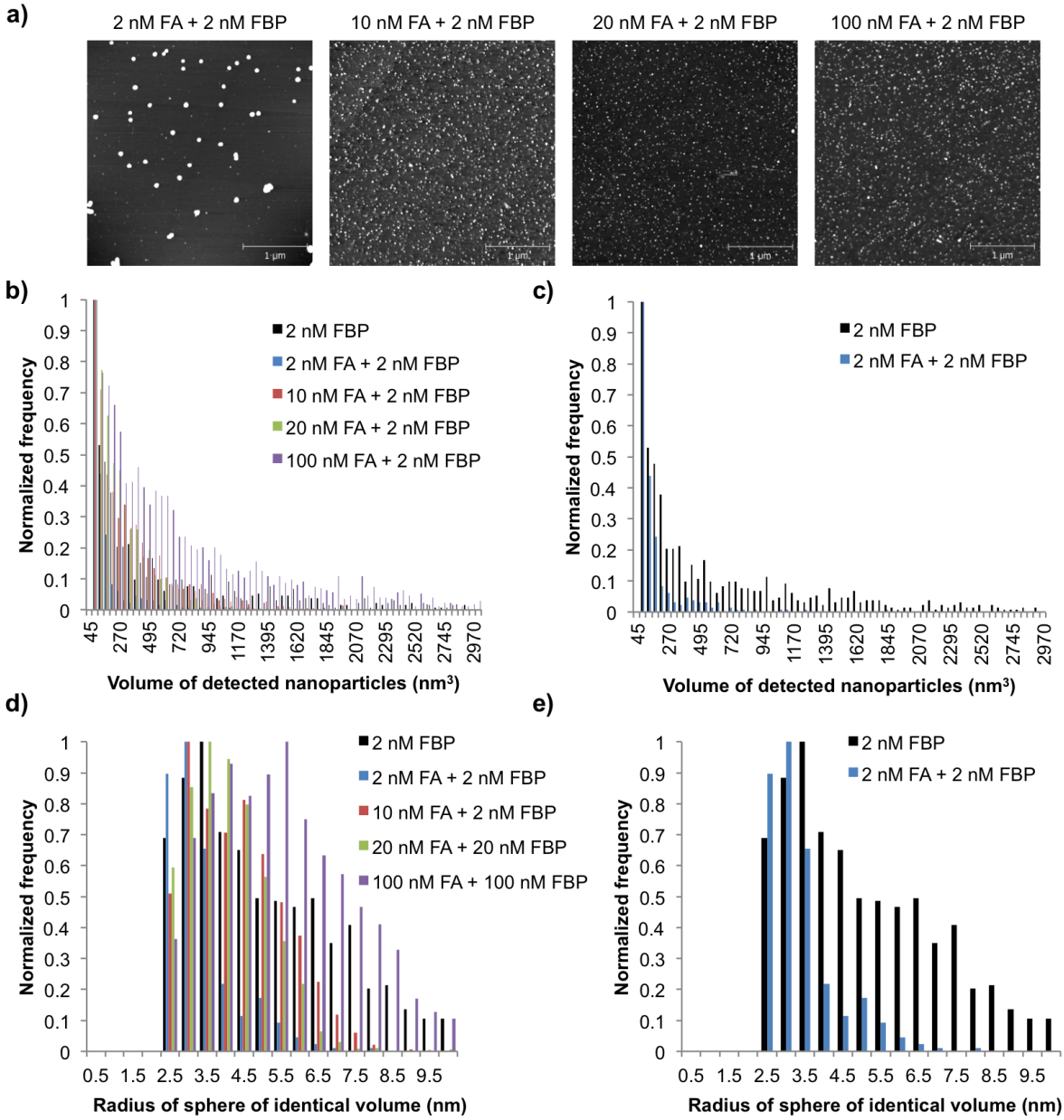

Figure 3.3. (a) AFM images of FBP nanoparticles formed from a range of FA : FBP ratios. For all samples, the FBP concentration was held constant at 2 nM in 1× PBS. AFM images were captured by spin-coating the solutions onto freshly-cleaved mica. As is evident from the 2 nM FA + 2 nM FBP image in panel A, the addition of FA to 2 nM FBP disrupts the FBP self-aggregation observed for FBP alone, resulting in a bimodal distribution (only the smaller nanoparticles are shown in the histograms, see Figure A.3 for the full distribution). (b) Histogram of the volumes of the FBP nanoparticles for all the FA : FBP ratios. With the exception of the 2 nM FA sample, apo- and ligand-bound FBPNP display similarly wide volume distributions. (c) Histogram of the volumes of FBP nanoparticles in only 2 nM FBP and 2 nM FA + 2 nM FBP. Most of the FA-bound FBP nanoparticles are smaller and contained within a narrower distribution than observed for the 2 nM FBP. However, the large FBPNP contain 96% of the FBP material. (d) Histogram showing the distribution of nanoparticle radii extrapolated from the detected FBP nanoparticle volumes. (e) Histogram of only 2 nM FBP and 2 nM FA + 2 nM FBP nanoparticle radii. The narrower distribution of the FA-bound FBP nanoparticles is clearly evident.

The self-aggregation behavior observed for FBP below 10 nM runs counter to previous reports of FBP behavior.[30,34] The existence of FBPNP at these physiologically relevant concentrations suggests self-aggregated FBP is a naturally occurring nanostructure and potentially critical to the transport and delivery of FA, MTX, LEUC, and other aFAs. It is also worthwhile to consider these findings in the context of the self-aggregation results of apo-FBP at 100 nM – the concentration of FBP in human breast milk. This sample displays a high degree of FBPNP formation, pointing towards the potential importance of the nanoparticulate form of the protein in the trafficking and delivery of folate to infants. These results are especially interesting given that infants have higher intestinal expression of megalin,[23,37] which was recently reported to play a role in cellular uptake of FBP and FA.[23,24,37] As demonstrated here (*vide infra*) and in our recently published work,[38] FA binds to FBP and alters the distribution of FBPNP present in solution. The high degree of aggregation at 100 nM FBP provides a potential mechanism for the protection and transport of FA from mother to infant.

3.2.2. Nanoparticles of FA-FBP at physiological pH, protein, and salt concentrations

Although by AFM we observed self-aggregation of FBP at concentrations as low as 0.2 nM in 1× PBS, our data indicate that the addition of folic acid (FA) affects FBPNP properties and composition. That is, FA binds to already self-aggregated FBP, altering the nanoparticle volume distribution. This is consistent with previous work demonstrating that at close to neutral pH values, FA binds FBP with a nanomolar dissociation constant and induces a structural change in the protein.[19,20,31,39,40] Recent reports of the crystal structures of FR-α and FR-β demonstrate the conformational changes in protein structure induced by ligand binding Figure 3.4).[19,20] A number of other studies, including recent work from our group, have investigated the ligand-induced changes in protein structure and intrinsic tryptophan fluorescence.[31,32,38] We

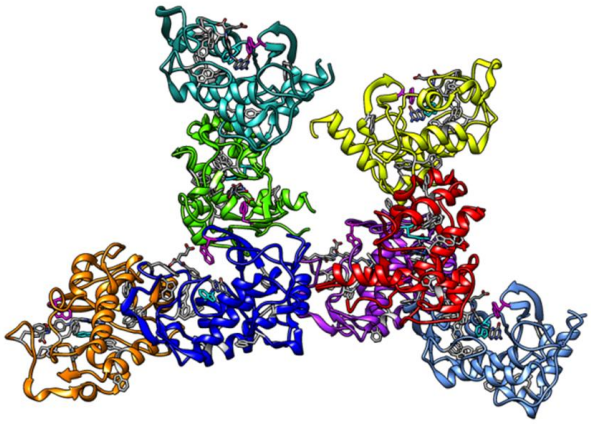

Figure 3.4. The 8-mer crystal structure of folate receptor-α (FBP without the GPI membrane anchor) with folic acid (FA) in the binding pocket.[19] All the tryptophan residues are shown. The tryptophan residues participating in the pi-stacking interaction with the pterin ring system in FA are highlighted in cyan. The tryptophan residues interacting with the benzamine ring in FA are shown in magenta. The rearrangement of these two tryptophan is likely responsible for the fluorescence quenching observed upon ligand binding.

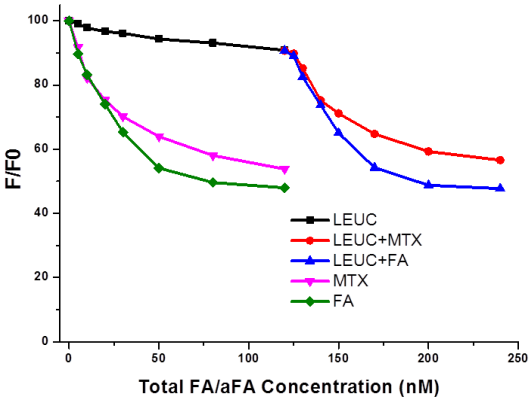

Figure 3.5. The FBP fluorescence is measured upon addition of different folate and folinate materials. Leucovorin (LEUC) did not induce significant fluorescence quenching of FBP (black). Further addition of folic acid (FA) leads to quenching of the intrinsic tryptophan fluorescence (blue) that resembles FA quenching alone (green). Similarly, when methotrexate (MTX) is added to LEUC (red), the fluorescence is quenched approximately the same level as when MTX only is added to FBP (purple). The FBP concentration in all cases is 58 nM (pH 7.4, 1× PBS solution).

demonstrated that upon titrating FBP with FA, approximately 50% of the native tryptophan fluorescence is quenched (Figure 3.5). The structural change in FBP upon ligand binding buries some of the more hydrophobic residues in the interior of the protein and exposes a more hydrophilic surface. The studies referenced above illustrate how the ligand-induced hydrophilic association of FBP has been well-documented by bulk measurements, but AFM has allowed characterization of this phenomenon on a particle-by-particle basis over physiologically-relevant concentration ranges.

When FBP was exposed to FA at a 1:1 ratio (2 nM FA + 2 nM FBP), a bimodal distribution of FBPNP was formed (Figure 3.3a, Table 3.2), clearly indicating that the binding of FA to FBP disrupts the apo-FBP nanoparticles resulting from self-aggregation. The larger FBPNP within the bimodal distribution had a mean volume of ~27,500 nm^3 (n ~ 611, radius = 17.7 nm). For the smaller FBPNP, we observed a mode of approximately one FBP (n = 1) and mean volume of 167 nm^3 (n ~ 4, radius = 3.1). Interestingly, given the general consensus in the

literature that FA-binding induces aggregation,[9–11,30–34] most of the ligand-bound FBPNP were smaller and contained within a narrower distribution that was observed for the 2 nM FBP alone. However, the large FBPNP contain 96% of the FBP material. (The full analysis, including histograms and statistical plots for the 2 nM FA + 2 nM FBP sample, are included in Figure A.3. For clarity and scaling issues, only the smaller FBPNP from this sample are included in the figures in the main body, Figure 3.3) The non-uniform distribution of FBPNP observed at these low FA concentrations is particularly interesting, as 2 nM FA would represent a severe folate deficiency in humans, in whom normal serum folate levels range from 10 to 40 nM.[41] The non-uniform distribution of FBPNP is consistent with aggregation of apo- and holo-FBP, as has been previously documented at low FA concentrations.[11] A fluorescence quenching experiment in which FBP was titrated into FA yielded results consistent with these previous observations (Figure A.4). Although more experiments are required, particularly in the complex environment of blood serum, altered trafficking, biodistribution, and cellular uptake in the non-uniform FA-bound FBPNP may be associated with the symptoms resulting from folate deficiency.

When the FA:FBP stoichiometry was varied to higher concentrations of FA (10 nM to 100 nM), the FBPNP no longer exhibited bimodal distributions and gave mean volumes of ~300–700 nm^3 (n ~ 3–5, radii ~3–5 nm, Table 3.2, Figure 3.3), in close agreement with the volumes of apo-FBPNP (Table 3.1). Given the similarity between the FBPNP volumes in the higher ratio FA and the apo-FBP samples, it is interesting to consider the physiological role of the nanoparticulate form of FBP in the cellular endocytotic uptake pathway. Several recent studies of the role of folate and its cellular uptake have demonstrated that FA and FBP are taken up into cells via a complex mechanism involving several membrane-bound proteins. Birn *et al.* demonstrated the importance of megalin, a low density lipoprotein endocytotic receptor, in the

FBP uptake pathway.[23] Kur *et al.* examined embryotic neural tube development and demonstrated that uptake of folate into neuroepithelial cells involves an endocytotic mechanism with a complex of soluble FBP, membrane-bound folate receptors, and megalin.[24]

3.2.3. Nanoparticles of MTX-FBP at physiological pH, protein, and salt concentrations

Methotrexate (MTX) is a widely used antifolate (aFA) drug for the treatment of cancers, particularly pediatric leukemia, and rheumatoid arthritis (RA).[42,43] For cancer therapy, MTX is delivered systemically (intravenously), usually at doses in the 1–10 μM range. For the treatment of RA, MTX is traditionally given orally or intramuscularly, but reaches blood concentrations ranging from 500 nM at 5 hours post dosing, 100 nM at 30 hours post dosing, and 20 nM at 52 hours after dosing.[43] Therefore, there are substantial concentrations of MTX in blood available to interact with FBP. Although MTX functions as a dihydrofolate reductase (DHFR) antagonist, it is known to bind to FBP.[20,21] This is unsurprising given the structural similarities between FA and MTX (Figure 3.1), but MTX has 100–200× lower binding affinity to FBP than FA to FBP.[20,44–48] The binding interaction between MTX and membrane-bound folate receptors (from which FBP is derived) has been well characterized, including by X-ray crystallography.[20] In addition, our group and others[31] have characterized the tryptophan fluorescence quenching of FBP upon titration with MTX (Figure 3.5). Similar to FA, the native FBP tryptophan fluorescence was quenched by approximately 45%, suggesting ligand binding, protein reorganization, and disruption of apo-FBPNP.

As with FA, we examined the interaction of MTX with FBP at physiological pH, protein, and salt concentrations and characterized the resulting FBPNP using AFM (Table 3.2, Figure 3.6, and S3.5). Like the FA–FBP nanoparticles, the largest MTX-bound FBPNP volumes were observed when both ligand and protein were at 2 nM. In this case, the FBPNP had a mean

volume of 1,293 nm^3 (n ~ 29, radius = 6.3). The histograms shown in Figure 3.6b (volume) and 3.6c (radius) demonstrate that unlike with FA at 2 nM, neither a bimodal distribution nor a narrowing of FBPNP volume distribution is observed with MTX. Above 2 nM MTX, up to 1,000 nM (1 μM) MTX, FBPNP sizes remained consistent at volumes of ~500–800 nm^3 (n ~ 11–18, radii ~4.5–5.5 nm). The variation FBPNP volume as a function of ligand concentration suggests that degree of protein aggregation could play an important role in the trafficking and cellular uptake of the drug.

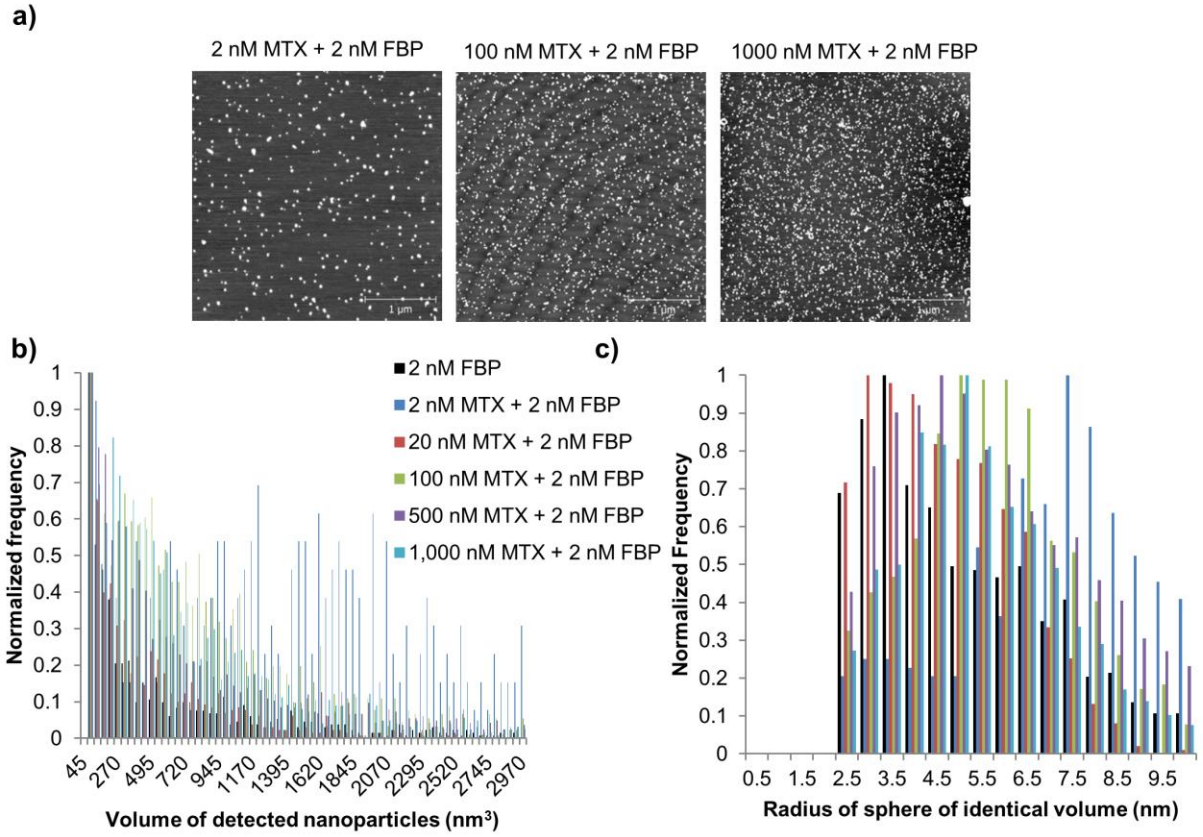

Figure 3.6. (a) Exemplar AFM images of FBP nanoparticles formed from a range of MTX : FBP ratios. For all samples, the FBP concentration was held constant at 2 nM in 1× PBS. FBP nanoparticles were captured by spin-coating solutions containing the nanoparticles onto freshly-cleaved mica. (AFM images of all of the MTX concentrations are provided in Figure A.5.) (b) Histogram of the volumes of the FBPNP for all the MTX : FBP ratios studied. A wide, tailing distribution is observed for all samples. (c) Histogram of the radii of the FBPNP for all MTX : FBP ratios. The radius data are extrapolated from the detected volumes of the FBPNP.

Table 3.2. Summary of mean, median, and mode of nanoparticle volumes formed upon exposure of 2 nM FBP to FA, MTX, or LEUC. Particle size and distributions were determined by analyzing AFM images of FBP nanoparticles captured by spin-coating the solutions onto freshly-cleaved mica

	Ligand conc. [nM]	Particle Count	Mean Volume [nm^3] (Mean Radius) [nm]	Mean # FBP per particle (*n*)	Volume Median [nm^3]	Volume Mode [nm^3]
Folic acid	2	45	27,500 ± 25, 200 (17.7 ± 4.0)	611	20,600	14,000
		282	167 ± 204 (3.1 ± 0.9)	4	96	72
	10[a)]	1836	356 ± 337 (4.0 ± 1.2)	8	246	71
	20[a)]	1862	275 ± 237 (3.8 ± 1.0)	6	203	65
	100	2024	720 ± 659 (5.0 ± 1.7)	16	504	47
Methotrexate	2	289	1293 ± 803 (6.3 ± 1.7)	29	1219	57
	20[b)]	798	495 ± 495 (4.4 ± 1.5)	11	309	57
	100[b)]	1425	795 ± 640 (5.3 ± 1.6)	18	628	97
	500[b)]	1912	757 ± 719 (5.1 ± 1.8)	17	474	46
	1000[c)]	1660	697 ± 620 (5.0 ± 1.6)	15	490	74
Leucovorin	2		No particles observed			
	20	1580	224 ± 235 (3.5 ± 1.0)	5	146	55
	100	730	503 ± 458 (4.5 ± 1.4)	11	386	58
	500	1384	665 ± 634 (4.9 ± 1.7)	15	461	57
	1000	1888	299 ± 316 (3.8 ± 1.1)	7	198	47

3.2.4. Nanoparticles of LEUC-FBP at physiological pH, protein, and salt concentrations

Leucovorin (LEUC, folinic acid) is a vitamer of folic acid and is used in folic acid rescue following treatment of cancer or arthritis with MTX.[43,49–52] The mechanism of action of

leucovorin in folic acid rescue is still debated. Interestingly, LEUC is effective at reducing toxicity of MTX but FA is not, and the reason for this is not yet fully understood.

Using the same AFM techniques described above, we imaged solutions of LEUC and FBP at physiological protein concentration (Table 3.2, Figure A.6). No FBPNP formation was observed at 2 nM LEUC + 2 nM FBP, in direct contrast with the FA and MTX solutions. This indicates that the presence of LEUC both disrupts the normal FBP aggregation process and fails to cause ligand-induced aggregation. Some initial formation of FBPNP was observed at a 10:1 ratio of LEUC:FBP (20 nM LEUC + 2 nM FBP), but substantial FBPNP were not observed until the LEUC concentration was increased to 100 nM. Examination of the crystal structure of FA bound to FBP shows two tryptophan residues participate in the strong binding interaction through pi–pi stacking with both the benzamine ring and the pteridine ring (Figure 3.4). Groups who have examined the binding of FA and MTX to FBP in detail have remarked on the importance of this pi-stacking interaction in the binding of FA and MTX to FBP.[19,20] LEUC, however, lacks the pteridine ring, and in fact, lacks planar geometry due to the presence of a quaternary carbon, preventing the pi–pi stacking interaction (Figure 3.1). When present in high enough concentration, however, LEUC induced formation of FBPNP of comparable volume to the FBPNP containing FA and MTX.

Our FBP fluorescence quenching data also suggest that the interaction between FBP and LEUC is different than FA/FBP and MTX/FBP interaction. As shown in Figure 3.5, LEUC did not induce a conformational change in the FBP protein structure that is known to lead to quenching of the intrinsic tryptophan fluorescence. Sequential titration of FBP with LEUC followed by FA or MTX did result in quenching of the intrinsic fluorescence to the same level

observed with FA or MTX alone. This indicates that FA and MTX are capable of displacing LEUC from the FBP binding pocket.

3.2.5. Statistical evaluation of FBP nanoparticle distributions: implications for transport and delivery of FA, MTX, and LEUC

We employed quantile–quantile (Q–Q) plots to provide a qualitative comparison of FBPNP distributions. The technique plots the quantiles (*i.e.*, a percentage or fraction of a data set below a given value) of one data set against the quantiles of the second data set. In Figure 3.7, we plotted the FBPNP volume distributions of FA- and MTX-containing FBP against the FBPNP distribution formed from apo-FBP at 2 nM. In all cases, the dashed lines pass through the first and third quartiles (25^{th} and 75^{th} percentiles) of the data. We note that at 2 nM FA or MTX the FBPNP size distributions are substantially different (Figure 3.7a). (Only the smaller FBPNP in the 2 nM FA + 2 nM FBP distribution are plotted so different ligand concentrations can be easily compared. Figure A.3 shows the full Q–Q and CDF plots of 2 nM FA + 2 nM FBP.) At 20 nM FA or MTX, the two FBPNP distributions are more similar, but both populations of ligand-bound FBPNP are systematically smaller than the 2 nM apo FBPNP (Figure 3.7b). When the ligand concentrations are increased to 100 nM FA and 1000 nM MTX, the ligandbound and ligand-free FBPNP distributions are nearly identical (Figure 3.7c). That is, at high MTX concentrations, the resulting FBPNP distribution closely resembles the distributions of nanoparticles present in solutions of both apo-FBP and FBP with 100 nM FA. However, the FBPNP formed at these high MTX concentrations (mimicking therapeutic blood levels) did not have the same volume distribution as those formed from physiological levels of FA (10–40 nM). The different FBPNP size distribution may be consistent with different mechanisms of cellular uptake of FA and MTX. A number of in vitro studies have presented evidence that FA and MTX follow different cellular internalization pathways: MTX is postulated to enter cells via the

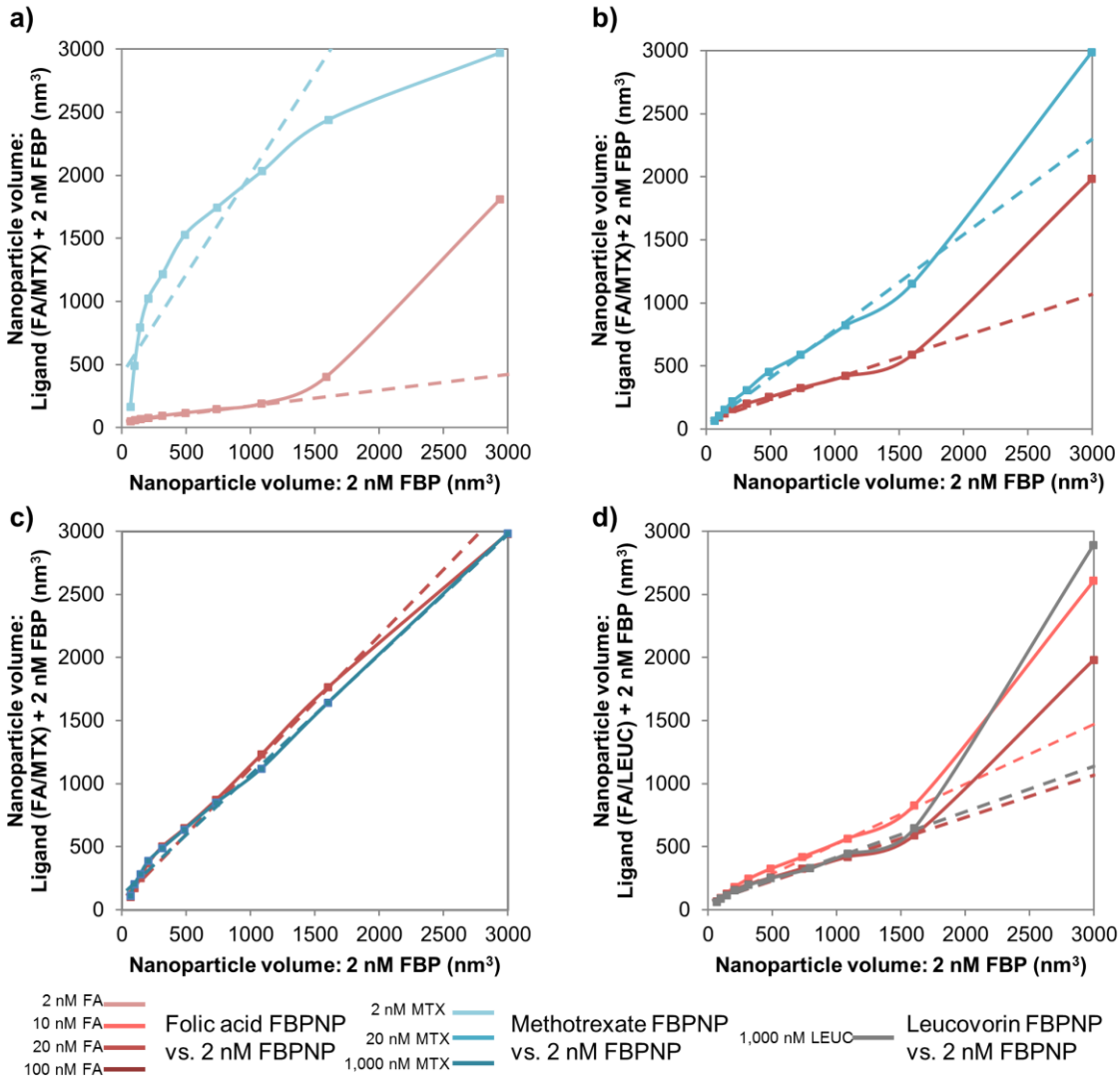

Figure 3.7. Quantile–quantile (Q–Q) plots of the volumes of FA-, MTX-, and LEUC-containing FBP nanoparticle plotted against ligand-free 2 nM FBP nanoparticle volumes. The square markers represent each decile of data. The dashed lines in the charts pass through the 1st and 3rd quartiles (25th and 75th percentiles) of the data. (a) Q–Q plot of the volumes of 2 nM FA- and MTX-containing FBP nanoparticles against the volumes of 2 nM apoFBP nanoparticles. (b) Q–Q plot of the volumes of 20 nM FA- and MTX-containing FBP nanoparticles against the volumes of 2 nM apo-FBP nanoparticles. (c) Q–Q plot of the volumes of 100 nM FA- and MTX-containing FBP nanoparticles against the volumes of 2 nM FBP nanoparticles. These data suggests that at high MTX concentrations, the resulting FBP nanoparticles closely resembles the native form of FBP in both size and distribution, enabling effective transport and delivery to target cells. (d) Q–Q plot of the volumes of 10 nM FA-, 20 nM FA-, and 1000 nM LEUC-containing FBP nanoparticles against the volumes of 2 nM FBP nanoparticles. These data indicate that at therapeutic levels of LEUC, the resulting FBP nanoparticles have a similar volume distribution as FBPNP formed at healthy levels of FA. This suggests that FBP nanoparticles containing LEUC follow the same trafficking and biodistribution pathways as FBP nanoparticles formed at healthy, or potentially even scarce, FA concentrations, facilitating cellular uptake of the vitamer and folic acid rescue.

reduced folate carrier while FA is taken up through membrane-bound folate receptors.[8,53]

However, these studies have been performed in vitro without controlling for FBP concentration

or considering the implications of FBPNP-mediated transport. Further studies both in vitro and in vivo controlling for the FBP concentration are necessary to establish the role of FBP in the cellular internalization of FA and MTX.

We also compared the LEUC-containing FBPNP volume distributions with the FBPNP made from 10 nM FA + 2 nM FBP and 20 nM FA + 2 nM FBP. As can be seen in Figure 3.7d, the LEUC-containing FBPNP have a similar distribution to the FBPNP induced by both 10 nM and 20 nM FA, but the FBPNP in all these ligand-containing populations are systematically smaller than 2 nM apo-FBPNP. This suggests that at therapeutic levels of LEUC, the FBPNP formed resemble the FBPNP present at both slightly deficient and healthy levels of FA. We hypothesize this indicates that FBPNP containing LEUC follow the same trafficking and biodistribution pathways as FBPNP formed at these FA concentrations. These data could indicate a passive targeting mechanism, which facilitates cellular uptake of LEUC because the FBPNP resemble proteins carrying healthy levels of folate. It is interesting to note that at high (micromolar) LEUC concentrations, the FBPNP distribution differs significantly from the FBPNP at the same MTX concentration, but matches that of the FA-containing FBPNP at normal physiological levels. This suggests that LEUC is trafficked to cells similarly to FA, and at high concentrations is able to bypass the MTX uptake pathway to facilitate folic acid rescue. This hypothesis provides a mechanistic explanation for the perplexing observation that high concentrations of FA fail to provide a therapeutic benefit. Note that the FBPNP generated from apo-FBP, 1,000 nM MTX, and 100 nM FA have the same volume distributions (Figure 3.7c).

To obtain quantitative comparisons of the ligand-free and ligand-containing FBPNP volume distributions, we plotted the data as cumulative density functions (CDFs) and employed the Kolmogorov–Smirnov (K–S) test (Figure 3.8). Consistent with the Q–Q plots, the K–S test

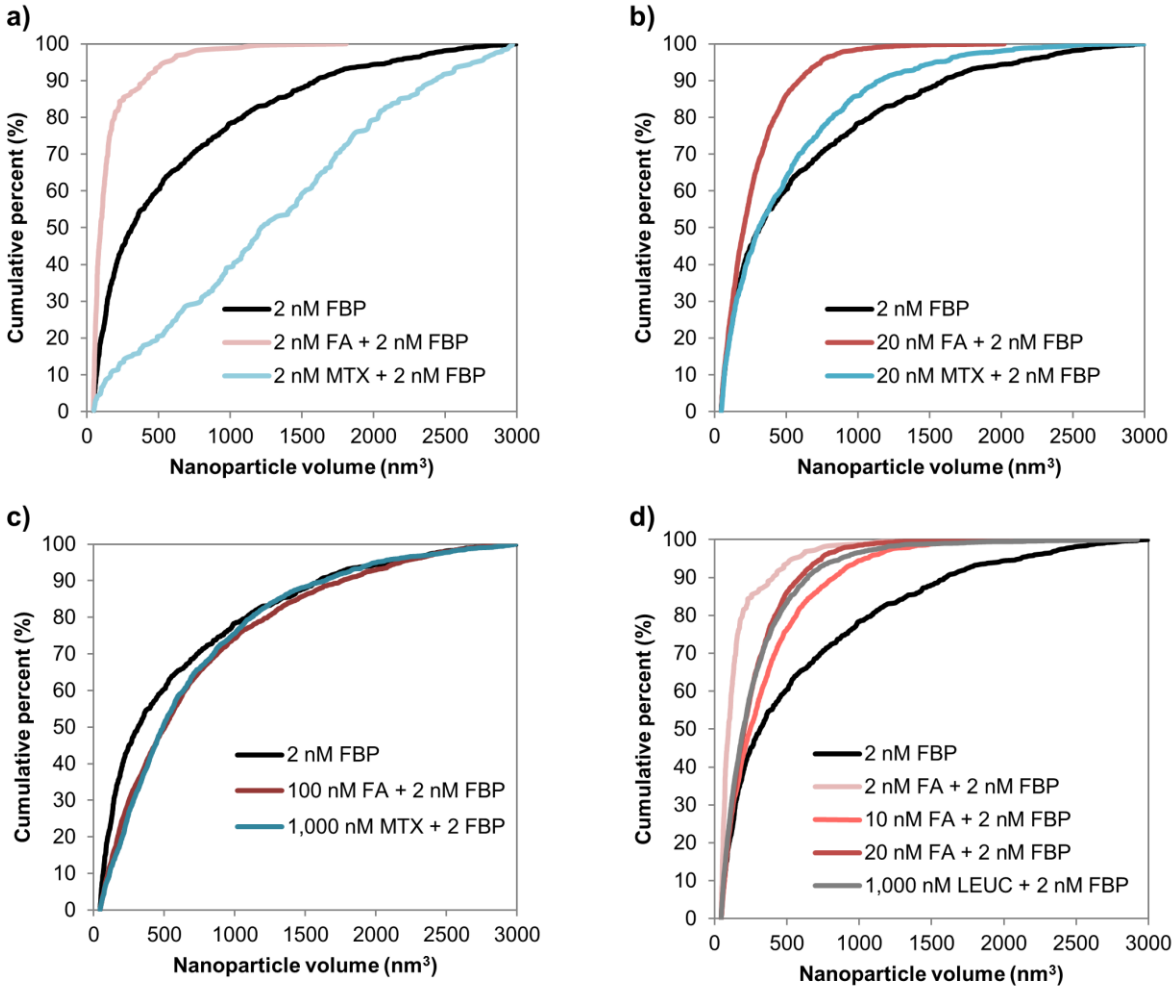

Figure 3.8. Cumulative density function (CDF) plots of selected the measured volumes FA-, MTX-, and LEUC-containing FBP nanoparticles. The similarity of the nanoparticle volume distributions was assessed using K–S statistics. The K–S testing showed the volume distributions of FBP nanoparticles formed from 20 nM FA + 2 nM FBP and 1000 nM LEUC + 2 nM FBP are not statistically different (p = 0.310). All other nanoparticle volume distributions were shown to be statistically different when evaluated with the K–S test. We hypothesize LEUC is effective as a folic acid rescue agent because the FBP nanoparticles formed at therapeutic concentrations of LEUC have the same volume distribution as the nanoparticles formed at healthy FA concentrations (20 nM) and a similar distribution to nanoparticles containing physiologically low FA concentrations (10 nM).

indicated that FBPNP volume distributions of 20 nM FA + 2 nM FBP and 1000 nM LEUC + 2 nM FBP are not statistically different (p = 0.31, Figure 3.8d). All other K–S test comparisons rejected the null hypothesis, signifying that other FBPNP volume distributions are statistically significant from each other ($p < 0.05$). For example, the FBPNP volume distribution of 2 nM FA + 2 nM FBP is different from the distributions of 2 nM FBP and 2 nM MTX + 2 nM FBP.

However, we do not ascribe biological significance to some of these statistically significant populations, particularly in the case of 2 nM apo-FBP, 100 nM FA + 2 nM FBP, and 1000 nM MTX + 2 nM FBP. (The K–S test comparison of FBPNP with 100 nM FA and 1000 nM MTX indicated the samples are statistically different with $p = 0.018$). The Q–Q plot comparing these samples (Figure 3.8c) shows the FBPNP to be nearly identical in volume distribution. These samples are likely to behave similarly biologically and may indicate FA and MTX are trafficked via the same pathways.

The quantitative results of our CDF and K–S test analysis are consistent with the Q–Q plot analysis of FBPNP volume distributions. Based on the consistency of the qualitative and quantitative statistical analyses, we propose LEUC is effective as a folic acid rescue agent because the FBPNP formed at therapeutic concentrations of LEUC have the same volume distribution as the FBPNP formed at healthy FA concentrations and a similar distribution the FBPNP formed at physiologically low FA concentrations (10 nM). We hypothesize this enables LEUC to bypass the MTX trafficking pathway and be delivered to cells at high enough concentrations to be therapeutic.

The likelihood of proteins to aggregate has been a matter of extensive study due to the role of aggregates in Alzheimer's disease. Methods, such as the TANGO simulation,[54–56] have been developed to assess the propensity for aggregation of particular protein sequences. Although the TANGO simulation has limitations for our system (it was developed to study amyloid-β formation and the code assumes a concentration of at least 10 μM), the program output indicated that analogous sequences near the N-terminii of both bovine and human FBP have a 99% aggregation tendency (Figure A.7 and Figure A.8). These sequences are in ideal positions for initiating aggregation between proteins. We note with interest that these sequences

that have been associated with disease-based aggregation may also play a role in the protein aggregation for a normal, healthy physiological process. While we are still investigating the aggregation process (*via* NMR and further AFM studies), the TANGO analysis does suggest one potential mechanism. Similar conclusions regarding the presence of a hydrophobic patch on FBP were previously reached by Holm *et al.* based upon disruption of the FBP aggregates using 1-anilinonapthalene-8-sulfonate (ANS).[33]

3.2.6. Biotrafficking, drug transport, and uptake

Our AFM imaging studies indicate that FBPNP are formed at healthy levels of FA and under therapeutically relevant concentrations of MTX and LEUC (Table 3.2), with FBPNP volumes ranging generally from ~300–800 nm^3 (n ~ 4–15, radii ~ 3–6 nm). The consistency in volume across several orders of magnitude of ligand binding affinity point to the potentially biologically robust nature of FBPNP and suggest a role in the lifetime and biodistribution of the vitamin and drugs, as well as in cellular uptake. However, we have demonstrated that the overall distribution of FBPNP volumes vary as a function ligand concentration. We hypothesize these changes in FBPNP volume distributions dictate the trafficking and biodistribution of the bound small molecules, pointing towards important differences in the mechanism of cellular delivery of FA, MTX, and LEUC.

The conventional view has been that FA is taken up into cells via direct interaction between the vitamin and membrane-bound folate receptors, followed by receptor-mediated endocytosis.[12–17] This mechanism has been invoked for the uptake of FA-targeted drug conjugate systems and imaging agents. This strategy has demonstrated some success in vitro but as of yet, has failed to successfully transfer to in vivo systems and the clinic. Recent reports have shown that megalin (LRP2) is critical for the cellular uptake of FBP, and consequently FA.[23,57] Megalin

is highly expressed in the epithelial tissues in the brain, kidney, yolk sac, and intestines, all areas known to have high folate resorption. Kur *et al.* demonstrated in vivo the importance of megalin in folate uptake and its role in embryonic neural tube development using megalin knockdown mice embryos.[24] They showed that megalin and membrane-bound folate receptors are critical for the receptor-mediated endocytosis of the FA–FBP complex. These studies demonstrate that the cellular uptake pathway of FA is a complex, multi-component process in which we are continuing to investigate the role of FBPNP.

3.2.7. Implications for drug delivery: pre-formation of FBP nanoparticle and dosing schedule

The highly robust formation process of FBPNP suggests that relatively simple modifications to the delivery and/or dosing schedule of MTX could potentially improve drug efficacy and decrease toxicity for cancer and rheumatoid arthritis therapies. Taking advantage of the natural FBPNP formation process, the MTX-bound FBPNP could be pre-formed and the drug administered as a protein nanoparticle. Given the binding of MTX to FBP, dosing schedules could also be modified from existing protocols in order to accommodate the production rate of FBP. The drug would only be injected at a frequency that would ensure FBP is available to traffic the drug to intended locations, helping to prevent off-target toxicity and improving the therapeutic index of MTX.

These ligand-driven aggregation phenomena are important from the point of view of drug biodistribution and may also have key roles in delivery and uptake.[58] For example, materials of ~30 kDa or with a hydrodynamic radius of ~5 nm are below the kidney filtration limit and are excreted in urine, whereas larger particles are trafficked to the liver. The presence of strong aFA–protein interactions may also provide alternate pathways for drug transport into cancer cells[57] and cells infected by pathogens utilizing protein transporter pathways.[23]

3.2.8. Trafficking mechanism for leucovorin

This report presents evidence as to why LEUC is an effective folic acid rescue agent while FA itself is not, a phenomenon that is not well understood. The FBPNP formed at therapeutic concentrations of LEUC have the same volume distribution as FA-containing FBPNP at healthy FA concentrations. We propose that this allows LEUC at high enough concentrations to have a therapeutic effect by following the same trafficking and biodistribution pathways as FA. This passive targeting mechanism allows a high dose of LEUC to be delivered to cells, facilitating folic acid rescue.

3.3. Conclusions

Using primarily AFM, we have examined the self- and ligand-induced aggregation of folate binding protein (FBP) over the physiological concentration range of 0.2 nM to 100 nM. We have discussed some potential implications for vitamin and antifolate drug trafficking resulting from FBP nanoparticle (FBPNP) formation. Upon analyzing our AFM data on the FBPNP, our major conclusions and related biological hypotheses for future work are as follows:

C1. Even in the absence of ligand, FBP at physiological concentrations of ~2 nM self-aggregates to form nanoparticles with a mean of ~12–14 proteins.

C2. In the presence of 2 nM folic acid (FA, which is below healthy human blood serum levels of 10–40 nM) FBP at 2 nM demonstrates complex aggregation properties, resulting in a bimodal distribution of FBPNP. The FBPNP comprising this bimodal population differs significantly in both volume and distribution from the FBPNP formed at healthy levels of FA.

C2-H. It is possible the change in aggregation properties at low FA levels contributes to the deleterious health effects resulting from folate deficiency.

C3. In the presence of 2 nM methotrexate (MTX), FBP at 2 nM aggregates into FBPNP of a different volume distribution than the nanoparticles formed at 2 nM FA. The FBPNP formed at 100 nM FA or 1,000 nM MTX and 2 nM FBP are similar in volume distribution to both each other and to apo-FBPNP at 2 nM.

C3-H. This suggests that at therapeutically relevant concentrations, MTX-containing FBPNP are biologically trafficked like the native protein.

C4. Low concentrations of 2 nM leucovorin (LEUC) disrupt already existing apo-FBPNP and inhibit new nanoparticle formation, in contrast to the strong binding of FA and MTX to FBP that maintain the aggregation properties of FBP.

C5. The distribution of FBPNP in the presence of 1,000 nM LEUC, the approximate therapeutic blood serum concentration, is similar to the FBPNP distribution at physiologically healthy FA concentrations.

C5-H. This new insight provides a hypothesis for the transport of LEUC in the folic acid rescue procedure: the LEUC-containing FBP aggregates resemble the 10–40 nM FA-containing FBPNP distribution, allowing LEUC to be trafficked like FA and enhancing cellular uptake and facilitating its therapeutic effect.

FBP nanoparticles could potentially be exploited for targeted drug delivery applications. Protein nanoparticles are already critical formulations currently used in the clinic. Particularly, albumin has been extensively exploited as a scaffold for increasing efficacy and decreasing toxicity of small molecule therapeutics and imaging agents.[1] There are currently drug delivery and imaging systems employing an albumin scaffold, with applications in the treatment of metastatic breast cancer and diabetes and imaging of cardiovascular and cerebral circulation and lymph nodes. Of particular interest is Abraxane®, a formulation of paclitaxel (Taxol®) and albumin to give nanoparticle albumin-bound paclitaxel (nab-paclitaxel). The formulation process yields nanoparticles with a reported diameter of ~130 nm (DLS measurement). While Abraxane® has had marked success in treating advanced stages of metastatic breast cancer, non-small cell lung cancer, and pancreatic cancer, therapies with an albumin scaffold suffer from the promiscuous nature of albumin in regards to small molecule binding and biological trafficking. Conversely, small molecule–FBP binding interactions, and thus the resulting FBPNP, are highly specific, pointing to the critical role of the protein and the aggregation process in the transport and delivery of FA and aFA drugs to cells.

3.4. Experimental

3.4.1. Materials

All materials purchased from commercial sources were used without further purification, unless otherwise noted. Folic acid (FA), methotrexate (MTX), and leucovorin (LEUC) were purchased from Sigma-Aldrich and used as received. FA, MTX, and LEUC were shielded from light when handling.

3.4.2. Extraction and purification of FBP

FBP was purified from whey protein powder using a folic acid affinity column as previously described.[38] In brief, Sepharose 4B beads (200 mL) were activated with cyanogen bromide and subsequently conjugated to FA. A pH 7.0 2% (w/v) solution of whey protein was centrifuged (20,000g) for 20 minutes, and the supernatant was isolated and run through the affinity column. Unbound protein was washed away with 1 M NaCl (2 L) until the solution ran clear, and then the column was washed with nanopure water (at least 2 L). FBP was released from the column using 0.3 M acetic acid solution (300 mL) and the desired protein was collected in fractions. Fractions containing FBP with at least 90% purity were combined and the pH was adjusted to 7.0 by addition of 5.0 M NaOH. Purity of the isolated FBP was assessed by SDS-PAGE and MALDI-TOF-MS (Figure A.9).

3.4.3. AFM sample preparation

FBP and ligand + FBP solutions were made using serial dilutions. In all cases, FBP was added to 1× PBS (free of Mg^{2+} and Ca^{2+}), and then the ligand was added. For example, to form 100 nM FA + 2 nM FBP, 20 μL of 20 nM FBP in PBS was added to 160 μL PBS, after which 20 μL of 1 μM FA was added to the diluted FBP solution. The resulting nanoparticle solutions were stored at 4°C and shielded from light. Before AFM imaging, mica was glued onto 15 mm

diameter steel AFM pucks. The mica was cleaved using adhesive tape immediately before using. Samples were spin-coated at 3,000 RPM onto the freshly cleaved mica. Samples dissolved in PBS were rinsed with nanopure water (~0.5 mL) to remove the salt and dried under a stream of N_2 for ~5 minutes. Samples containing FA, MTX, or LEUC were shielded from light during the spin-coating process.

3.4.4. Atomic force microscopy (AFM) imaging and image analysis

All AFM imaging was carried out in air-dry conditions using a PicoPlus 5500 AFM (Agilent). Imaging was performed in tapping mode using Aspire CT300R probes (NanoScience, AZ; silicon cantilever, nominal radius 8 nm, force constant 40 N m^{-1}, resonance frequency 300 kHz, length 125 μm). For the 3.5 × 3.5 μm images in which FBPNP were quantified, line scan rates were set at 0.5 Hz and at 1024 pixels per line (~3.4 nm per pixel). Random locations on the mica surface were imaged.

The AFM images were analyzed and the volume of the FBP nanoparticles (FBPNP) were determined using SPIP (v6.2.6, Image Metrology, Hørsholm, Denmark). For the FBPNP size/ volume analysis, AFM images were processed and analyzed as follows: all images were flattened with a 2^{nd} degree global plane correction and with the Z offset with the "Bearing Height to Zero" (SPIP "Best Practices" for particle detection). The image was then further filtered with a 1st order linewise leveling and the background set to zero. Finally, the image was smoothed using the Mean 3 × 3 filter. (The Mean 3 × 3 filter improved the signal-to-noise and allowed for faster FBPNP volume calculation over the entire image.) For each image, 10 FBPNP of a range of sizes randomly distributed over the field were selected. A line scan was performed across each FBPNP, and the diameter and Z-range (height) recorded. Then, using the "Particle & Pore Analysis" feature in SPIP, the volumes of the 10 selected FBPNP were measured. For each

FBPNP, the threshold (bottom plane) of each particle was set so that the detected particle size matched the markers used to measure the FBPNP diameter in the line scan. The "Detected Diameter," "Detected Height," and "Detected Volume" were recorded. A threshold for the overall image was selected based on the modal threshold from measuring the 10 FBPNP individually. This global threshold was applied to all the FBPNP in the image. The radii of the particles were extrapolated using the "Detected Volume" data, assuming the FBPNP are spherical in solution. Because the FBPNP were sometimes close together or overlapping, the selected global threshold sometimes registered distinct FBPNP as one object. There were also sometimes very large aggregates or contaminants (dust) in the images. In order to account for this, FBPNP with volumes larger than 3,000 nm^3 (~67 FBP) were excluded from the mean volume and radius calculations. (The exception is 2 nM FA + 2 nM FBP in which we treated the sample as bimodal). We checked our statistical analyses including the FBPNP larger than 3000 nm^3, and the differences when those particles were included was negligible. For the 10 FBPNP originally analyzed in order to determine the threshold, we compared their volumes determined from the globally applied threshold with the manually measured volumes; in all cases the difference was less than 10%.

In order to ensure that the Mean 3 × 3 filter was not changing the detected shapes or volumes of the FBPNP, line scans of several FBPNP before and after the Mean 3 × 3 smoothing filter was applied were compared. The two line scans showed no difference in height or shape, and there was less than 4% difference in particle volume for the same FBPNP in images processed by the two different methods. We also wanted to ensure that the same particle volumes were reproducibly measured across different image sizes and pixel densities. For select cases, the above procedure was followed to characterize FBPNP volumes in 1.5 × 1.5 μm images of the

same sample. In the 1.5 × 1.5 μm images, FBPNP volumes within 10% of the 3.5 × 3.5 μm analysis were obtained.

The number of FBP in each FBPNP was determined by first calculating the volume of one FBP, assuming a molecular weight of 30 kDa and a density of 1.1 g cm^{-3}. The volume of one FBP was estimated to be 45 nm^3.

3.4.5. Fluorescence measurements

Full experimental details can be found in previously published work.[38] Briefly, all fluorescence experiments were performed on a Varian Cary Eclipse Fluorescence Spectrophotometer. The excitation wavelength was 280 nm. The temperature was controlled to 22°C.

Supplementary information in Appendix A.

3.5. Acknowledgements

RLM thanks the NSF for a Graduate Research Fellowship. This material is based upon work supported by the National Science Foundation Graduate Research Fellowship under Grant No. DGE 1256260.

3.6. References

1. B. Elsadek and F. Kratz, *J. Controlled Release*, 2012, **157**, 4-28.
2. F. Kratz and B. Elsadek, *J. Controlled Release*, 2012, **161**, 429-445.
3. D. E. Owens III and N. A. Peppas, *Int. J. Pharm.*, 2006, **307**, 93-102.
4. I. Lynch and K. A. Dawson, *Nano Today*, 2008, **3**, 40-47.
5. R. L. Merzel, J.-J. Chen, E. N. G. Marsh and M. M. B. Holl, *Chin. Chem. Lett.*, 2015, **26**, 426-430.
6. F. Chiti and C. M. Dobson, *Nat. Chem. Biol.*, 2009, **5**, 15-22.
7. G. B. Henderson, *Annu. Rev. Nutr.*, 1990, **10**, 319-335.

8. A. C. Antony, *Annu. Rev. Nutr.*, 1996, **16**, 501-521.

9. J. Holm, L. N. Babol, N. Markova, A. J. Lawaetz and S. I. Hansen, *Biochimica et Biophysica Acta (BBA) - Proteins and Proteomics*, 2014, **1844**, 512-519.

10. S. W. Bruun, J. Holm, S. I. Hansen and S. Jacobsen, *Appl. Spectrosc.*, 2006, **60**, 737-746.

11. J. Holm, C. Schou, L. N. Babol, A. J. Lawaetz, S. W. Bruun, M. Z. Hansen and S. I. Hansen, *Biochimica Et Biophysica Acta-General Subjects*, 2011, **1810**, 1330-1339.

12. P. S. Low and S. A. Kularatne, *Curr. Opin. Chem. Biol.*, 2009, **13**, 256-262.

13. N. A. Bandara, M. J. Hansen and P. S. Low, *Mol. Pharm.*, 2014, **11**, 1007-1013.

14. E. Sega and P. Low, *Cancer Metastasis Rev.*, 2008, **27**, 655-664.

15. A. R. Hilgenbrink and P. S. Low, *J. Pharm. Sci.*, 2005, **94**, 2135-2146.

16. C. P. Leamon and J. A. Reddy, *Adv. Drug Del. Rev.*, 2004, **56**, 1127-1141.

17. S. Kularatne and P. Low, in *Cancer Nanotechnology*, eds. S. R. Grobmyer and B. M. Moudgil, Humana Press, 2010, vol. 624, ch. 17, pp. 249-265.

18. L. B. Bailey and J. F. Gregory, *The Journal of Nutrition*, 1999, **129**, 779-782.

19. C. Chen, J. Y. Ke, X. E. Zhou, W. Yi, J. S. Brunzelle, J. Li, E. L. Yong, H. E. Xu and K. Melcher, *Nature*, 2013, **500**, 486-489.

20. A. S. Wibowo, M. Singh, K. M. Reeder, J. J. Carter, A. R. Kovach, W. Meng, M. Ratnam, F. Zhang and C. E. Dann, *Proc. Natl. Acad. Sci.*, 2013, **110**, 15180-15188.

21. J. J. McGuire, *Curr. Pharm. Des.*, 2003, **9**, 2593-2613.

22. J. Yuvaniyama, P. Chitnumsub, S. Kamchonwongpaisan, J. Vanichtanankul, W. Sirawaraporn, P. Taylor, M. D. Walkinshaw and Y. Yuthavong, *Nat. Struct. Mol. Biol.*, 2003, **10**, 357-365.

23. H. Birn, X. Y. Zhai, J. Holm, S. I. Hansen, C. Jacobsen, E. I. Christensen and S. K. Moestrup, *FEBS J.*, 2005, **272**, 4423-4430.

24. E. Kur, N. Mecklenburg, R. M. Cabrera, T. E. Willnow and A. Hammes, *J. Cell Sci.*, 2014, **127**, 2261-2268.

25. J. Ghitis, *Am. J. Clin. Nutr.*, 1967, **20**, 1-4.

26. M. Hoier-Madsen, J. Holm and S. I. Hansen, *Biosci. Rep.*, 2008, **28**, 153-160.

27. B. A. Kamen, in *Targeted Drug Strategies for Cancer and Inflammation*, eds. A. L. Jackman and C. P. Leamon, Springer, 2011.

28. L. Nygren-Babol and M. Jagerstad, *Crit. Rev. Food Sci. Nutr.*, 2012, **52**, 410-425.

29. E. Sadasivan and S. P. Rothenberg, *J. Biol. Chem.*, 1989, **264**, 5806-5811.

30. S. I. Hansen, J. Holm, J. Lyngbye, T. G. Pedersen and I. Svendsen, *Arch. Biochem. Biophys.*, 1983, **226**, 636-642.

31. S. W. Bruun, J. Holm, S. I. Hansen, C. M. Andersen and L. Norgaard, *Appl. Spectrosc.*, 2009, **63**, 1315-1322.

32. U. Christensen, J. Holm and S. I. Hansen, *Biosci. Rep.*, 2006, **26**, 291-299.

33. J. Holm, A. J. Lawaetz and S. I. Hansen, *Biochem. Biophys. Res. Commun.*, 2012, **425**, 19-24.

34. T. Pedersen, I. Svendsen, S. Hansen, J. Holm and J. Lyngbye, *Carlsberg Res. Commun.*, 1980, **45**, 161-166.

35. T. A. Betley, M. M. Banaszak Holl, B. G. Orr, D. R. Swanson, D. A. Tomalia and J. R. Baker, *Langmuir*, 2001, **17**, 2768-2773.

36. T. A. Betley, J. A. Hessler, A. Mecke, M. M. Banaszak Holl, B. G. Orr, S. Uppuluri, D. A. Tomalia and J. R. Baker, *Langmuir*, 2002, **18**, 3127-3133.

37. E. I. Christensen and H. Birn, *Nature Reviews Molecular Cell Biology*, 2002, **3**, 258-268.

38. J. Chen, M. A. van Dongen, R. L. Merzel, C. A. Dougherty, B. G. Orr, A. K. Kanduluru, P. S. Low, E. N. G. Marsh and M. M. Banaszak Holl, *Biomacromolecules*, 2016, **17**, 922-927.

39. M. A. van Dongen, J. E. Silpe, C. A. Dougherty, A. K. Kanduluru, S. K. Choi, B. G. Orr, P. S. Low and M. M. Banaszak Holl, *Mol. Pharm.*, 2014, **11**, 1696-1706.

40. N. C. Kaarsholm, A.-M. Kolstrup, S. E. Danielsen, J. Holm and S. I. Hansen, *Biochem. J*, 1993, **292**, 921-925.

41. WHO. Serum and red blood cell folate concentrations for assessing folate status in populations. Vitamin and Mineral Nutrition Information System, World Health Organization, Geneva, 2015.

42. W. E. Evans, W. R. Crom, M. Abromowitch, R. Dodge, A. T. Look, W. P. Bowman, S. L. George and C.-H. Pui, *New Engl. J. Med.*, 1986, **314**, 471-477.

43. J. M. Kremer, J. Galivan, A. Streckfuss and B. Kamen, *Arthritis Rheum.*, 1986, **29**, 832-835.

44. B. A. Kamen and A. Capdevila, *Proc. Natl. Acad. Sci.*, 1986, **83**, 5983-5987.

45. A. C. Antony, C. Utley, K. Van Horne and J. Kolhouse, *J. Biol. Chem.*, 1981, **256**, 9684-9692.

46. S. G. Nandini-Kishore and W. A. Frazier, *Proc. Natl. Acad. Sci.*, 1981, **78**, 7299-7303.

47. S. Rijnboutt, G. Jansen, G. Posthuma, J. B. Hynes, J. H. Schornagel and G. J. Strous, *The Journal of cell biology*, 1996, **132**, 35-47.

48. M.-H. Li, S. K. Choi, T. P. Thomas, A. Desai, K.-H. Lee, A. Kotlyar, M. M. Banaszak Holl and J. R. Baker Jr, *European Journal of Medicinal Chemistry*, 2012, **47**, 560-572.

49. D. G. Priest, J. C. Schmitz and M. A. Bunni, *J. Natl. Cancer Inst.*, 1991, **83**, 1806-1812.

50. E. Frei, R. H. Blum, S. W. Pitman, J. M. Kirkwood, I. C. Henderson, A. T. Skarin, R. J. Mayer, R. C. Bast, M. B. Garnick and L. M. Parker, *The American journal of medicine*, 1980, **68**, 370-376.

51. L. Matherly, C. Barlowe, V. Phillips and I. D. Goldman, *J. Biol. Chem.*, 1987, **262**, 710-717.

52. A. E. Van Ede, R. F. Laan, H. J. Blom, R. A. De Abreu and L. B. van de Putte, *Semin. Arthritis Rheum.*, 1998, **27**, 277-292.

53. L. H. Matherly, Z. Hou and Y. Deng, *Cancer Metastasis Rev.*, 2007, **26**, 111-128.

54. F. Rousseau, J. Schymkowitz and L. Serrano, *Curr. Opin. Struct. Biol.*, 2006, **16**, 118-126.

55. A.-M. Fernandez-Escamilla, F. Rousseau, J. Schymkowitz and L. Serrano, *Nat. Biotechnol.*, 2004, **22**, 1302-1306.

56. R. Linding, J. Schymkowitz, F. Rousseau, F. Diella and L. Serrano, *J. Mol. Biol.*, 2004, **342**, 345-353.

57. H. Y. Xue and H. L. Wong, *Eur. J. Pharm. Biopharm.*, 2012, **81**, 24-32.

58. P. L. Kastritis and A. M. Bonvin, *J. R. Soc. Interface*, 2013, **10**, 20120835.

CHAPTER 4. Conjugation Dependent Interaction of Folic Acid with Folate Binding Protein

Reprinted with permission from:
Rachel L. Merzel [Wallace], Carolina Frey, Junjie Chen, Rachel Garn, Mallory van Dongen, Casey A. Dougherty, Ananada Kumar Kanduluru, Philip S. Low, E. Neil G. Marsh, and Mark M. Banaszak Holl
Bioconjugate Chemistry **2017**, *28*, 2350-2360.

4.1. Abstract

Serum proteins play a critical role in the transport, uptake, and efficacy of targeted drug therapies, and here we investigate the interactions between folic acid−polymer conjugates and serum folate binding protein (FBP), the soluble form of the cellular membrane-bound folate receptor. We demonstrate that both choice of polymer and method of ligand conjugation affect the interactions between folic acid−polymer conjugates and serum FBP, resulting in changes in the folic acid-induced protein aggregation process. We have previously demonstrated that individual FBP molecules self-aggregate into nanoparticles at physiological concentrations. When poly(amidoamine) dendrimer−folic acid conjugates bound to FBP, the distribution of nanoparticles was preserved. However, the dendritic conjugates produced larger nanoparticles than those formed in the presence of physiologically normal human levels of folic acid, and the conjugation method affected particle size distribution. In contrast, poly(ethylene glycol)−folic acid conjugates demonstrated substantially reduced binding to FBP, did not cause folic acid-induced aggregation, and fully disrupted FBP self-aggregation. On the basis of these results, we

discuss the potential implications for biodistribution, trafficking, and therapeutic efficacy of targeted nanoscale therapeutics, especially considering the widespread clinical use of poly(ethylene glycol) conjugates. We highlight the importance of considering specific serum protein interactions in the rational design of similar nanocarrier systems. Our results suggest that prebinding therapeutic nanocarriers to serum FBP may allow folate-specific metabolic pathways to be exploited for delivery while also affording benefits of utilizing an endogenous protein as a vector.

4.2. Introduction

Nanoparticles have been investigated for targeted therapeutic applications, and protein coronas often define their biological identity, biodistribution, therapeutic efficacy, and ultimate fate.[1−7] As such, the formation of unwanted protein coronas that remove targeted nanoparticles from their therapeutic pathway has proven a major challenge in the clinical development of therapeutic nanoscale drug conjugates (nanocarriers). There has been substantial effort invested in trying to understand how protein coronas form and to mitigate their deleterious effects on the biotransport and off-target fate of nanoscale therapeutics.[8−13] However, there are over 100,000 blood serum proteins,[14,15] which makes predicting the interactions between serum proteins and nanocarriers a particularly challenging task. The most notable advance on prevention of protein coronas is the development of “stealth nanocarriers”, most commonly achieved by conjugating poly(ethylene glycol) (PEG) onto the nanocarrier’s surface.[5,16,17]

Generally, protein coronas are discussed as forming around nonendogenous nanoscale objects, but we argue that the selfaggregation of endogenous serum proteins into nanoparticles should also be considered a type of protein corona. The selfaggregation of serum proteins carrying vitamins, drugs, other small molecules, and nanocarrier conjugates affects the

biotransport and cellular uptake of the materials, just as with protein coronas that form around exogenous nanoparticles. As we discuss, it may be possible to exploit serum protein selfaggregation into natural protein coronas for targeted drug delivery.

This work explores the interaction of folate binding protein (FBP) with folic acid (FA)−polymer conjugates. FBP is a glycoprotein (~30 kDa) present in 1−2 nM concentration in human blood serum and 100 nM concentration in human breast milk.[18−20] Serum FBP is likely derived from two isoforms of membrane-bound folate receptors (FRs) via cleavage of their glycosylphosphatidylinositol (GPI) anchors.[21,22] The concentration-dependent self-aggregation of serum FBP has been well-documented over the past several decades, and it has generally been observed that FBP molecules have an increasing tendency to self-associate with increasing concentration.[23−26]

Researchers have also extensively studied FA-induced FBP aggregation and particle formation.[24−31] This aggregation is important in the context of the substantial amount of research and attention FA targeting on a variety of different platforms has received.[32−39] FA is an attractive targeting ligand in drug delivery systems due to its (1) high binding affinity to FR/FBP, (2) stability, (3) ability to be conjugated to a variety of different nanoparticulate and polymeric platforms, and (4) affinity for membrane-bound FRs that are overexpressed on many human cancers. In the field of targeted drug delivery, including in research on FA-targeted therapeutics, the majority of the work has focused at the cellular level, *i.e.*, with the assumption that vectors are delivered to the targeted tissues as administered and that conjugated FA is free to interact with FRs on the cell surface.[40−42] It is assumed that once the targeted vectors interact with the FRs, the therapeutic will be taken up via receptor-mediated endocytosis. However, intravenously administered FA-targeted therapeutics will interact with and bind to serum FBP just as strongly

as they will to cellular FRs. In large part, the design process is missing the critical consideration of specific serum protein interactions (and not just the nonspecific formation of potentially deleterious serum protein coronas) between the targeted nanocarrier and serum proteins during transport to the cell. In this report, we probe the interaction of FA-dendrimer and FA-PEG conjugates with serum FBP and characterize the resulting particle distributions.

FA binding to FBP is important for its biotransport and delivery and enhances both symmetric (apo−apo or holo− holo) and asymmetric (apo−holo) protein aggregation.[25,28] The increased tendency toward both symmetric and asymmetric aggregation has been attributed to conformational changes in the FBP that occur upon FA binding. There are limited data on the binding of other small molecules, such as FA-antagonist drugs (antifolates) like methotrexate (MTX), to FBP. A 2009 study by Bruun *et al.* compared FA- versus MTXinduced changes to the intrinsic FBP fluorescence, relating the results to changes in protein conformational structure. Crystal structures of FA and MTX bound to FR were published by Chen *et al.* (2013)[43] and Wibowo *et al.* (2014),[44] confirming the conformational changes that occur with ligand binding.

Our group recently examined FBP aggregation in the presence of FA, MTX, and leucovorin (LEUC, a vitamer of FA).[45,46] Due to technique and detection level limitations, the earlier studies on serum FBP were carried out at FBP concentrations at least an order of magnitude above physiological levels. In our recent report, we used atomic force microscopy (AFM) to investigate FBP aggregation as a function of protein and ligand concentration and ligand identity at FBP concentrations similar to those found in human blood (~1−2 nM) or other bodily fluids (100 nM). FBP aggregation was observed at all protein concentrations, but the degree of aggregation varied as a function of ligand identity and concentration. That FBP aggregation was maintained at physiologically normal or therapeutically relevant concentrations

of FA, MTX, and LEUC indicated the importance of self- aggregated FBP in the biotransport and cellular uptake of FBP-bound small molecules. Previous reports have noted that FBP aggregates are quite stable,[29] further supporting this hypothesis. Additionally, cell culture media contain very high concentrations of FA (~10 μM), and therefore, aggregation of FBP in the media and of FRs in the membranes is expected in cell culture experiments. This is in fact consistent with reports of FR clustering, as well observations that many FRs are taken up in one endocytosis event.[47,48] The recent work of Birn *et al.*[49] and Kur *et al.*,[50] in which they demonstrated *in vitro* and *in vivo* the critical role of FBP in cellular uptake of FA, further supports these conclusions.

In addition to our work with small molecules, we also recently studied the binding interaction of FA−polymer (dendrimer and PEG) conjugates[51,52] and FA-conjugated iron oxide nanoparticles with FBP.[53] The FA-dendrimer conjugates had an equal or greater affinity for FBP as compared with free FA; one FA-dendrimer conjugate was able to displace FA from the FBP binding pocket and was not removed with large excesses of free FA. In the presence of FA-iron oxide, FBP aggregation was significantly enhanced. These results highlight the importance of considering the interactions of FBP with FA-targeted materials.

On the basis of these observations and given the extensive efforts employing FA-dendrimer and FA-PEG conjugates as targeted drug imaging delivery agents,[51−66] in this report we have investigated interactions of serum FBP with four different FA-targeted dendrimer and PEG conjugates and have characterized the resulting nanoparticle distributions. We demonstrate the formation of a natural protein corona and highlight how this process is likely critical for the trafficking of therapeutic nanocarriers to their intended physiological targets. We discuss the potential implications of this particular interaction for FA-targeted drug nanocarriers. We further

consider how it may be possible to take advantage of FBP-specific metabolic pathways in order to use the protein itself as a targeted carrier and/or drug delivery agent.

4.3. Results and discussion

In these studies, we used fluorescence spectroscopy and AFM to investigate the interaction of FBP (2 nM) with several FA− polymer conjugates, which have applications in targeted drug delivery. The binding of these conjugates to FBP directly affects FBP aggregation around the conjugate, sometimes resulting in FBP nanoparticles (FBPNP). Therefore, an understanding of the binding-induced FBP aggregation (or lack thereof) is crucial for accurately assessing the biotransport and cellular uptake of the FA-targeted conjugates. In this case, AFM afforded us the ability to directly acquire data on the volume distribution of a statistically relevant number of FBPNP on a particle-by-particle basis. AFM analysis of the FBPNP volume distribution generally showed that both the type of polymer conjugated to FBP and the method of conjugation itself played a critical role in the FBP self-aggregation process. We demonstrated that by changing the polymer we could either completely inhibit or substantially enhance FBP aggregation. Our attempts to use techniques such as dynamic light scattering to analyze these samples were inhibited by the necessity to work at low physiologically relevant concentrations of FBP, the low scattering cross section of the polymeric nanoparticles, and the bias of the technique toward larger particles.

The FA−polymer conjugate and FBP binding interactions were explored as a function of FA-conjugate:FBP ratio, under solution conditions that mimicked the pH and salt concentration of human blood serum (1× PBS). Samples were prepared using 10−20 nM stock solutions of FBP or the FA conjugate. For example, a 1:1 ratio FBP:FA-conjugate sample was created by adding 20 μL of 20 nM FBP to 160 μL of PBS, then adding 20 μL of 20 nM FA-conjugate,

resulting in a clear, colorless solution. The resulting nanoparticles were captured by spin-coating at 3,000 rpm 20 μL of the FBPNP solution onto a freshly cleaved mica surface. We have previously found this to be a useful method for isolating nanoparticles from solution and avoiding aggregation associated with concentrating solutions or drying samples.[67,68] After spin-coating, the mica surface was washed to remove the buffer salt. AFM imaging was performed in tapping mode, and the volumes of the FBPNP were extracted directly from the AFM data. We estimated the number of FBP in each particle by calculating the volume of one FBP using a protein mass of 29.1 kDa and a density of 1.1 cm^3 g^{-1}. Assuming a spherical aggregate in solution, the detected volume of each FBPNP was used to extrapolate the nominal radius of each particle in solution.

4.3.1. Polymer conjugates

Highly water-soluble polymers such as PEG and poly(amidoamine) (PAMAM) dendrimers have been popular in the development of FA-targeted delivery systems because they solubilize hydrophobic FA and drugs.[69−71] In the case of dendrimers, multiple attachment points are available for small molecules. As such, in this work we investigated the interaction of serum FBP with four FA− polymer conjugates: two PAMAM conjugates and two PEG conjugates of different polymer lengths. Both generation 5 (G5) PAMAM species were fully acetylated after ligand conjugation in order to make the polymer neutral under physiological conditions, thereby decreasing the cytotoxicity of the polymer.[54,59,72] The use of these four different polymer−FA conjugates illustrated how both polymer type and method of conjugation can significantly alter interactions with serum proteins.

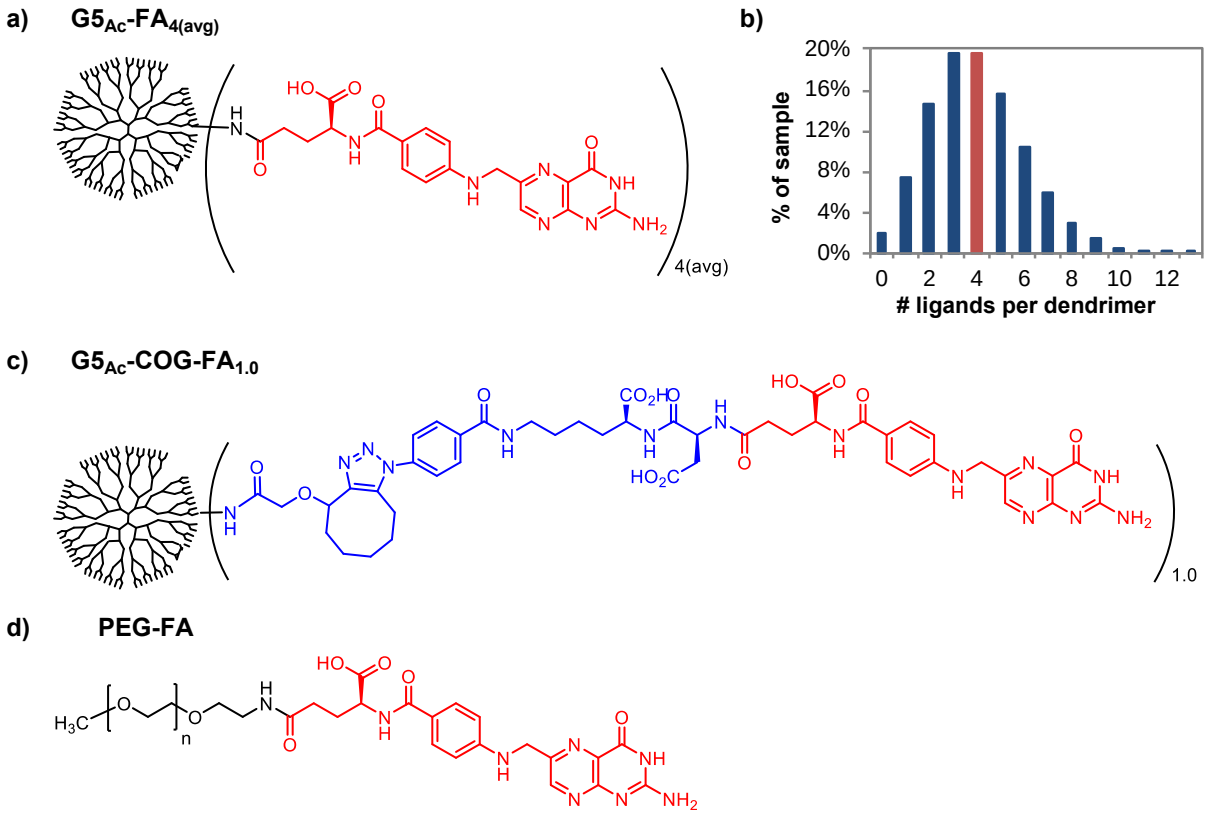

Figure 4.1. Representations of polymer-conjugate materials used in this work. For the PAMAM dendrimers, all terminal amines are acetylated following ligand conjugation. (a) Folic acid (FA, red) conjugated directly to G5 PAMAM (black), producing $G5_{Ac}$-$FA_{4(avg)}$; (b) distribution resulting from a stochastic conjugation with an average of 4 ligands and 93 arms; (c) FA (red) conjugated to G5 PAMAM (black) via a cyclooctyne glycolic acid (COG)–amino acid linker (blue), producing $G5_{Ac}$-COG-$FA_{1.0}$; (d) FA (red) conjugated to poly(ethylene glycol) (black).

The first of these polymer conjugate studied was G5 PAMAM with a stochastic average of four FA ($G5_{Ac}$-$FA_{4(avg)}$) conjugated directly to each dendrimer through an amide bond Figure 4.1a). The average of four FA per dendrimer was the goal of the synthesis and determined to have been achieved by ^{1}H NMR (Figure B.1 in Supporting Information), but since the number of ligands on a dendrimer follows a Poisson distribution,[69,73–75] approximately 20% of the sample had the average four FA molecules per dendrimer (Figure 4.1b). (This polymer conjugate also has an average of two fluorescein isothiocyanate molecules per dendrimer.)

The second G5 PAMAM polymer conjugate studied had one FA per dendrimer conjugated through a cyclooctyne glycolic acid−amino acid linker ($G5_{Ac}$-COG-$FA_{1.0}$) (Figure

4.1c). Our methods for generating a sample with a precise ratio of ligand to dendrimer have been reported in detail elsewhere.[51,76–78] In brief, reverse-phase high performance liquid chromatography was used to isolate a G5 PAMAM sample with one COG linker per dendrimer. Copper-free, strain-promoted click chemistry was then used to conjugate FA to the dendrimer. The driving motivation for this early work was to remove heterogeneity from polymer conjugate samples in order to identify which species were producing observed biological effects. The third and fourth polymer conjugates used in this work were commercially available FA conjugated to either 2 kDa or 30 kDa PEG, respectively (Nanocs, Inc.) (Figure 4.1d). NMR spectroscopy was used to quantify the percentage of FA-conjugated material in the purchased materials (PEG_{2kDa}-FA ~25%; PEG_{30kDA}-FA ~15%).

4.3.2. FBP tryptophan fluorescence quenching as a function of polymer conjugate

As reported in the work of Hansen and Holm[27,31] and by our group,[45,46,52,53] quenching of the native tryptophan fluorescence can be used to assess structural reorganization of FBP upon ligand binding. In our previous work, we particularly compared the fluorescence quenching observed when free FA and FA−polymer conjugates were titrated into FBP.[52] Notably, $G5_{Ac}$-COG-$FA_{1.0}$ produced a high degree of fluorescence quenching as compared to free FA or $G5_{Ac}$-$FA_{4(avg)}$, even at $G5_{Ac}$-COG-$FA_{1.0}$ concentrations as low as 0.1 equivalent per FBP. This suggests that each $G5_{Ac}$-COGFA1.0 was capable of influencing the conformation, and therefore the fluorescent properties, of more than one, and up to 10, FBP. That is, not every $G5_{Ac}$-COG-$FA_{1.0}$ was necessarily bound to FBP, but those that were only directly interacted with the binding pocket of one FBP. The conformational changes from these binding events propagated throughout the protein population, resulting in substantially decreased intrinsic fluorescence. AFM data presented in this report (*vide infra*) support this conclusion of induced protein

conformational change. For PEG-FA conjugates, the magnitude of quenching was the same as with free FA, but the extent of binding decreased with increasing polymer chain length, leading to the hypothesis that the PEG chain was inhibiting access of the FA to the FBP binding site.

Here, we have extended our investigation of FBP fluorescence quenching upon ligand binding by performing the titration in the reverse order so that FBP was added in increasing concentrations into FA or FA−polymer conjugates (Figure 4.2). The excitation wavelength for the intrinsic tryptophan fluorescence was 280 nm, and emission was detected at 342 nm. The presence of FA or any FA-conjugated material resulted in less FBP fluorescence intensity, as compared to apo-FBP (7.4 AU/nM). These data indicate that even when FBP was present in excess, FA or an FA-conjugate enhanced symmetric and asymmetric FBP self-aggregation and induced conformational changes throughout the protein population. This is a well-known effect;[23−31] our method of titrating the FBP into the FA or FA conjugate clearly demonstrated that the conformational change continued up to 4 or 5 equivalents of protein. Interestingly, the trace for the $G5_{Ac}COG\text{-}FA_{1.0}$ fluorescence intensity shows two distinct slopes: the first slope (0.7 AU/nM FBP) corresponds to fluorescence up to approximately stoichiometric ratios of FBP and $G5_{Ac}$COG-FA1.0, and the second slope (2.8 AU/nM FBP) corresponds to superstoichiometric

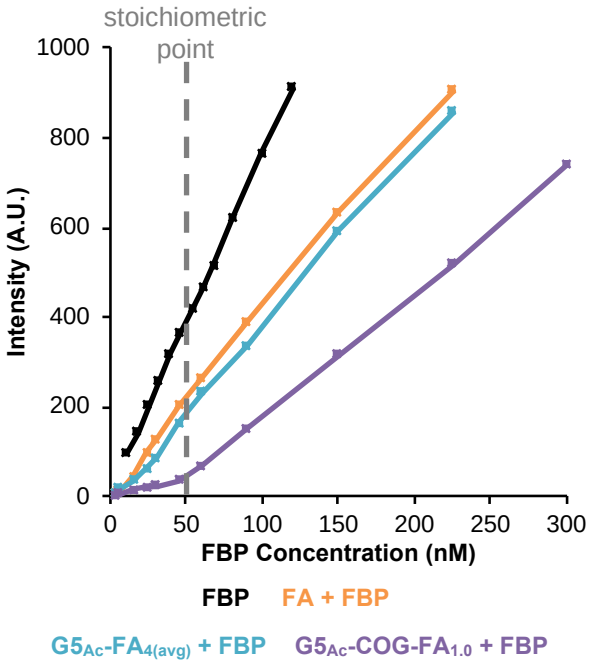

Figure 4.2. Titration of FBP into FA (50 nM) and $G5_{Ac}$-FA PAMAM polymer conjugates (50 nM). All curves with FA materials demonstrated that the presence of FA resulted in a decreased rate of fluorescence increase, as compared to apo-FBP (7.3 A.U./nM). These data indicate that even at greater than stoichiometric FBP concentrations, the FA materials produced conformational changes throughout the protein population.

FBP concentrations. The curves showing a slower rate of change for $G5_{Ac}$-COG-$FA_{1.0}$ compared to FA and $G5_{Ac}$-$FA_{4(avg)}$ (4.0 and 3.8 AU/nM FBP, respectively) indicate that $G5_{Ac}$-COG-$FA_{1.0}$ induced a greater conformational change in FBP as compared to the conformational change induced by other FA materials. This resulted in enhanced asymmetric aggregation of bound and unbound FBP, as demonstrated by the AFM data in following sections.

4.3.3. AFM imaging and analysis: $G5_{Ac}$ + FBP

To determine if acetylated G5 PAMAM ($G5_{Ac}$) itself affected the FBP aggregation process, FBP (2 nM) was exposed to $G5_{Ac}$ at varying concentrations. The volume distributions of the resulting FBPNP (Table 4.1, Figure 4.3) were compared to apo-FBPNP (2 nM).[46] $G5_{Ac}$ + FBP nanoparticles (radius of ~4.4− 5.5 nm) comprised on average 10−13 30 kDa species (FBP monomers and G5 PAMAM dendrimers) compared to the mean of 13 protein molecules for apo-FBPNP (radius of ~4.6 nm). (See Figure B.2 for histograms of the FBPNP volume and radius distribution.) Statistical analyses of the $G5_{Ac}$ + FBP nanoparticles showed the volume distributions were similar to the apo-FBP for all $G5_{Ac}$ concentrations. At 0.5 nM and 2 nM $G5_{Ac}$, a Kolmogorov−Smirnov (K−S) test demonstrated that the volume distributions were not statistically different from the apo-FBPNP volume distribution (p = 0.13 and 0.26, respectively). All other pairwise comparisons indicated that the populations were statistically different, but we do not necessarily ascribe biological or physiological difference to them. Cumulative density function (CDF) plots (Figure 4.3b) and quantile−quantile (Q−Q) plots (Figure 4.3c) illustrate the similarities of the distributions, indicating that $G5_{Ac}$ itself did not substantially interfere with natural FBP aggregation. Previously reported fluorescence quenching data support this conclusion.[52]

Table 4.1. Summary of mean, median, and mode of nanoparticle volumes formed upon exposure of 2 nM FBP to varying concentrations of $G5_{Ac}$ (1x PBS). Particle size and distributions were determined by analyzing AFM images of FBP nanoparticles captured by spin-coating the solutions onto freshly-cleaved mica.

2 nM FBP	N/A	738	610 ± 1160 [4.6 ± 1.8]	13	320	60
2 nM FBP + $G5_{Ac}$ PAMAM	0.5	457	550± 560 [4.5 ± 1.6]	12	330	70
	2	339	570 ± 650 [5.4 ± 1.5]	13	280	50
	5	406	460 ± 470 [4.4 ± 1.4]	10	300	120
	50	216	580 ± 600 [4.6 ± 1.6]	13	370	80

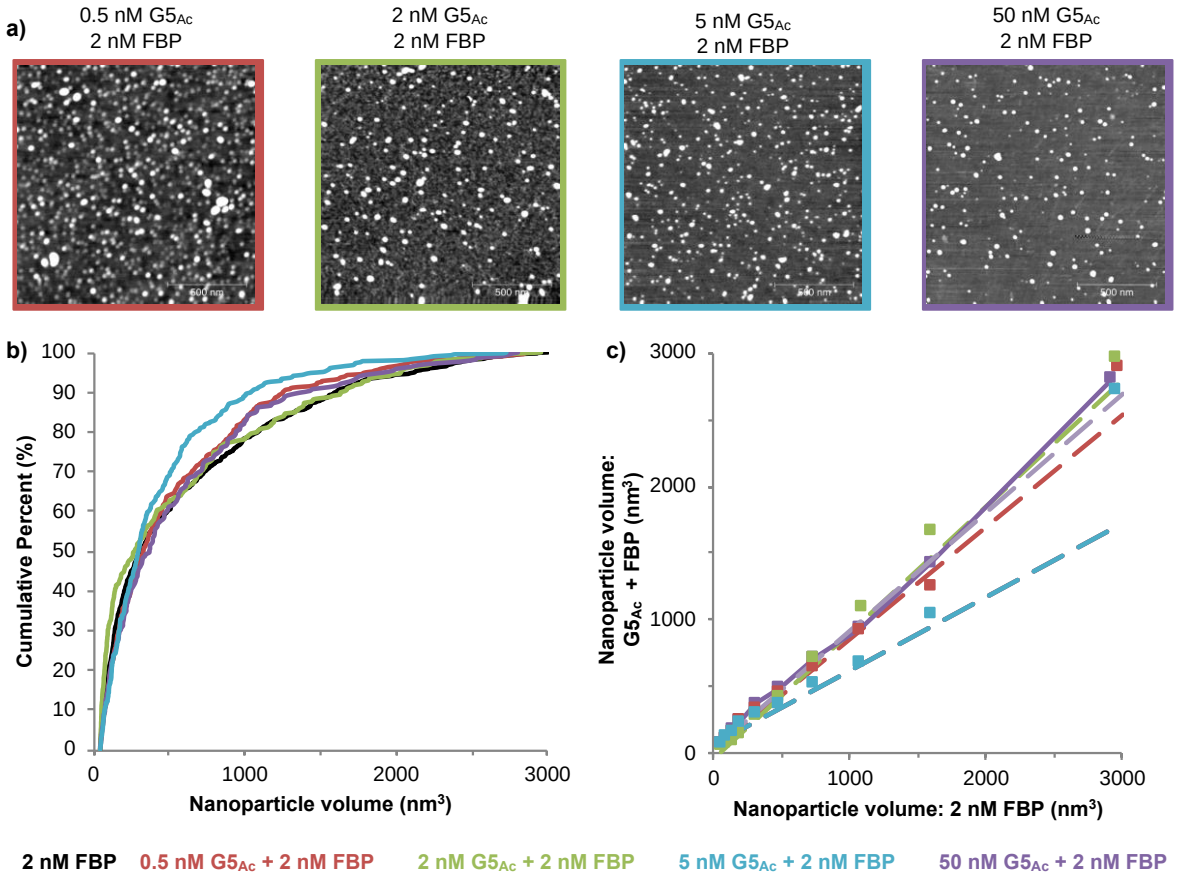

Figure 4.3. a) AFM images of FBP nanoparticles resulting from the addition of $G5_{Ac}$ to FBP (2 nM in 1x PBS). AFM images were captured by spin coating the solutions onto freshly-cleaved mica; b) Cumulative density function (CDF) plots the measured volumes $G5_{Ac}$ + FBP nanoparticles; c) Quantile-quantile (Q-Q) plots of the volumes of $G5_{Ac}$ + FBP nanoparticles plotted against the distribution of ligand-free 2 nM FBP nanoparticle volumes. The square markers represent each decile of data. The straight lines in the charts pass through the 1st and 3rd quartiles (25th and 75th percentiles) of the data. Q-Q plots compare the quantiles of one population against the quantiles of a second population.

4.3.4. AFM imaging and analysis: $G5_{Ac}$-$FA_{4(avg)}$ + FBP

In the presence of $G5_{Ac}$-$FA_{4(avg)}$ (0.5−50 nM polymer), FBP (2 nM) remained aggregated in well-defined, discrete nanoparticles (Table 4.2, Figure 4.4a). FBP and G5 PAMAM both have similar molecular weights (~30 kDa) and volumes. Therefore, the measured volumes of FBPNP include both 30 kDa species. The volume data provided no information on the ratio of protein to polymer; only an estimate of the number of 30 kDa species could be extrapolated. We expected that each $G5_{Ac}$-$FA_{4(avg)}$ was directly bound to only one FBP, *i.e.*, no multivalent binding.[52] However, it is possible that the conformational change in FBP resulting from binding event induced asymmetrical apo−holo aggregation.

Table 4.2. Summary of mean, median, and mode of nanoparticle volumes formed upon exposure of 2 nM FBP to varying concentrations of $G5_{Ac}$-$FA_{4(avg)}$, $G5_{Ac}$-COG-$FA_{1.0}$, and PEG-FA conjugates (1x PBS). Particle volume and distributions were determined by analyzing AFM images of FBP nanoparticles captured by spin-coating the solutions onto freshly-cleaved mica.

Polymer Conj. + 2 nM FBP	Conc. [FA conc.] (nM)	Particle Count	Mean Volume [nm³] [Mean Radius] (nm)	Mean #30kDa species (*n*)	Volume Median (nm³)	Volume Mode (nm³)
$G5_{Ac}$-$FA_{4(avg)}$	0.5 [2]	1,813	640± 600 [4.9 ± 1.6]	14	450	60
	2 [8]	1,087	790 ± 580 [5.4 ± 1.5]	18	660	100
	5 [20]	618	1,120 ± 820 [6.0 ± 1.8]	25	928	60
	50 [200]	multilayers of particles → could not measure volume accurately				
$G5_{Ac}$-COG-$FA_{1.0}$	0.2	410	227 ± 251 [3.5 ± 1.0]	4	150	100
	0.5	243	820 ± 746 [5.3 ± 1.8]	18	594	100
	1.0	multilayers of particles/polymer → could not measure volume accurately				
	2.0	15	32700 ± 20600 [19 ± 3.9]	730	very few particles	
PEG(2kDa)-FA	2-200	no particles observed				
PEG(30kDa)-FA	2-200	no particles observed				

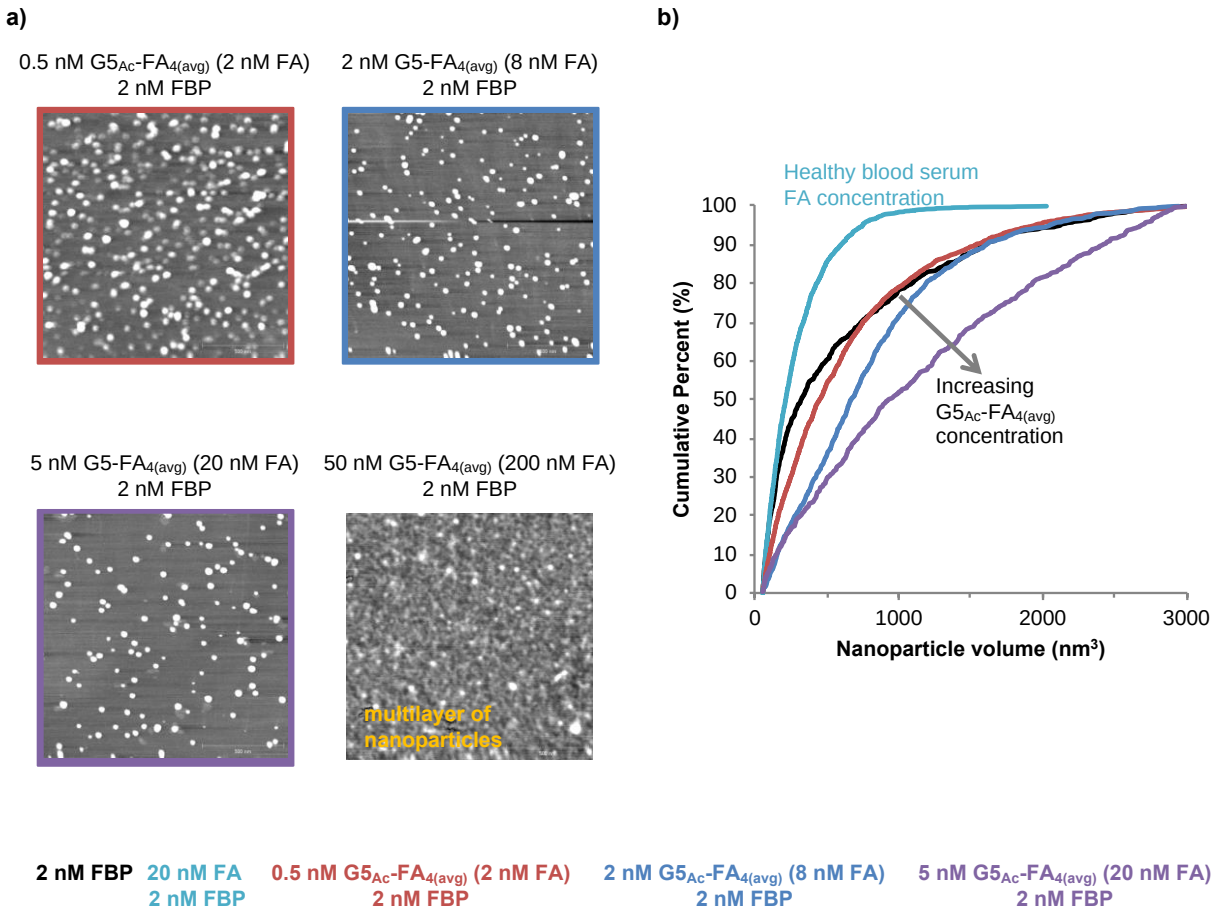

Figure 4.4. a) AFM images of FBP nanoparticles resulting from the addition of $G5_{Ac}$-$FA_{4(avg)}$ to FBP (2 nM in 1x PBS). AFM images were captured by spin coating the solutions onto freshly-cleaved mica; b) Cumulative density function (CDF) plots of the measured volume distributions of 2 nM FBP, 20 nM FA + 2 nM FBP,[46] and $G5_{Ac}$-$FA_{4(avg)}$ + FBP nanoparticles. The similarity of the nanoparticle volume distributions was assessed using K-S statistics, which showed all nanoparticle volume distributions to be statistically different. Analysis of the volume distributions indicated that FBP nanoparticle size increases with increasing $G5_{Ac}$-$FA_{4(avg)}$ concentration.

The binding of $G5_{Ac}$-$FA_{4(avg)}$ to FBP preserved the natural nanoparticulate form of the protein, but the resulting particles were slightly larger than apo-FBPNP and dramatically larger than FBPNP formed in the presence of physiological levels of FA (Figure 4.4b).[46] FBPNP volume increased with $G5_{Ac}$-$FA_{4(avg)}$ concentration. The Q–Q plots of these data further highlight this result. In Figure 4.5a, the Q–Q plots show that the volume distributions of $G5_{Ac}$-$FA_{4(avg)}$ + FBP nanoparticles were similar to the volume distribution of apo-FBPNP. In Figure 4.5b, the Q–

Q plots demonstrate that the volumes of $G5_{Ac}$-$FA_{4(avg)}$ + FBP nanoparticles were significantly larger than nanoparticles generated from 20 nM FA + 2 nM FBP.

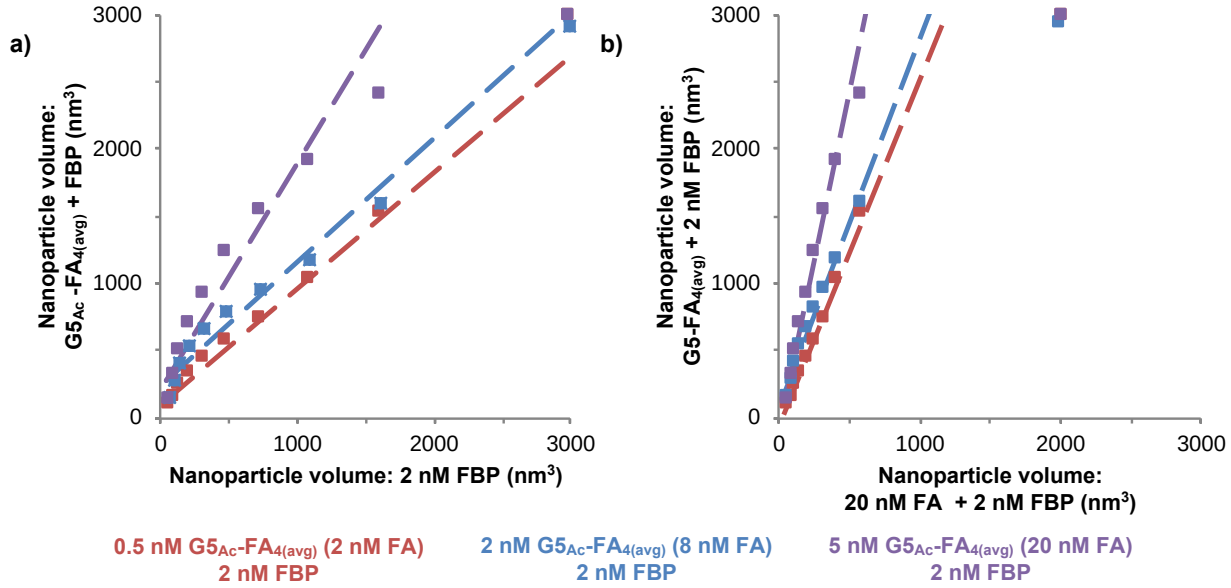

Figure 4.5. Quantile-quantile (Q-Q) plots of nanoparticle volume distributions. The square markers represent each decile of data. The dashed lines pass through the 1st and 3rd quartiles (25th and 75th percentiles) of the data. a) Q-Q plots of the volumes of $G5_{Ac}$-$FA_{4(avg)}$ + FBP nanoparticles plotted against the ligand-free volume distribution of 2 nM FBP nanoparticles; b) Q-Q plots of the volume distribution of $G5_{Ac}$-$FA_{4(avg)}$ + FBP nanoparticles plotted against the nanoparticle volume distribution of 20 nM FA + 2 nM FBP. This is approximately the healthy physiological concentration of FA in blood serum. Q-Q plots compare the quantiles of one population against the quantiles of a second population.

4.3.5. AFM imaging and analysis: $G5_{Ac}$-COG-$FA_{1.0}$ + FBP

FBP (2 nM) was exposed to $G5_{Ac}$-COG-$FA_{1.0}$ over a concentration range of 0.2−20 nM (Table 4.2, Figure 4.6). Substantially lower concentrations of conjugate as compared to the $G5_{Ac}$-$FA_{4(avg)}$ experiments were used in this case because at higher concentrations of $G5_{Ac}$-COG-$FA_{1.0}$ very large aggregates and multilayers of polymer were observed in the AFM images. It is interesting to compare these AFM results with the fluorescence quenching data highlighted in our previous work, particularly the fact that $G5_{Ac}$-COG-$FA_{1.0}$ induced a large conformational change in FBP (see discussion above).[52] By AFM, this phenomenon was observed as asymmetric

aggregation between apo and holo FBP. Our AFM results showed substantial aggregation at substoichiometric levels of $G5_{Ac}$-COG-$FA_{1.0}$, with excess polymer observed on the mica surface, which is particularly evident in the images of 2 nM and 8 nM $G5_{Ac}$-COG-$FA_{1.0}$ + 2 nM FBP (Figure 4.6). While the present studies demonstrate a much more dramatic effect, this is consistent with our previous AFM work showing that at low concentrations of FA, FBP undergoes asymmetrical apo−holo aggregation.[46]

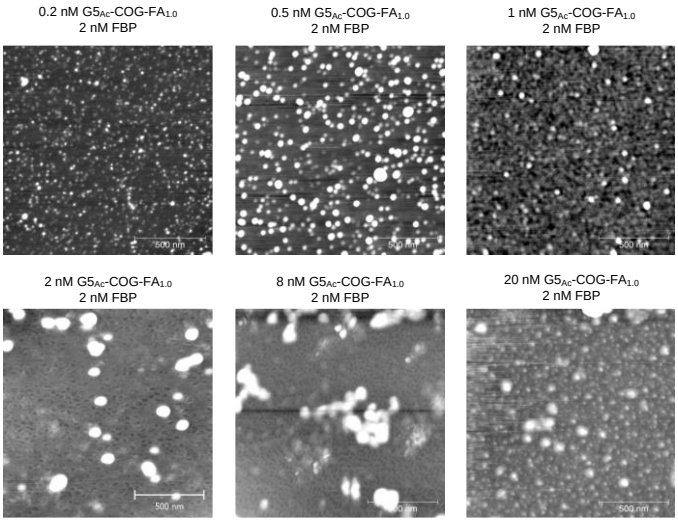

Figure 4.6. AFM images of FBP nanoparticles resulting from the addition of $G5_{Ac}$-COG-$FA_{1.0}$ to FBP (2 nM in 1x PBS). AFM images were captured by spin coating the solutions onto freshly-cleaved mica.

We hypothesize that $G5_{Ac}$-COG-$FA_{1.0}$ induced much more fluorescence quenching52 and FBP aggregation compared to $G5_{Ac}$-$FA_{4(avg)}$ because of the long glycolic acid−amino acid linker between the polymer and the ligand (Figure 4.1c). The distance afforded the G5 PAMAM arms sufficient room to interact with the FBP once it underwent a conformational change upon ligand binding. This hypothesis is consistent with previous work from our group in which we demonstrated that $G5_{Ac}$-COG-$FA_{1.0}$ bound irreversibly to FBP due to a network of nonspecific van der Waals interactions between the G5 PAMAM and the protein (a slow-onset, tight-binding mechanism).[51,76] In the case of $G5_{Ac}$-$FA_{4(avg)}$, the G5 PAMAM was held more closely to the FA and the binding pocket, and we hypothesize that the dendrimer arms could not interact with large enough area of the protein surface to form a strong van der Waals network.

4.3.6. AFM imaging and analysis: PEG-FA + FBP

PEG_{2kDa}-FA and PEG_{30kDa}-FA at both 2 and 20 nM were added to FBP (2 nM), a concentration at which apo-FBPNP are known to be present.46 (Higher PEG-FA concentrations resulted in a multilayer coating of polymer on the mica surface.) In all cases, the PEG-FA conjugates disrupted the existing FBP nanoparticles, and very few were observed by AFM (Table 4.2, compare Figure B.3to Figure 4.4a and Figure 4.6). That is, PEG-FA conjugates upset the natural FBP aggregation process.

Our previously published fluorescence quenching data indicated that the shorter PEG-FA conjugates do bind to FBP and induce a conformational change in the FBP, but the binding affinity was significantly decreased due to the interference of the PEG chain blocking access to the binding pocket.[52] The steric constraints imposed by the longer PEG chains resulted in greatly reduced binding and subsequent fluorescence quenching. Given that PEG-FA did demonstrate some binding interaction with FBP, it is likely that the PEG chain in close proximity to the protein blocked FBP self-aggregation, observed by the lack of FBPNP in the AFM images.

4.3.7. Potential implications for drug delivery: targeted biotransport and efficiency

Our recent work demonstrated that when physiological concentrations of FBP are exposed to free FA at healthy serum levels, FBPNP formed that comprised an average of six proteins subunits.[46] We hypothesize that the nanoparticulate form of FA-carrying FBP is critical for the delivery and cellular uptake of the vitamin, consistent with the hypotheses of Birn[49] and Kur.[50]

With FA-targeted drug delivery, the goal is to have the targeted conjugates trafficked similarly to FA in order to take advantage of cellular overexpression of FRs on diseased cells. Therapeutic efficacy and decreased toxicity are dependent on targeted biological transport to and

successful uptake by the intended tissues. However, FBPNP containing PAMAM-FA conjugates were larger than natural FBPNP (apo and FA-bound), which could have implications for the trafficking, biodistribution, and efficacy of the targeted conjugates. In direct contrast to the effect of PAMAM on FBP aggregation, PEG disrupted the natural and healthy FBP aggregation processes, suggesting that PEG-containing FA-targeted vectors may not be trafficked as intended. PEG is the most commonly used polymer for biomedical applications, including in nanocarrierbased drug delivery, and therefore, its use and role in preventing protein coronas warrant consideration in the rational design of targeted vectors. Furthermore, the disruption of natural FBP aggregation may also impact normal FA distribution and metabolism.

Given the highly specific metabolic pathway of FBP and the critical role we postulate FBP plays in the trafficking process, we propose that FBPNP itself can be used as a targeted nanocarrier, leading to decreased off-target toxicity and increased efficacy. That is, we propose to take advantage of this naturally occurring protein corona for use in targeted drug delivery. This could be accomplished by prebinding the drug to FBP before administering it. We are currently carrying out in vivo experiments with MTX to test this hypothesis. The ability demonstrated in this paper to tune the size of the generated FBPNP using different polymers and conjugation methods also presents the attractive possibility of expanding this work to include polymer nanocarriers. The use of self-aggregated serum proteins as targeted therapeutic nanocarriers is not unprecedented. Abraxane, formulation of albumin and paclitaxel, yields nanoparticles with a reported 130 nm diameter.[14,15] Abraxane is the only solid nanoparticle therapy currently in the clinic, but it has demonstrated substantial success in the treatment of breast, lung, and pancreatic cancers. In this case, it is believed the drug remains bound to albumin, and the uptake into cells follows the albumin trafficking pathways. However, albumin

is the most common human serum protein, and as a result, the treatment suffers from its promiscuous nature and widespread distribution throughout the body. The metabolic pathway of FBP is much more specific, which presents the possibility of using it in a targeted fashion as an endogenous protein nanocarrier.

4.4. Conclusions

Using fluorescence spectroscopy and AFM, we examined the aggregation of FBP in the presence of four different FA− polymer conjugates with applications in FA-targeted drug delivery. The degree of aggregation of FBP varied with both polymer type and conjugation method. These data demonstrate the importance of considering the interactions between targeted polymer nanocarriers and serum proteins to which they bind.

In general, when G5 PAMAM-FA conjugates bound to FBP, the natural FBP self-aggregation process was preserved, although with some notable differences in FBPNP size as compared to the natural aggregation process. Conversely, PEGFA conjugates completely disrupted FBP self-aggregation. The disruption of natural FA-trafficking pathways from PEG conjugation will likely have important implications for delivery and efficacy of the targeted therapeutic, which may point toward why FA-targeted PEG conjugates have yet to be widely adopted in the clinic. To be successful in designing and deploying targeted polymer vectors, researchers must consider the effect of PEG on FBP self-aggregation and protein corona formation. Additionally, the disruption of FBPNP will likely also have the unintended side effect of interfering with free FA transport and metabolism.

The data and discussion presented here solely focus on FA− polymer conjugates, but we suggest that the necessary considerations of serum protein interactions and aggregation apply generally to the field of drug delivery research. Along with attention to solubility, stability,

toxicity, and immunogenicity, researchers designing targeted nanocarrier systems must take into account (and possibly even beneficially exploit) these natural protein coronas.

4.5. Experimental Procedures

4.5.1. Materials

All materials were purchased from commercial sources. G5 PAMAM dendrimers were purchased from Dendritech, Inc. (Midland, MI) and were purified before conjugation procedure as previously reported.[51,76–78] Folic acid and sepharose 4B beads were purchased from Sigma-Aldrich (St. Louis, MO) and used as received. PEG-FA conjugates were purchased from Nanocs, Inc. (Pittsburgh, PA) and used as received following characterization of active FA material by ^{1}H NMR. HPLC grade water, acetonitrile, and methanol were purchased from Fisher-Scientific (Waltham, MA) and used as received. A 500 MHz Varian NMR instrument was used for all ^{1}H NMR measurements. FA and FA-containing materials were shielded from light when handling.

4.5.2. Extraction and purification of FBP

FBP was purified from whey protein powder using a FA affinity column as previously described.[52] In brief, sepharose 4B beads (200 mL bed volume) were activated with cyanogen bromide and subsequently conjugated to FA. A pH 7.0 2% (w/v) solution of whey protein was centrifuged (20,000g) for 20 min at 4 °C. The supernatant was transferred to the affinity column. Unbound protein was washed away with 1× phosphate buffer containing 1 M NaCl (pH 7, 1 L). The column was then washed with nanopure water (at least 2 L) until no protein was detected in the eluent. FBP was released from the column using 0.2 M acetic acid (300 mL). The first 30 mL of the acid wash was discarded because this volume was shown to contain very little protein, and what was present was not pure. For the remaining 270 mL of FBP-containing acetic acid solution the pH was adjusted to 7 by the addition of 5 and 1 M NaOH. The neutralized protein solutions

were frozen in liquid N_2 and lyophilized to yield a white powder comprising sodium acetate salt and FBP. The concentration (w/w) of the FBP in the powder was determined using a NanoDrop fluorospectrometer with absorption at 280 nm. The purity of the FBP was assessed by fluorescence spectroscopy, AFM, SDS−PAGE, and MALDITOF-MS (sinapic acid matrix). Fractions containing FBP with at least 90% purity were combined. Note that bovine FBP was used for this study. Bovine FBP and human FBP have >80% homology overall, including 100% homology in the binding pocket. The human and bovine forms have been shown to exhibit similar aggregation phenomena. For this work, we have employed the substantially more accessible bovine FBP.

4.5.3. Synthesis of G5 PAMAM-FA polymer conjugates

Biomedical grade G5 PAMAM was purified using reverse phase HPLC to obtain G5 dendrimer without trailing generations (G1−G4), dimers, and trimers.[78,75] $G5_{Ac}$ and G5Ac-COG-$FA_{1.0}$ were synthesized according to previously reported methods.[51]

Synthesis of $G5_{Ac}$-$FA_{4(avg)}$ was based on previous methods.[54,79,80] Small changes were made to the procedure and are briefly described here. Amine-terminated G5 PAMAM dissolved in methanol was reacted with fluorescein isothiocyanate (FITC) for 24 h. The resulting material was purified by dialysis against a 10,000 MWCO membrane. $G_5(NH_2)$-FITC was allowed to react with FA which was preactivated with EDC and NHS. The reaction was stirred for 3 days. The product was purified using dialysis and centrifugation against 10 000 MWCO membranes. After lyophilization to dryness, ^{1}H NMR analysis demonstrated the presence of both FITC and FA conjugated to the dendrimer. Finally, the remaining terminal amine groups were fully acetylated by exposing the dendrimer conjugate to excess acetic anhydride in the presence of triethylamine. The product was purified by centrifugation against a 10,000 MWCO membrane.

Remaining unconjugated small molecules were removed by dialysis to yield $G5_{Ac}$-$FA_{4(avg)}$. Ultraperformance liquid chromatography and ^{1}H NMR analyses demonstrated the removal of small molecules. ^{1}H NMR integration determined an average of 4.2 folic acids and 2.2 FITC per G5 dendrimer (Figure B.1).

4.5.4. Fluorescence experiments

Fluorescence experiments were performed on a Varian Cary Eclipse fluorescence spectrophotometer. The excitation wavelength for tryptophan was 280 nm, and the detected emission wavelength was 342 nm. The temperature was controlled to 22 °C. Experiments were carried out in a 1× PBS without Ca^{2+} and Mg^{2+}. Fluorescence measurements were taken after the solutions had reached equilibrium.

4.5.5. AFM sample preparation

Full experimental details have been previously reported.[46] Briefly, FBP and FA−polymer conjugate solutions were made using serial dilutions in 1× PBS. In all cases, the FA−polymer conjugate solution was added to the FBP solution. The resulting FBPNP solutions were stored at 4 °C and shielded from light. To image the nanoparticles, FBPNP solution was spin-coated onto freshly cleaved mica. The mica surface was rinsed with nanopure water to remove the salt and dried under a stream of N_2.

For PEG-FA samples, the percent FA-conjugation of the commercial material was assessed by ^{1}H NMR (PEG_{2kDa}-FA ~25%; PEG_{30kDa} ~15%). The amount of PEG-FA conjugate used in each solution was adjusted to account for the fact that not all of the material was active.

4.5.6. AFM imaging and analysis

The AFM imaging procedures and nanoparticle analysis have been previously reported.[46] Briefly, all AFM imaging was carried out in air using a PicoPlus 5500 AFM (Agilent) or a Nanoscope III (Digital Instruments). Imaging was performed in tapping mode using Aspire CT300R probes (NanoScience, AZ; silicon cantilever, nominal radius 8 nm, force constant 40 N/m, resonance frequency 300 kHz, length 125 μm). For the $G5_{Ac}$, $G5_{Ac}FA_{4(avg)}$, and $G5_{Ac}$-COG-$FA_{1.0}$ samples, FBPNP were quantified in 1.5 μm × 1.5 μm images, with line scan rates set at 1.5 Hz and 512 pixels per line (~2.9 nm/pixel). Random locations on the mica surfaces were imaged.

The AFM images were analyzed and the volume of the FBPNP was determined using the automated "Particle & Pore Analysis" feature in SPIP (version 6.2.6, Image Metrology, Hørsholm, Denmark). See our previous report for full details on the image processing and nanoparticle measurement methods.[46] Histograms of the nanoparticle volumes and radii are shown in Figure B.2.

Supporting information in Appendix B.

4.6. Acknowledgements

R.L.M. thanks the National Science Foundation for a Graduate Research Fellowship. This material is based upon work supported by the National Science Foundation Graduate Research Fellowship under Grant DGE 1256260.

4.7. References

1. Cedervall, T., Lynch, I., Lindman, S., Berggård, T., Thulin, E., Nilsson, H., Dawson, K. A., and Linse, S. (2007) Understanding the nanoparticle-protein corona using methods to quantify exchange rates and affinities of proteins for nanoparticles. Proc. Natl. Acad. Sci. U. S. A. 104, 2050–5.

2. Lynch, I., Cedervall, T., Lundqvist, M., Cabaleiro-Lago, C., Linse, S., and Dawson, K. A. (2007) The nanoparticle–protein complex as a biological entity; a complex fluids and surface science challenge for the 21st century. Adv. Colloid Interface Sci. 134, 167–174.

3. Salvati, A., Åberg, C., Dawson, K. A., Monopoli, M. P., Åberg, C., Salvati, A., Dawson, K. A., Aberg, C., Salvati, A., and Dawson, K. A. (2012) Biomolecular coronas provide the biological identity of nanosized materials. Nat. Nanotechnol. 7, 779–786.

4. Aggarwal, P., Hall, J. B., McLeland, C. B., Dobrovolskaia, M. A., and McNeil, S. E. (2009) Nanoparticle interaction with plasma proteins as it relates to particle biodistribution, biocompatibility and therapeutic efficacy. Adv. Drug Deliv. Rev. 61, 428–437.

5. Owens III, D. E., and Peppas, N. A. (2006) Opsonization, biodistribution, and pharmacokinetics of polymeric nanoparticles. Int. J. Pharm. 307, 93–102.

6. Walczyk, D., Bombelli, F. B., Monopoli, M. P., Lynch, I., and Dawson, K. A. (2010) What the cell "sees" in bionanoscience. J. Am. Chem. Soc. 132, 5761–5768.

7. Lynch, I., and Dawson, K. A. (2008) Protein-nanoparticle interactions. Nano Today 3, 40–47.

8. Cedervall, T., Lynch, I., Foy, M., Berggård, T., Donnelly, S. C., Cagney, G., Linse, S., and Dawson, K. A. (2007) Detailed Identification of Plasma Proteins Adsorbed on Copolymer Nanoparticles. Angew. Chemie Int. Ed. 46, 5754–5756.

9. Monopoli, M. P., Walczyk, D., Campbell, A., Elia, G., Lynch, I., Baldelli Bombelli, F., and Dawson, K. A. (2011) Physical-Chemical aspects of protein corona: Relevance to in vitro and in vivo biological impacts of nanoparticles. J. Am. Chem. Soc. 133, 2525–2534.

10. Deng, Z. J., Liang, M., Monteiro, M., Toth, I., and Minchin, R. F. (2011) Nanoparticle-induced unfolding of fibrinogen promotes Mac-1 receptor activation and inflammation.

11. Röcker, C., Pötzl, M., Zhang, F., Parak, W. J., and Nienhaus, G. U. (2009) A quantitative fluorescence study of protein monolayer formation on colloidal nanoparticles. Nat. Nanotechnol. 4, 577–580.

12. Wang, F., Yu, L., Monopoli, M. P., Sandin, P., Mahon, E., Salvati, A., and Dawson, K. A. (2013) The biomolecular corona is retained during nanoparticle uptake and protects the cells from the damage induced by cationic nanoparticles until degraded in the lysosomes. Nanomedicine Nanotechnology, Biol. Med. 9, 1159–1168.

13. Wan, S., Kelly, P. M., Mahon, E., Stöckmann, H., Rudd, P. M., Caruso, F., Dawson, K. A., Yan, Y., and Monopoli, M. P. (2015) The "Sweet" Side of the Protein Corona: Effects of Glycosylation on Nanoparticle–Cell Interactions. ACS Nano 9, 2157–2166.

14. Kratz, F., and Elsadek, B. (2012) Clinical impact of serum proteins on drug delivery. J. Control. Release 161, 429–445.

15. Elsadek, B., and Kratz, F. (2012) Impact of albumin on drug delivery — New applications on the horizon. J. Control. Release 157, 4–28.

16. Li, S.-D., and Huang, L. (2010) Stealth nanoparticles: high density but sheddable PEG is a key for tumor targeting. J. Control. Release 145, 178–81.

17. Otsuka, H., Nagasaki, Y., and Kataoka, K. (2003) PEGylated nanoparticles for biological and pharmaceutical applications. Adv. Drug Deliv. Rev. 55, 403–419.

18. Henderson, G. B. (1990) Folate Binding Proteins. Annu. Rev. Nutr. 10, 319–335.

19. Antony, A. C. (1996) Folate Receptors. Annu. Rev. Nutr. 16, 501–521.

20. Nygren-Babol, L., Sternesjö, Å., and Björck, L. (2004) Factors influencing levels of folate-binding protein in bovine milk. Int. Dairy J. 14, 761–765.

21. Hoier-Madsen, M., Holm, J., Hansen, S. I., Høier-madsen, M., Holm, J., and Hansen, S. I. (2008) α Isoforms of soluble and membrane-linked folate-binding protein in human blood. Biosience Reports 28, 153–160.

22. Kamen, B. A. (2011) Folate Receptors and Therapeutic Applications, in Targeted Drug Strategies for Cancer and Inflammation (Jackman, A. L., and Leamon, C. P., Eds.). Springer.

23. Pedersen, T., Svendsen, I., Hansen, S., Holm, J., and Lyngbye, J. (1980) Aggregation of a folate-binding protein from cow's milk. Carlsberg Res. Commun. 45, 161–166.

24. Hansen, S. I., Holm, J., Lyngbye, J., Pedersen, T. G., and Svendsen, I. (1983) Dependence of aggregation and ligand affinity on the concentration of the folate-binding protein from cow's milk. Arch. Biochem. Biophys. 226, 636–642.

25. Holm, J., Schou, C., Babol, L. N., Lawaetz, A. J., Bruun, S. W., Hansen, M. Z., and Hansen, S. I. (2011) The interrelationship between ligand binding and self-association of the folate binding protein. The role of detergent-tryptophan interaction. Biochim. Biophys. Acta - Gen. Subj. 1810, 1330–1339.

26. Holm, J., Lawaetz, A. J., and Hansen, S. I. (2012) Ligand binding induces a sharp decrease in hydrophobicity of folate binding protein assessed by 1-anilinonaphthalene-8-sulphonate which suppresses self-association of the hydrophobic apo-protein. Biochem. Biophys. Res. Commun. 425, 19–24.

27. Christensen, U., Holm, J., and Hansen, S. I. (2006) Stopped-flow kinetic studies of the interaction of bovine folate binding protein (FBP) and folate. Biosci. Rep. 26, 291–299.

28. Kaarsholm, N. C., Kolstrup, A.-M., Danielsen, S. E., Holm, J., and Hansen, S. I. (1993) Ligand-induced conformation change in folate-binding protein. Biochem. J. 292, 921–925.

29. Holm, J., Babol, L. N., Markova, N., Lawaetz, A. J., and Hansen, S. I. (2014) The interrelationship between ligand binding and thermal unfolding of the folate binding protein. The role of self-association and pH. Biochim. Biophys. Acta - Proteins Proteomics 1844, 512–519.

30. Bruun, S. W., Holm, J., Hansen, S. I., and Jacobsen, S. (2006) Application of Near-Infrared and Fourier Transform Infrared Spectroscopy in the Characterization of Ligand-Induced Conformation Changes in Folate Binding Protein Purified from Bovine Milk: Influence of Buffer Type and pH. Appl. Spectrosc. 60, 737–746.

31. Bruun, S. W., Holm, J., Hansen, S. I., Andersen, C. M., Norgaard, L., and Nørgaard, L. (2009) A chemometric analysis of ligand-induced changes in intrinsic fluorescence of folate binding protein indicates a link between altered conformational structure and physico-chemical characteristics. Appl. Spectrosc. 63, 1315–1322.

32. Low, P. S., and Kularatne, S. A. (2009) Folate-targeted therapeutic and imaging agents for cancer. Curr. Opin. Chem. Biol. 13, 256–262.

33. Sega, E., and Low, P. (2008) Tumor detection using folate receptor-targeted imaging agents. Cancer Metastasis Rev. 27, 655–664.

34. Hilgenbrink, A. R., and Low, P. S. (2005) Folate receptor-mediated drug targeting: From therapeutics to diagnostics. J. Pharm. Sci. 94, 2135–2146.

35. Leamon, C. P., and Reddy, J. A. (2004) Folate-targeted chemotherapy. Adv. Drug Deliv. Rev. 56, 1127–1141.

36. Sudimack, J., and Lee, R. J. (2000) Targeted drug delivery via the folate receptor. Adv. Drug Deliv. Rev. 41, 147–162.

37. Wu, Y., Guo, R., Wen, S., Shen, M., Zhu, M., Wang, J., and Shi, X. (2014) Folic Acid-Modified Laponite Nanodisks for Targeted Anticancer Drug Delivery. J. Mater. Chem. B Mater. Biol. Med. 2, 7410–7418.

38. Hu, Y., Wang, R., Wang, S., Ding, L., Li, J., Luo, Y., Wang, X., Shen, M., and Shi, X. (2016) Multifunctional Fe3O4 @ Au core/shell nanostars: a unique platform for multimode imaging and photothermal therapy of tumors. Sci. Rep. 6, 28325.

39. Zheng, M., Zhao, P., Luo, Z., Gong, P., Zheng, C., Zhang, P., Yue, C., Gao, D., Ma, Y., and Cai, L. (2014) Robust ICG theranostic nanoparticles for folate targeted cancer imaging and highly effective photothermal therapy. ACS Appl. Mater. Interfaces 6, 6709–6716.

40. Kularatne, S., and Low, P. (2010) Targeting of Nanoparticles: Folate Receptor, in Cancer Nanotechnology (Grobmyer, S. R., and Moudgil, B. M., Eds.), pp 249–265. Humana Press.

41. Bandara, N. A., Hansen, M. J., and Low, P. S. (2014) Effect of Receptor Occupancy on Folate Receptor Internalization. Mol. Pharm. 11, 1007–1013.

42. Kennedy, M., Jallad, K., Lu, J., Low, P., and Ben-Amotz, D. (2003) Evaluation of Folate Conjugate Uptake and Transport by the Choroid Plexus of Mice. Pharm. Res. 20, 714–719.

43. Chen, C., Ke, J., Zhou, X. E., Yi, W., Brunzelle, J. S., Li, J., Yong, E.-L., Xu, H. E., and Melcher, K. (2013) Structural basis for molecular recognition of folic acid by folate receptors. Nature 500, 486–489.

44. Wibowo, A. S., Singh, M., Reeder, K. M., Carter, J. J., Kovach, A. R., Meng, W., Ratnam, M., Zhang, F., and Dann, C. E. (2013) Structures of human folate receptors reveal biological trafficking states and diversity in folate and antifolate recognition. Proc. Natl. Acad. Sci. 110, 15180–15188.

45. Merzel, R. L., Chen, J.-J., Marsh, E. N. G., and Holl, M. M. B. (2015) Folate binding protein—Outlook for drug delivery applications. Chinese Chem. Lett. 26, 426–430.

46. Merzel, R. L., Boutom, S. M., Chen, J., Frey, C., Shedden, K., Marsh, E. N. G., and Banaszak Holl, M. M. (2017) Folate binding protein: therapeutic natural nanotechnology for folic acid, methotrexate, and leucovorin. Nanoscale 9, 2603–2615.

47. Rothberg, K. G., Ying, Y. S., Kolhouse, J. F., Kamen, B. A., and Anderson, R. G. (1990) The glycophospholipid-linked folate receptor internalizes folate without entering the clathrin-coated pit endocytic pathway. J. Cell Biol. 110.

48. Rothberg, K. G., Ying, Y. S., Kamen, B. A., and Anderson, R. G. (1990) Cholesterol controls the clustering of the glycophospholipid-anchored membrane receptor for 5-methyltetrahydrofolate. J. Cell Biol. 111.

49. Birn, H., Zhai, X. Y., Holm, J., Hansen, S. I., Jacobsen, C., Christensen, E. I., and Moestrup, S. K. (2005) Megalin binds and mediates cellular internalization of folate binding protein. FEBS J. 272, 4423–4430.

50. Kur, E., Mecklenburg, N., Cabrera, R. M., Willnow, T. E., and Hammes, A. (2014) LRP2 mediates folate uptake in the developing neural tube. J. Cell Sci. 127, 2261–2268.

51. van Dongen, M. A., Silpe, J. E., Dougherty, C. A., Kanduluru, A. K., Choi, S. K., Orr, B. G., Low, P. S., and Banaszak Holl, M. M. (2014) Avidity Mechanism of Dendrimer–Folic Acid Conjugates. Mol. Pharm. 11, 1696–1706.

52. Chen, J., van Dongen, M. A., Merzel, R. L., Dougherty, C. A., Orr, B. G., Kanduluru, A. K., Low, P. S., Marsh, E. N. G., and Banaszak Holl, M. M. (2016) Substrate-Triggered Exosite Binding: Synergistic Dendrimer/Folic Acid Action for Achieving Specific, Tight-Binding to Folate Binding Protein. Biomacromolecules 17, 922–927.

53. Chen, J., Klem, S., Jones, A. K., Orr, B., and Banaszak Holl, M. M. (2017) Folate-Binding Protein Self-Aggregation Drives Agglomeration of Folic Acid Targeted Iron Oxide Nanoparticles. Bioconjug. Chem. 28, 81–87.

54. Mullen, D. G., McNerny, D. Q., Desai, A., Cheng, X., DiMaggio, S. C., Kotlyar, A., Zhong, Y., Qin, S., Kelly, C. V, Thomas, T. P., Majoros, I., Orr, B. G., Baker, J. R., and Banaszak Holl, M. M. (2011) Design, Synthesis, and Biological Functionality of a Dendrimer-Based Modular Drug Delivery Platform. Bioconjug. Chem. 22, 679–689.

55. Landmark, K. J., DiMaggio, S., Ward, J., Kelly, C., Vogt, S., Hong, S., Kotlyar, A., Myc, A., Thomas, T. P., Penner-Hahn, J. E., Baker, J. R., Holl, M. M. B., and Orr, B. G. (2008) Synthesis, characterization, and in vitro testing of superparamagnetic iron oxide nanoparticles targeted using folic acid-conjugated dendrimers. ACS Nano 2, 773–783.

56. Kukowska-Latallo, J. F., Candido, K. A., Cao, Z., Nigavekar, S. S., Majoros, I. J., Thomas, T. P., Balogh, L. P., Khan, M. K., and Baker, J. R. (2005) Nanoparticle Targeting of Anticancer Drug Improves Therapeutic Response in Animal Model of Human Epithelial Cancer. Cancer Res. 65.

57. Majoros, I. J., Thomas, T. P., Mehta, C. B., and Baker, J. R. (2005) Poly(amidoamine) dendrimer-based multifunctional engineered nanodevice for cancer therapy. J. Med. Chem. 48, 5892–5899.

58. Gillies, E. R., and Fréchet, J. M. J. (2005) Dendrimers and dendritic polymers in drug delivery. Drug Discov. Today 10, 35–43.

59. Lee, C. C., MacKay, J. A., Fréchet, J. M. J., and Szoka, F. C. (2005) Designing dendrimers for biological applications. Nat. Biotechnol. 23, 1517–1526.

60. Stella, B., Arpicco, S., Peracchia, M. T., Desmaële, D., Hoebeke, J., Renoir, M., D'Angelo, J., Cattel, L., and Couvreur, P. (2000) Design of folic acid-conjugated nanoparticles for drug targeting. J. Pharm. Sci. 89, 1452–1464.

61. Sunoqrot, S., Bugno, J., Lantvit, D., Burdette, J. E., and Hong, S. (2014) Prolonged blood circulation and enhanced tumor accumulation of folate-targeted dendrimer-polymer hybrid nanoparticles. J. Control. Release 191, 115–122.

62. Luo, Y., Zhao, L., Li, X., Yang, J., Guo, L., Zhang, G., Shen, M., Zhao, J., and Shi, X. (2016) The design of a multifunctional dendrimer-based nanoplatform for targeted dual mode SPECT/MR imaging of tumors. J. Mater. Chem. B 4, 7220–7225.

63. Li, X., Xiong, Z., Xu, X., Luo, Y., Peng, C., Shen, M., and Shi, X. (2016) 99m Tc-Labeled Multifunctional Low-Generation Dendrimer-Entrapped Gold Nanoparticles for Targeted SPECT/CT Dual-Mode Imaging of Tumors. ACS Appl. Mater. Interfaces 8, 19883–19891.

64. Zhou, B., Zhao, L., Shen, M., Zhao, J., and Shi, X. (2017) A multifunctional polyethylenimine-based nanoplatform for targeted anticancer drug delivery to tumors in vivo. J. Mater. Chem. B 5, 1542–1550.

65. Wang, Y., Cao, X., Guo, R., Shen, M., Zhang, M., Zhu, M., and Shi, X. (2011) Targeted delivery of doxorubicin into cancer cells using a folic acid–dendrimer conjugate. Polym. Chem. 2, 1754.

66. Pearson, R. M., Sen, S., Hsu, H., Pasko, M., Gaske, M., Král, P., and Hong, S. (2016) Tuning the Selectivity of Dendron Micelles Through Variations of the Poly(ethylene glycol) Corona. ACS Nano 10, 6905–6914.

67. Betley, T. A., Banaszak Holl, M. M., Orr, B. G., Swanson, D. R., Tomalia, D. A., and Baker, J. R. (2001) Tapping Mode Atomic Force Microscopy Investigation of Poly(amidoamine) Dendrimers: Effects of Substrate and pH on Dendrimer Deformation. Langmuir 17, 2768–2773.

68. Betley, T. A., Hessler, J. A., Mecke, A., Banaszak Holl, M. M., Orr, B. G., Uppuluri, S., Tomalia, D. A., and Baker, J. R. (2002) Tapping Mode Atomic Force Microscopy Investigation of Poly(amidoamine) Core−Shell Tecto(dendrimers) Using Carbon Nanoprobes. Langmuir 18, 3127–3133.

69. van Dongen, M. A., Dougherty, C. A., and Banaszak Holl, M. M. (2014) Multivalent Polymers for Drug Delivery and Imaging: The Challenges of Conjugation. Biomacromolecules 15, 3215–3234.

70. Petros, R. A., and DeSimone, J. M. (2010) Strategies in the design of nanoparticles for therapeutic applications. Nat. Rev. Drug Discov. 9, 615–627.

71. Peer, D., Karp, J. M., Hong, S., Farokhzad, O. C., Margalit, R., and Langer, R. (2007) Nanocarriers as an emerging platform for cancer therapy. Nat Nano 2, 751–760.

72. Hong, S., Bielinska, A. U., Mecke, A., Keszler, B., Beals, J. L., Shi, X., Balogh, L., Orr, B. G., Baker, J. R., and Banaszak Holl, M. M. (2004) Interaction of poly(amidoamine) dendrimers with supported lipid bilayers and cells: Hole formation and the relation to transport. Bioconjug. Chem. 15, 774–782.

73. Mullen, D. G., Fang, M., Desai, A., Baker, J. R., Orr, B. G., and Banaszak Holl, M. M. (2010) A Quantitative Assessment of Nanoparticle−Ligand Distributions: Implications for Targeted Drug and Imaging Delivery in Dendrimer Conjugates. ACS Nano 4, 657–670.

74. Mullen, D. G., and Banaszak Holl, M. M. (2011) Heterogeneous Ligand–Nanoparticle Distributions: A Major Obstacle to Scientific Understanding and Commercial Translation. Acc. Chem. Res. 44, 1135–1145.

75. van Dongen, M. A., Desai, A., Orr, B. G., Baker, J. R., Banaszak Holl, M. M., Baker Jr, J. R., and Banaszak Holl, M. M. (2013) Quantitative analysis of generation and branch defects in G5 poly(amidoamine) dendrimer. Polymer (Guildf). 54, 4126–4133.

76. van Dongen, M. A., Rattan, R., Silpe, J., Dougherty, C., Michmerhuizen, N. L., Van Winkle, M., Huang, B., Choi, S. K., Sinniah, K., Orr, B. G., and Banaszak Holl, M. M. (2014) Poly(amidoamine) Dendrimer–Methotrexate Conjugates: The Mechanism of Interaction with Folate Binding Protein. Mol. Pharm. 11, 4049–4058.

77. Dougherty, C. A., Furgal, J. C., van Dongen, M. A., Goodson, T., Banaszak Holl, M. M., Manono, J., and DiMaggio, S. (2014) Isolation and Characterization of Precise Dye/Dendrimer Ratios. Chem. – A Eur. J. 20, 4638–4645.

78. Mullen, D. G., Desai, A., van Dongen, M. A., Barash, M., Baker, J. R., and Banaszak Holl, M. M. (2012) Best Practices for Purification and Characterization of PAMAM Dendrimer. Macromolecules 45, 5316–5320.

79. Majoros, I. J., Myc, A., Thomas, T., Mehta, C. B., and Baker, J. R. (2006) PAMAM dendrimer-based multifunctional conjugate for cancer therapy: Synthesis, characterization, and functionality. Biomacromolecules 7, 572–579.

80. Quintana, A., Raczka, E., Piehler, L., Lee, I., Myc, A., Majoros, I., Patri, A. K., Thomas, T., Mulé, J., and Baker, J. R. (2002) Design and function of a dendrimer-based therapeutic nanodevice targeted to tumor cells through the folate receptor. Pharm. Res. 19, 1310–1316.

CHAPTER 5. Folate Binding Protein Inhibits Tumor Growth

Rachel L. Merzel [Wallace], Junjie Chen, Carolina Frey, Alexis Jones, Mark Vartanian, Brent Ward, Mark M. Banaszak Holl

This chapter was submitted to *Molecular Pharmaceutics* as a Communication.

5.1. Abstract

Using a KB xenograft model in severe combined immunodeficient (SCID) mice, we investigated whether pre-binding the chemotherapeutic methotrexate (MTX) to folate binding protein (FBP) would enable the protein to serve as a targeted therapeutic vector, enhancing uptake into tumor cells and improving therapeutic efficacy. Three concentrations of FBP were tested (MTX dose was held constant between the groups), in addition to FBP alone. Despite displaying substantial toxicity, FBP alone inhibited tumor growth compared to the saline control and free MTX. This is the first time this effect of FBP has been reported. We hypothesize the excess unbound FBP resulted in folate starvation of the tumors. The groups treated with MTX and FBP also showed inhibition of tumor growth, but toxicity increased with FBP concentration. It is likely that instead of specifically targeting the cancer cells, FBP facilitated widespread uptake of MTX, resulting in systemic toxicity. The substantial reduction observed in tumor volume suggest that FBP alone could be employed as a chemotherapeutic. As an endogenous serum protein, FBP avoids complications associated with synthetic nanoscale therapeutics, primarily immune reactions (*e.g.*, opsonization) and heterogeneity in manufacturing.

5.2. Introduction

Folic acid (FA) targeting has been widely explored as a targeting agent for cancer therapy.[1–14] High-affinity folate receptors (FRs), with which FA has a nanomolar dissociation constant, are overexpressed in a wide range of human cancers, including breast, ovary, endometrium, kidney, lung, brain, head, and neck.[3,4,15–19] Cancers are postulated to overexpress FRs because FA is a critical component in DNA synthesis, and rapidly dividing cancer cells must have access to a large amount of FA.[20–23] Researchers have sought to leverage this overexpression to achieve active, selective targeting to the cancer cells. Despite a number of clinical trials in humans,[1,2] FA-targeted cancer therapies have yet to be deployed in the clinic. In the mid-2000s an FA-targeted cancer therapeutic designed by colleagues was cleared to begin clinical trials. However, synthesizing consistent batches of material on the kilogram scale proved a challenge, and the trial was never started. At that time, we began investigating why FA-targeted therapies broadly were not performing as expected or desired and why the manufacturing scale-up of these materials was so difficult.

Over approximately the last decade, we have published a number of papers investigating this phenomenon.[13,24–27] In particular, we focused on the interaction between the targeted therapies and proteins, both FRs and serum proteins.[11,12,28–30] Based on these studies, we postulate that the role of *serum* folate binding protein (the soluble form of cellular membrane-bound FRs) may play an important role in trafficking and biotransport of the FA-targeted materials.

Folate binding protein (FBP) is derived from membrane-bound FRs through cleavage of the glycosylphosphatidylinositol (GPI) anchor and is present at 1-2 nM in human blood serum and <1 nM in human tissues.[31,32] The 21 residues in the binding pocket of FR-α (the isoform of

FR from which the majority of FBP is derived) and FBP are 100% homologous. Therefore, any targeted therapeutic will have the same strong binding interaction with FBP as it will with membrane-bound FRs. This binding event and subsequent FBP aggregation/protein corona formation we and others previously reported,[12,28–30,33–41] will dictate the biotransport and uptake of the therapeutic before it reaches the targeted cells. Therefore, FA-targeted therapies *in vivo* are likely to operate by a different mechanism that those predicted by *in vitro* experiments in the absence of soluble FBP.

In the research presented here, we sought to leverage the interaction of therapeutics with serum FBP present *in vivo*. We took advantage of the fact that members of the antifolate (aFA) class of drugs bind to FBP due to the structural similarities between FA and aFAs.[22,23,41] We and others have reported that the most commonly used aFA, methotrexate (MTX), causes FBP aggregation similar to the aggregation processes induced by FA.[12,41] Protein aggregation is often considered to be an indication of disease or physiological disfunction (*e.g.*, β-amyloid formation associated with Alzheimer's disease).[42] With FBP, however, self-aggregation is postulated to be a natural and healthy process.[12,33–41] It has been shown that the FBP aggregates are quite stable.[39] This is consistent with research demonstrating clusters of FBP and FRs taken up into cells in one endocytosis event.[43–46] *In vitro* and *in vivo* work by Birn *et al.*,[47]Kur *et al.*,[48] and Piedrahita *et al.*[49] highlight the critical role FBP plays in uptake of FA, in healthy cellular processes, and embryonic development. In unpublished research, we also demonstrated that one large dose of MTX administered once per week inhibited tumor growth and was significantly less toxic than the same cumulative amount being divided into daily doses. We hypothesize this is because the initial dose of FBP swamps out endogenous serum FBP, and time between doses

is needed for the FBP to regenerate. When another dose is administered too soon, off-target uptake and toxicity increase.

In the context of this previous work, we hypothesized that by pre-binding MTX to FBP we could actively target FR-overexpressing cancer cells. In addition to providing a transport vehicle to the MTX, pre-binding the drug to FBP avoids the problem of over-saturating endogenous serum FBP, potentially leading to toxicity due to off-target uptake of MTX not bound to FBP.

Pre-binding already clinically approved drugs to serum proteins to increase targeting and efficacy is not unprecedented. Abraxane® is a 130 nm albumin-bound form of paclitaxel (Taxol ®) that is used to treat metastatic breast and pancreatic cancer and advanced lung cancer.[50,51] The biotrafficking of the drug is coupled to albumin trafficking and absorption, likely as a complex of one drug and one protein. A number of other albumin-based therapies are also already in the clinic or in clinical trials.[50,51] One of the major problems associated with using albumin, however, is that it is highly promiscuous – it is the most common human serum protein (0.6-0.7 mM). FBP is present at much lower concentrations than albumin and functions on a much more *specific* metabolic pathway associated with FA trafficking and cellular delivery. We therefore hypothesized that we could take advantage of the specific FBP trafficking pathway to deliver targeted therapy. The following *Communication* describes our first efforts testing this hypothesis using a KB xenograft model in mice.

5.3. Results and discussion

5.3.1. FBP as a therapeutic.

In this study we investigated whether pre-binding the antifolate cancer therapeutic MTX to FBP provided enhanced targeting of tumor cells and reduced toxicity. In an *in vivo* study using

a KB xenograft model in SCID mice, we compared how well three different ratios of MTX to FBP controlled tumor growth. Free MTX, free FBP, and saline were used as controls. Table 5.1 shows a summary of the treatment groups and survival outcomes. In all treatment groups with MTX (Groups A-D), the drug was administered at 0.3 mg/kg (approximately 10 μM in blood serum), giving a maximum cumulative dose of 5 mg/kg. FBP doses ranged from approximately 5-80 mg/kg (3-45 μM). Mouse blood volume was estimated at 1.2 mL.

Table 5.1. Summary of treatment groups and survival statistics. The cumulative mass ratio gives the theoretical maximum mass ratio of MTX and FBP that would have been administered if the mouse survived the entire 56-day trial (15 injections).

Group	Treatment	Molar ratio MTX:FBP	Dose (mg/kg) ratio MTX : FBP	Cumulative mass (mg/kg) ratio MTX:FBP	Day at LD_{50} (<3 mice surviving)	Day by which mice died/sacrificed
A	MTX only	1 : 0	0.3 : 0	5 : 0	N/A	56
B	MTX : FBP	1 : 0.25	0.3 : 5	5 : 80	31	56
C	MTX : FBP	1 : 1.1	0.3 : 24	5 : 353	35	38
D	MTX : FBP	1 : 3.7	0.3 : 79	5 : 1,186	18	21
E	FBP only	0 : 3.7	0 : 79	0 : 1,186	24	28
F	Saline	N/A	N/A	N/A	N/A	56

Figure 5.1 shows measured tumor volume as a function of time. The solid lines represent tumor growth up to lethality of (LD_{50}), and the dashed lines show the tumor growth for the remaining two mice past that point. Figure 5.2 shows the survival rate of the mice. All of the mice dosed with free MTX (Group A) survived the entirety of the 56-day trial, while mice given any MTX + FBP (Groups B-D) or FBP alone (Group E) experienced substantial toxicity effects. As discussed in detail below, this likely due to a combination of adverse responses to both FBP itself and increased toxicity from enhanced systemic uptake of MTX.

Despite concerns relating to the toxicity of the FBP-containing treatment and the survival rate of the mice, FBP alone (Group E) suppressed tumor growth. In fact, this group had the smallest tumors of all the treatment groups. This indicates that the protein itself can act as a

therapeutic. This effect of FBP has never before been reported, and its physiological mechanism is unknown. We hypothesize that FBP inhibited tumor growth by acting as a competitor for uptake of FA-bound FBP into the cancer cells, thus effectively starving the tumors of folate. In these studies, each dose in Group E (as well as Group D) resulted in serum FBP concentrations approximately four orders of magnitude higher than natural human FBP concentrations (40 µM after injection vs. 1-2 nM). It is unclear whether the folate starvation was a result of the tumors taking up the more available apo-FBP or if the tumors rejected apo-FBP (signaled by the conformational change in the protein upon ligand binding) but did not have sufficient access to FA-bound FBP. The mechanism and therapeutic efficacy of this potential treatment warrant further study.

Taking both survival and tumor inhibition into account, Group B fared the best. Based on these data, it is unclear whether the observed effect was due to the FBP only or a synergistic effect between FBP and MTX. Based on the slow rate of tumor growth as compared to free MTX (Group A) and the toxicity of the treatment – Group B was lethal (LD_{50}) by 31 days – it

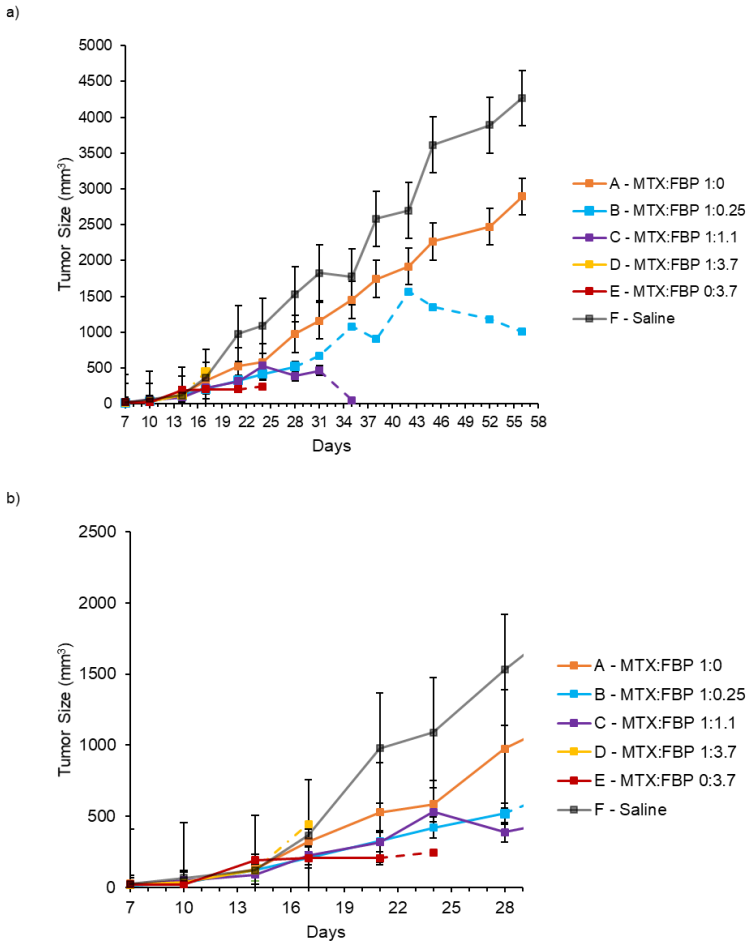

Figure 5.1. Tumor growth in SCID mice with KB xenografts during treatment with MTX+FBP, free MTX, free FBP, or saline (control). Solid lines represent the tumor growth up to lethality (LD_{50}) and the dashed lines represent the tumor growth for the remaining two mice in the treatment group. The vertical lines represent the standard deviation. a) Tumor growth over 56 days; b) Zoomed view of tumor growth over the first 28 days of the experiment.

appears that FBP is the primary contributor to the observed physiological outcomes. It is also possible that the combination of equal parts MTX and FBP (Group C) suppressed tumor growth, but none of the mice survived far enough into the study to know whether this trend would hold. The drop in tumor volume between Day 31 and Day 35 for the last remaining mouse in Group C is anomalous and unexplained. Regardless, these data indicate that FBP administered at lower doses than tested in this study could be therapeutically useful in inhibiting tumor growth. FBP could be used alone or synergistically with other drugs.

5.3.2. Toxicity of FBP-containing treatments

Despite the potential therapeutic properties of FBP or FBP+MTX, the data presented in Table 5.1, Figure 5.1, and Figure 5.2 demonstrate that high doses of FBP – even without any MTX present – were toxic. In Groups D and E, both of which had 3.7 equivalents of FBP, none of the mice survived past day 28, even with the tumor growth inhibition demonstrated in Group E. LD_{50} for Group D was 17 days, and all the animals in Group D died by day 21. It should also be noted that several mice in Groups D and E died approximately 30 seconds after injection, likely from stroke. If this phenomenon were to occur again in future experiments, the mice would be sent to a pathologist for further study. Mice given lower concentrations of FBP (Groups B and C) survived longer, but none lived to the end of the 56-day trial like the mice administered free MTX (Group A) and saline (Group F).

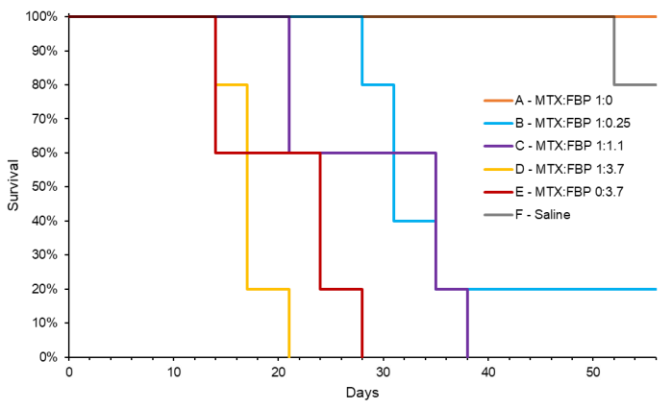

Figure 5.2. Survival rate of SCID mice bearing KB xenograft tumors treated with MTX+FBP, free MTX, free FBP, or saline (control). Each treatment group comprised five mice.

We propose several possible explanations for the toxicity results, some or all of which could have contributed to

the observed outcomes. The first is that the FBP itself was acutely toxic when administered at concentrations much higher than natural physiological levels. The animals may have experienced an adverse reaction to the rapid infusion of high concentrations of exogenous protein. In particular, this hypothesis may explain the sudden deaths (within one minute of injection) of several mice in Groups D and E. It is unclear why FBP was highly toxic to animals who survived immediately following the injection. Based on previous reports an immune response to the bovine FBP is not expected.[53]

The data from Group D suggest that in Groups B-D, the high toxicity was not due solely to the FBP itself, but from the FBP carrying MTX as well. As mentioned above and shown in the figures, the animals in Group D died most quickly. In designing this study, our hypothesis was that FBP would provide a vehicle for active targeting of the KB tumor cells. Additionally, the FBP would facilitate uptake of the MTX into the tumor cells. The results indicate, however, that FBP enhanced widespread, systemic uptake of MTX, not just targeted uptake into tumor cells. Combined the adverse reaction to FBP itself, the Group D treatment was highly toxic, which countered our initial hypotheses. In Groups B and C, the mice likely experienced toxicity effects from both FBP alone and enhanced, widespread uptake of MTX facilitated by FBP.

In general, these data suggest that FBP can therapeutically suppress tumor growth. Research testing lower concentrations of FBP that were used in this study will help to assess whether the toxicity effects can be minimized to acceptable levels. It is possible that the observed tumor growth inhibition was a toxicity-related effect. That is, sick mice do not grow big tumors, and the longer-surviving mice in Groups B and C did lose up to 30% of their body weight (mice in the other FBP groups did not experience such a weight loss because they did not survive long enough). However, this study was carried out at FBP concentrations approximately four orders

of magnitude higher than healthy blood serum levels, and the data show that even the lowest dose of FBP may have been therapeutic. Future dose-response studies should clarify the effect of FBP concentrations, both for the protein alone and in combination therapy.

5.3.3. Comparison to another folic acid-targeted polymer therapeutic.

As mentioned in the Introduction, we have unpublished data showing that a single dose of MTX is less toxic than the same cumulative dose spread out over multiple injections. Despite this, we designed this study to have a direct comparison to previous research carried out by colleagues (Kukowska-Latallo *et al.*) in which they tested poly(amidoamine) (PAMAM) dendrimers as a scaffold for a nanoscale therapeutic, injected twice weekly.[54] A dendrimer conjugate very similar to this one was eventually approved for Phase I clinical trials, and we wanted to be able to assess the tumor growth suppression our method achieved in that context. Furthermore, the more frequent dosing schedule provided a method of testing the hypothesis that MTX toxicity associated with more frequent dosing was caused by consumption of endogenous FBP – by pre-binding the MTX to FBP the deleterious effect could potentially be avoided.

The PAMAM dendrimers were conjugated to FA (targeting agent), MTX (therapeutic), and a fluorescent dye (imaging agent). In that study, the dose of MTX on the targeted conjugate was equal to the lowest dose of free MTX tested. In the research presented here, Groups A-D were administered MTX at the same concentration as the lowest dose tested in the Kukowska-Latallo *et al.* study.[54] The targeted PAMAM conjugate suppressed tumor growth to approximately 45% the volume of the tumors in mice administered saline, free MTX, or the carrier control. Additionally, the conjugate was not toxic over the course of the 56-day trial. Comparatively, the Group E treatment (FBP only) was lethal by day 24, but the tumors were suppressed to approximately 22% of the volume of the tumors in the saline group at the same

time point. In Group B, the group administered the lowest concentration of FBP, at lethality the tumor volume was 34% of the tumors in the mice treated with saline. At 56 days, the surviving mouse had a tumor approximately 24% the volume of the tumors in the saline-treated mice and 35% the volume of the mice treated with free MTX (Group A).

FBP offers potential advantages over synthetic (*e.g.* polymer, micelle, quantum dot) scaffolds. FBP is an endogenous serum protein and, therefore, avoids common immune reactions. The trafficking and biodistribution of nanomaterials injected into the bloodstream are often dictated by opsonization processes (formation of protein coronas) affecting their therapeutic efficacy. FBP will likely not induce the formation of further protein coronas, as aggregated FBP can be considered a type of protein corona itself.[12,28,30] The use of a serum protein as the targeted scaffold also avoids complications related to conjugation heterogeneity. Synthesizing targeted conjugates with multiple types of ligands (*i.e.*, targeting agents, drugs, and dyes) often results in thousands of different species.[13,24–27,55,56] When the resulting mixtures are tested *in vitro* and *in vivo*¸ it is impossible to know materials are inducing the observed outcomes. Given these advantages of FBP, we will pursue further research into using FBP itself as a therapeutic.

5.4. Conclusions and ongoing studies

This *Communication* presents new data demonstrating the possibility of using FBP targeted carrier for aFA therapies. Surprisingly, the results suggested that FBP itself may act as a cancer therapeutic. We demonstrated that FBP suppressed tumor growth. We hypothesize that the presence of unligated FBP at concentrations higher than serum FA led to folate starvation of the tumor cells. *In vitro* assays examining the effect of excess FBP on FA uptake and directly measuring FA levels in tissues will provide insights into this hypothesis. The studies presented

here did not include treatment of comparatively low doses of FBP alone (no pre-binding of MTX to FBP), but future studies will include an investigation of the therapeutic efficacy of FBP over a wide range of concentrations. The treatment group with the lowest dose of FBP (which had MTX present) still displayed tumor suppression. We predict that by decreasing the FBP concentration more and removing the MTX we can still achieve a therapeutic effect while decreasing the toxicity. Finally, future work will include research exploring how FBP-induced folate starvation could be synergistic with other therapies, *e.g.*, with 5-fluorouracil.[57,58] It will also include research on the observed systemic toxicity, by radiolabeling the FBP to examine which tissues take it up. Overall, these early results present a promising new endogenous protein therapy that negates the need for a toxic small molecule chemotherapeutic and avoids problems associated with the manufacturing process, immunogenicity, and biodegradability in synthetic targeted drug delivery scaffolds.

5.5. Materials and methods

5.5.1. Materials

All materials were purchased from commercial sources. Folic acid and methotrexate were purchased from Sigma-Aldrich (St. Louis, MO) and used as received. Whey powder was purchased from Z Natural Foods (West Palm Beach, FL).

5.5.2. FBP isolation and purification

FBP was isolated from bovine whey powder according to previously published methods.[11,30] Multiple isolations were performed to acquire enough protein, and all batches were combined and thoroughly mixed prior to characterization. The fully combined batch of FBP was used in the animal trials. The concentration (w/w) of the FBP in the powder was

determined using a NanoDrop Fluorospectrometer. FBP purity was assessed by fluorescence spectroscopy, AFM, SDS−PAGE, and MALDI TOF-MS as previously described.[11,30]

Note that bovine FBP was used for this study. Bovine FBP and human FBP have >80% homology overall, including 100% homology in the binding pocket.[22,52] The human and bovine forms have been shown to exhibit similar aggregation phenomena.[33–41] For this work, we have employed the substantially more accessible bovine FBP. Previous *in vivo* studies found no adverse effects of homologous (*e.g.*, goat FBP used in goats) versed heterologous (*e.g.*, goat FBP used in rats) FBP circulation.[53]

5.5.3. Preparation of treatment solutions

For all treatment solutions, 10% extra volume was prepared (0.220 mL total) to account for loss in the syringe.

MTX+FBP solutions: The powder resulting from the FBP isolation was 1.71% (w/w) FBP in sodium acetate. The powder was dissolved in water and centrifuged against a 10,000 MWCO filter to remove the sodium acetate. The final solution contained 8.4 mg/mL FBP. Given this constraint, the highest molar ratio of MTX:FBP that could be delivered was 1:3.7. FBP in PBS solutions were prepared at concentrations such that, for each treatment group, the correct amount of FBP could be delivered in a 0.2 mL injection. The solutions were aliquoted into individual vials and 20 μL of MTX stock solution added so that the final MTX dose was 0.33 mg/kg (5 mg/kg total over 15 doses). The three molar ratios of MTX:FBP were 1:0.25, 1:1.1, and 1:3.7.

FBP only solution: The highest concentration FBP solution was aliquoted (0.2 mL) as described above, but instead of adding MTX, 20 μL of PBS was added to bring the final volume to 220 μL.

MTX only solutions: A solution of MTX in PBS at 0.33 mg/kg/dose (0.033 mg/mL) and aliquoted.

5.5.4. Animal model

Female Fox Chase severe combined immunodeficient (SCID CB17) mice were purchased from Charles River (Wilmington, MA). The mice were housed in a specific animal-care facility at the University of Michigan Medical Center in accordance with the regulations of the University's Committee on the Use and Care of Animals as well as with

federal guidelines. Animals were fed *ad libitum* with folic acid deficient mouse chow from Test Diets (Richmond, IN) for three weeks before tumor cell injections.

5.5.5. Xenograft tumor treatment

Directly after lifting and collecting the cells, the cell suspension ($4x10^6$ cells in 0.2 mL PBS) was injected s.c. into the right flank of each mouse. The tumors were allowed to grow for seven days before starting treatment. Twice a week, the animals were injected via the tail vein with MTX + FBP (three ratios), FBP only, MTX only, or saline. Each treatment group comprised five mice. Each dose was administered in 0.2 mL of PBS (saline). In all treatment groups with MTX, each MTX dose was 0.3 mg/kg, to give a theoretical maximum cumulative dose of 5 mg/kg if a mouse received all 15 treatments in the 56-day trial. The final cumulative doses were not identical due to different survival rates between the groups. Tumors were measured using calipers. Tumor volume was estimated using the standard formula of an ellipsoid: $V = 4/3\pi(l/2 * w/2 * d/2)$, where l = length, w=width, and d=depth. Using the assumption that $\pi=3$ and width=depth, the equation used to calculate tumor volume simplifies to: $V = (l*w^2)/2$. The body weight of all the mice was monitored throughout the study as an indication of adverse toxicity effects.

5.6. References

(1) Low, P. S.; Henne, W. A.; Doorneweerd, D. D. Discovery and Development of Folic-Acid-Based Receptor Targeting for Imaging and Therapy of Cancer and Inflammatory Diseases. *Acc. Chem. Res.* **2008**, *41* (1), 120–129.

(2) Low, P. S.; Kularatne, S. A. Folate-Targeted Therapeutic and Imaging Agents for Cancer. *Curr. Opin. Chem. Biol.* **2009**, *13* (3), 256–262.

(3) Sega, E.; Low, P. Tumor Detection Using Folate Receptor-Targeted Imaging Agents. *Cancer Metastasis Rev.* **2008**, *27* (4), 655–664.

(4) Hilgenbrink, A. R.; Low, P. S. Folate Receptor-Mediated Drug Targeting: From Therapeutics to Diagnostics. *J. Pharm. Sci.* **2005**, *94* (10), 2135–2146.

(5) Leamon, C. P.; Reddy, J. A. Folate-Targeted Chemotherapy. *Adv. Drug Deliv. Rev.* **2004**, *56* (8), 1127–1141.

(6) Assaraf, Y. G.; Leamon, C. P.; Reddy, J. A. The Folate Receptor as a Rational Therapeutic Target for Personalized Cancer Treatment. *Drug Resistance Updates*. 2014.

(7) Sudimack, J.; Lee, R. J. Targeted Drug Delivery via the Folate Receptor. *Adv. Drug Deliv. Rev.* **2000**, *41* (2), 147–162.

(8) Wu, Y.; Guo, R.; Wen, S.; Shen, M.; Zhu, M.; Wang, J.; Shi, X. Folic Acid-Modified Laponite Nanodisks for Targeted Anticancer Drug Delivery. *J. Mater. Chem. B Mater. Biol. Med.* **2014**, *2* (42), 7410–7418.

(9) Hu, Y.; Wang, R.; Wang, S.; Ding, L.; Li, J.; Luo, Y.; Wang, X.; Shen, M.; Shi, X. Multifunctional Fe_3O_4 @ Au Core/shell Nanostars: A Unique Platform for Multimode Imaging and Photothermal Therapy of Tumors. *Sci. Rep.* **2016**, *6* (February), 28325.

(10) Ward, B. B.; Dunham, T.; Majoros, I. J.; Baker, J. R. Targeted Dendrimer Chemotherapy in an Animal Model for Head and Neck Squamous Cell Carcinoma. *J. Oral Maxillofac. Surg.* **2011**, *69* (9), 2452–2459.

(11) Chen, J.; van Dongen, M. A.; Merzel, R. L.; Dougherty, C. A.; Orr, B. G.; Kanduluru, A. K.; Low, P. S.; Marsh, E. N. G.; Banaszak Holl, M. M. Substrate-Triggered Exosite Binding: Synergistic Dendrimer/Folic Acid Action for Achieving Specific, Tight-Binding to Folate Binding Protein. *Biomacromolecules* **2016**, *17* (3), 922–927.

(12) Merzel, R. L.; Boutom, S. M.; Chen, J.; Frey, C.; Shedden, K.; Marsh, E. N. G.; Banaszak Holl, M. M. Folate Binding Protein: Therapeutic Natural Nanotechnology for Folic Acid, Methotrexate, and Leucovorin. *Nanoscale* **2017**, *9* (7), 2603–2615.

(13) van Dongen, M. A.; Silpe, J. E.; Dougherty, C. A.; Kanduluru, A. K.; Choi, S. K.; Orr, B. G.; Low, P. S.; Banaszak Holl, M. M. Avidity Mechanism of Dendrimer–Folic Acid Conjugates. *Mol. Pharm.* **2014**, *11* (5), 1696–1706.

(14) Mullen, D. G.; McNerny, D. Q.; Desai, A.; Cheng, X.; DiMaggio, S. C.; Kotlyar, A.; Zhong, Y.; Qin, S.; Kelly, C. V; Thomas, T. P.; *et al.* Design, Synthesis, and Biological Functionality of a Dendrimer-Based Modular Drug Delivery Platform. *Bioconjug. Chem.* **2011**, *22* (4), 679–689.

(15) Weitman, S. D.; Weinberg, A. G.; Coney, L. R.; Zurawski, V. R.; Jennings, D. S.; Kamen, B. A. Cellular Localization of the Folate Receptor: Potential Role in Drug Toxicity and Folate Homeostasis. *Cancer Res.* **1992**, *52* (23), 6708–6711.

(16) Campbell, I. G.; Jones, T. A.; Foulkes, W. D.; Trowsdale, J. Folate-Binding Protein Is a Marker for Ovarian Cancer Folate-Binding Protein Is a Marker for Ovarian Cancer. *CANCER Res.* **1991**, *51* (33), 5329–5338.

(17) Weitman, S. D.; Lark, R. H.; Coney, L. R.; Fort, D. W.; Frasca, V.; Zurawski, V. R.; Kamen, B. A. Distribution of the Folate Receptor GP38 in Normal and Malignant Cell Lines and Tissues. *Cancer Res.* **1992**, *52* (12), 3396–3401.

(18) Ross, J. F.; Chaudhuri, P. K.; Ratnam, M. Differential Regulation of Folate Receptor Isoforms in Normal and Malignant Tissues in Vivo and in Established Cell Lines. Physiologic and Clinical Implications. *Cancer* **1994**, *73* (9), 2432–2443.

(19) Bandara, N. A.; Hansen, M. J.; Low, P. S. Effect of Receptor Occupancy on Folate Receptor Internalization. *Mol. Pharm.* **2014**, *11* (3), 1007–1013.

(20) Bailey, L. B.; Gregory, J. F. Folate Metabolism and Requirements. *J. Nutr.* **1999**, *129* (4), 779–782.

(21) Kompis, I. M.; Islam, K.; Then, R. L. DNA and RNA Synthesis: Antifolates. *Chemical Reviews*. American Chemical Society 2005, pp 593–620.

(22) Chen, C.; Ke, J.; Zhou, X. E.; Yi, W.; Brunzelle, J. S.; Li, J.; Yong, E.-L.; Xu, H. E.; Melcher, K. Structural Basis for Molecular Recognition of Folic Acid by Folate Receptors. *Nature* **2013**, *500* (7463), 486–489.

(23) Wibowo, A. S.; Singh, M.; Reeder, K. M.; Carter, J. J.; Kovach, A. R.; Meng, W.; Ratnam, M.; Zhang, F.; Dann, C. E. Structures of Human Folate Receptors Reveal Biological Trafficking States and Diversity in Folate and Antifolate Recognition. *Proc. Natl. Acad. Sci.* **2013**, *110* (38), 15180–15188.

(24) van Dongen, M. A.; Rattan, R.; Silpe, J.; Dougherty, C.; Michmerhuizen, N. L.; Van Winkle, M.; Huang, B.; Choi, S. K.; Sinniah, K.; Orr, B. G.; *et al.* Poly(amidoamine) Dendrimer–Methotrexate Conjugates: The Mechanism of Interaction with Folate Binding Protein. *Mol. Pharm.* **2014**, *11* (11), 4049–4058.

(25) van Dongen, M. A.; Dougherty, C. A.; Banaszak Holl, M. M. Multivalent Polymers for Drug Delivery and Imaging: The Challenges of Conjugation. *Biomacromolecules* **2014**, *15* (9), 3215–3234.

(26) Mullen, D. G.; Banaszak Holl, M. M. Heterogeneous Ligand–Nanoparticle Distributions: A Major Obstacle to Scientific Understanding and Commercial Translation. *Acc. Chem. Res.* **2011**, *44* (11), 1135–1145.

(27) Mullen, D. G.; Fang, M.; Desai, A.; Baker, J. R.; Orr, B. G.; Banaszak Holl, M. M. A Quantitative Assessment of Nanoparticle−Ligand Distributions: Implications for Targeted Drug and Imaging Delivery in Dendrimer Conjugates. *ACS Nano* **2010**, *4* (2), 657–670.

(28) Merzel, R. L.; Chen, J.-J.; Marsh, E. N. G.; Holl, M. M. B. Folate Binding protein—Outlook for Drug Delivery Applications. *Chinese Chem. Lett.* **2015**, *26* (4), 426–430.

(29) Chen, J.; Klem, S.; Jones, A. K.; Orr, B.; Banaszak Holl, M. M. Folate-Binding Protein Self-Aggregation Drives Agglomeration of Folic Acid Targeted Iron Oxide Nanoparticles. *Bioconjug. Chem.* **2017**, *28* (1), 81–87.

(30) Merzel, R. L.; Frey, C.; Chen, J.; Garn, R.; van Dongen, M.; Dougherty, C. A.; Kandaluru, A. K.; Low, P. S.; Marsh, E. N. G.; Banaszak Holl, M. M. Conjugation Dependent Interaction of Folic Acid with Folate Binding Protein. *Bioconjug. Chem.* **2017**, *28* (9), 2350–2360.

(31) Hoier-Madsen, M.; Holm, J.; Hansen, S. I.; Høier-madsen, M.; Holm, J.; Hansen, S. I. α Isoforms of Soluble and Membrane-Linked Folate-Binding Protein in Human Blood. *Biosience Reports* **2008**, *28* (3), 153–160.

(32) Kamen, B. A. Folate Receptors and Therapeutic Applications. In *Targeted Drug Strategies for Cancer and Inflammation*; Jackman, A. L., Leamon, C. P., Eds.; Springer, 2011.

(33) Pedersen, T.; Svendsen, I.; Hansen, S.; Holm, J.; Lyngbye, J. Aggregation of a Folate-Binding Protein from Cow's Milk. *Carlsberg Res. Commun.* **1980**, *45* (2), 161–166.

(34) Hansen, S. I.; Holm, J.; Lyngbye, J.; Pedersen, T. G.; Svendsen, I. Dependence of Aggregation and Ligand Affinity on the Concentration of the Folate-Binding Protein from Cow's Milk. *Arch. Biochem. Biophys.* **1983**, *226* (2), 636–642.

(35) Holm, J.; Schou, C.; Babol, L. N.; Lawaetz, A. J.; Bruun, S. W.; Hansen, M. Z.; Hansen, S. I. The Interrelationship between Ligand Binding and Self-Association of the Folate Binding Protein. The Role of Detergent?tryptophan Interaction. *Biochim. Biophys. Acta - Gen. Subj.* **2011**, *1810* (12), 1330–1339.

(36) Holm, J.; Lawaetz, A. J.; Hansen, S. I. Ligand Binding Induces a Sharp Decrease in Hydrophobicity of Folate Binding Protein Assessed by 1-Anilinonaphthalene-8-Sulphonate Which Suppresses Self-Association of the Hydrophobic Apo-Protein. *Biochem. Biophys. Res. Commun.* **2012**, *425* (1), 19–24.

(37) Christensen, U.; Holm, J.; Hansen, S. I. Stopped-Flow Kinetic Studies of the Interaction of Bovine Folate Binding Protein (FBP) and Folate. *Biosci. Rep.* **2006**, *26* (4), 291–299.

(38) Kaarsholm, N. C.; Kolstrup, A.-M.; Danielsen, S. E.; Holm, J.; Hansen, S. I. Ligand-Induced Conformation Change in Folate-Binding Protein. *Biochem. J.* **1993**, *292* (3), 921–925.

(39) Holm, J.; Babol, L. N.; Markova, N.; Lawaetz, A. J.; Hansen, S. I. The Interrelationship between Ligand Binding and Thermal Unfolding of the Folate Binding Protein. The Role of Self-Association and pH. *Biochim. Biophys. Acta - Proteins Proteomics* **2014**, *1844* (3), 512–519.

(40) Bruun, S. W.; Holm, J.; Hansen, S. I.; Jacobsen, S. Application of Near-Infrared and Fourier Transform Infrared Spectroscopy in the Characterization of Ligand-Induced Conformation Changes in Folate Binding Protein Purified from Bovine Milk: Influence of Buffer Type and pH. *Appl. Spectrosc.* **2006**, *60* (7), 737–746.

(41) Bruun, S. W.; Holm, J.; Hansen, S. I.; Andersen, C. M.; Norgaard, L.; Nørgaard, L. A Chemometric Analysis of Ligand-Induced Changes in Intrinsic Fluorescence of Folate Binding Protein Indicates a Link between Altered Conformational Structure and Physico-Chemical Characteristics. *Appl. Spectrosc.* **2009**, *63* (12), 1315–1322.

(42) Chiti, F.; Dobson, C. M. Amyloid Formation by Globular Proteins under Native Conditions. *Nat. Chem. Biol.* **2009**, *5* (1), 15–22.

(43) Rothberg, K. G.; Ying, Y. S.; Kamen, B. A.; Anderson, R. G. Cholesterol Controls the Clustering of the Glycophospholipid-Anchored Membrane Receptor for 5-Methyltetrahydrofolate. *J. Cell Biol.* **1990**, *111* (6).

(44) Rothberg, K. G.; Ying, Y. S.; Kolhouse, J. F.; Kamen, B. A.; Anderson, R. G. The Glycophospholipid-Linked Folate Receptor Internalizes Folate without Entering the Clathrin-Coated Pit Endocytic Pathway. *J. Cell Biol.* **1990**, *110* (3).

(45) Smart, E. J.; Mineo, C.; Anderson, R. G. W. Clustered Folate Receptors Deliver 5-Methyltetrahydrofolate to Cytoplasm of MA104 Cells. *J. Cell Biol.* **1996**, *134* (5), 1169–1177.

(46) Moradi, E.; Vllasaliu, D.; Garnett, M.; Falcone, F.; Stolnik, S. Ligand Density and Clustering Effects on Endocytosis of Folate Modified Nanoparticles. *RSC Adv.* **2012**, *2* (7), 3025.

(47) Birn, H.; Zhai, X. Y.; Holm, J.; Hansen, S. I.; Jacobsen, C.; Christensen, E. I.; Moestrup, S. K. Megalin Binds and Mediates Cellular Internalization of Folate Binding Protein. *FEBS J.* **2005**, *272* (17), 4423–4430.

(48) Kur, E.; Mecklenburg, N.; Cabrera, R. M.; Willnow, T. E.; Hammes, A. LRP2 Mediates Folate Uptake in the Developing Neural Tube. *J. Cell Sci.* **2014**, *127* (10), 2261–2268.

(49) Piedrahita, J. A.; Oetama, B.; Bennett, G. D.; Van Waes, J.; Kamen, B. A.; Richardson, J.; Lacey, S. W.; Anderson, R. G. W.; Finnell, R. H. Mice Lacking the Folic Acid-Binding Protein Folbp1 Are Defective in Early Embryonic Development. *Nat. Genet.* **1999**, *23* (2),

228–232.

(50) Kratz, F.; Elsadek, B. Clinical Impact of Serum Proteins on Drug Delivery. *J. Control. Release* **2012**, *161* (2), 429–445.

(51) Elsadek, B.; Kratz, F. Impact of Albumin on Drug Delivery — New Applications on the Horizon. *J. Control. Release* **2012**, *157* (1), 4–28.

(52) Sadasivan, E.; Rothenberg, S. P. The Complete Amino-Acid Sequence of a Human Folate Binding Protein from KB Cells Determined from the cDNA. *J. Biol. Chem.* **1989**, *264* (10), 5806–5811.

(53) Rubinolf, M.; Abramson, R.; Schreiber, C.; Waxman, S. Effect of a Folate-Binding Protein on the Plasma Transport and Tissue Distribution of Folic Acid. *Acta Haematol.* **1981**, *65* (3), 145–152.

(54) Kukowska-Latallo, J. F.; Candido, K. A.; Cao, Z.; Nigavekar, S. S.; Majoros, I. J.; Thomas, T. P.; Balogh, L. P.; Khan, M. K.; Baker, J. R. Nanoparticle Targeting of Anticancer Drug Improves Therapeutic Response in Animal Model of Human Epithelial Cancer. *Cancer Res.* **2005**, *65* (12).

(55) Dougherty, C. A.; Furgal, J. C.; van Dongen, M. A.; Goodson, T.; Banaszak Holl, M. M.; Manono, J.; DiMaggio, S. Isolation and Characterization of Precise Dye/Dendrimer Ratios. *Chem. – A Eur. J.* **2014**, *20* (16), 4638–4645.

(56) Dougherty, C. A.; Vaidyanathan, S.; Orr, B. G.; Banaszak Holl, M. M. Fluorophore:Dendrimer Ratio Impacts Cellular Uptake and Intracellular Fluorescence Lifetime. *Bioconjug. Chem.* **2015**, *26* (2), 304–315.

(57) Backus, H. H. J.; Pinedo, H. M.; Wouters, D.; Padrón, J. M.; Molders, N.; Van Der Wilt, C. L.; Van Groeningen, C. J.; Jansen, G.; Peters, G. J. Folate Depletion Increases Sensitivity of Solid Tumor Cell Lines to 5-Fluorouracil and Antifolates. *Int. J. Cancer* **2000**, *87* (6), 771–778.

(58) Tucker, J. M.; Davis, C.; Kitchens, M. E.; Bunni, M. A.; Priest, D. G.; Spencer, H. T.; Berger, F. G. Response to 5-Fluorouracil Chemotherapy Is Modified by Dietary Folic Acid Deficiency in ApcMin/+mice. *Cancer Lett.* **2002**, *187* (1–2), 153–162.

CHAPTER 6. Conclusions

6.1. Summary and future outlook

The body of research presented in this dissertation focused on characterizing and understanding the self-aggregation of serum FBP into nanoparticles. We sought to develop greater scientific understanding of the connection between the structure of nanoparticulate FBP and its biological function and activity. Inspired by therapeutics using serum proteins as carriers,[1–5] our goal was to investigate the possibility of using FBP itself as a delivery vector.

Before now, other researchers have extensively investigated the self-aggregation of FBP as a function of both concentration and ligand binding.[6–14] In particular, they were interested in the role FA plays in these processes. FA is necessary for DNA synthesis and can only be obtained through diet.[15–18] FA binds strongly to both FRs and soluble FBP, and researchers postulated FBP assists in the biotransport and cellular uptake, helps prevent degradation, and protects against bacterial utilization of FA.[19–22] The aggregated, nanoparticulate form of FBP may play a role in these processes. The size of the FBP aggregates (*i.e.*, the degree of aggregation) likely acts as signaling mechanism to cells regarding what FBPNP is carrying. This hypothesis agrees well with microscopy images showing clustered FBP at sites of FA endocytosis, as well as data presented here on changes to FBPNP size as a function of ligand identity.[23,24] Recently, researchers have demonstrated *in vitro* and *in vivo* the critical role FBP plays in cellular uptake of FA and embryonic development.[25,26]

These earlier studies on concentration- and ligand-dependent aggregation of FBP were limited by the detection limits of the analytical techniques used: FBP concentrations were at least

an order of magnitude higher (and usually more) than physiological concentrations. In our work, we sought to build upon this previous research and extend the study of FBP aggregation and activity to biologically relevant conditions.

Chapter 2[27] is a mini-review on serum proteins as delivery vectors, as well as the specific advantages and challenges associated with FBP. It provides broader context for our research on FBP aggregation and outlines a general approach for our subsequent work. Data up to that point from our group and others indicated that FBP aggregation is natural, healthy, and occurs *in vivo.* In addition, some of our more recent research focused on the binding interactions of FA-PAMAM conjugates with FBP and their relationship to the FBP aggregation process.[28,29] We postulated it was possible to control the degree of aggregation and therefore influence the biological activity of the FBPNP through the conjugate. FBP has a key advantage over other serum proteins (primarily albumin) used as vectors: it has a particular role in folate metabolism and follows a specific trafficking pathway. This would allow it to function as a targeted vector. As a comparison, albumin, which is used in several clinically approved therapies, is present at much higher concentrations and much more promiscuous in terms of its binding of molecules, trafficking pathways, and biological activity.[1–5] As a critical component in the folate metabolic pathway, FBP is mechanistically linked to the antifolate class of drugs. We hypothesized that by pre-binding these drugs to FBP prior to injection, we could increase specificity and decrease toxicity. This key hypothesis informed the rest of the research presented here.

Chapter 3[30] focused on the binding interaction between FBP and FA, MTX, and LEUC. We examined FBP aggregation as a function of FBP concentration, ligand identity, and ligand

concentration on a particle-by-particle basis using AFM. Analysis of the FBPNP distributions, as opposed to reliance on averaged values obtained from bulk measurements, yielded valuable insights about the role of FBP in transporting small molecules. FBPNP with healthy levels of FA had a different distribution than FBPNP with therapeutic levels of MTX. These data suggest that the *in vivo* mechanism for MTX trafficking follows a different pathway than the pathway for FA. This is consistent with previous *in vitro* data showing that MTX is taken up into cells through different membrane receptor than FA. However, it is unclear the extent to which the role of soluble FBP was considered in these studies, and explicit inclusion of it in *in vitro* experiments could yield different results. Further investigation on the mechanism of action of MTX, and other antifolate drugs, would be a valuable line of research to pursue, particularly with the ultimate goal of developing methods to increase efficacy and decrease toxicity of these drugs. Analysis of distributions of FA-FBPNP and LEUC-FBPNP at therapeutically relevant concentrations of the ligands also produced surprising results. FBP exposed to high concentrations of FA resulted in FBPNP nearly identical to the distributions of unligated FBP and MTX-FBP at high MTX concentrations. Comparatively, FBPNP with of healthy levels of FA or therapeutically relevant levels LEUC and had distributions that were not statistically different. This suggests that therapeutic levels of FA are transported like MTX. As a result, high doses of FA cannot bypass the MTX trafficking pathway and mitigate toxicity effects. This is consistent with data indicating that healthy levels of FA and therapeutic MTX enter cells via different uptake pathways. The FBPNP formed with therapeutic levels of LEUC are indistinguishable from healthy FA-FBPNP, allowing LEUC to follow the FA trafficking pathways. These results provided the first mechanistic explanation for the puzzling phenomenon that LEUC must be used for FA rescue because FA itself has no therapeutic benefit at the required concentrations.

Chapter 4[31] built upon our work analyzing the small molecule-FBP interactions, as well as previous efforts in making and characterizing PAMAM dendrimers with precise numbers of ligands.[28,29,32–36] Using four different FA-polymer conjugates (two FA-PAMAM dendrimers and two FA-PEG conjugates), we examined the FBP aggregation process as a function of polymer identity and conjugation method. For these studies, we employed both AFM and fluorescence spectroscopy.[37] The complementary data obtained from both techniques provided important information on conformational changes in FBP upon ligand binding and FBP aggregation. Notably, the data illustrated the risks in relying only on bulk techniques (fluorescence spectroscopy in solution in this case) to reach conclusions on the structure of biological materials.

Fluorescence spectroscopy experiments showed that FA, either free or conjugated, induced conformational changes throughout the FBP population, even with an excess of FBP. Conformational changes in ligated FBP started a cascade through which unligated FBP also underwent a conformational rearrangement. The only way for this to have occurred was through aggregation, a result confirmed by AFM, as described below. By fluorescence spectroscopy, $G5_{Ac}$-$FA_{4(avg)}$ appeared to have a similar interaction with FBP as FA with FBP. They induced the same degree of fluorescence quenching, indicating comparable levels of FBP conformational change. In the absence of other information, it could be interpreted that $G5_{Ac}$-$FA_{4(avg)}$ could form the basis of a successful targeting vector. However, AFM studies showed that FA and $G5_{Ac}$-$FA_{4(avg)}$ induced dramatically different aggregation processes in FBP. The FA-FBPNP distribution was shifted towards smaller particles than the distributions of unligated FBPNP, while $G5_{Ac}$-$FA_{4(avg)}$-FBPNP distributions contained significantly larger particles than unligated FBPNP. $G5_{Ac}$-COG-$FA_{1.0}$ produced strong fluorescence quenching and very large FBP aggregates, even

at sub-stoichiometric concentrations. At stoichiometric concentrations of $G5_{Ac}$-COG-$FA_{1.0}$ and FBP, AFM images showed excess polymer on the surface, indicating that each $G5_{Ac}$-COG-$FA_{1.0}$ was aggregating more than one FBP. PEG-FA of all chain lengths and at all concentrations disrupted FBPNP and prevented the formation of new nanoparticles.

As argued above, the structure of FBPNP is critical for trafficking of FA, and our data show that the FA conjugates produced FBPNP that are significantly different than the FBPNP formed with free FA. As a result, the conjugates and FA would likely follow different biological pathways, diminishing the therapeutic targeting effects of the conjugations. Furthermore, PEG is the most common polymer in biomedical applications, and its inclusion in targeted therapeutics should be carefully considered. Disruption of natural FBP aggregation may not only result in off-target uptake of drugs but also artificially induce folate deficiency. These studies illustrate some of the challenges of clinical translation of targeted conjugates and highlight the importance of considering specific serum protein interactions in the rational design of delivery vectors.

As described in Chapter 5,[38] we applied our knowledge of distributions and our insights on the role of FBP in the folate metabolic pathway to testing our key hypothesis. Using KB xenograft tumor model in mice, we investigated whether pre-binding MTX to FBP would increase therapeutic efficacy and reduce toxicity. As a control, we included a group treated with only FBP, and we obtained the remarkable and entirely unexpected result that FBP alone dramatically reduced tumor growth. We hypothesize that the presence of unligated FBP at concentrations higher than serum FA led to folate starvation of the tumor cells. This means, there was no need for treatment to include a toxic chemotherapeutic such as MTX. The groups treated with MTX and FBP also showed inhibition of tumor growth, but toxicity increased with FBP

concentration. It is likely that instead of specifically targeting the cancer cells, FBP facilitated widespread uptake of MTX, resulting in systemic toxicity. These data indicate that by solely manipulating the serum concentration of FBP, by administering endogenous protein, it may be possible to treat a wide range of tumor types. This would be a completely novel approach to treating to treating a variety of cancers. The next step in this research is to follow up on these results by testing the therapeutic efficacy of lower concentrations of FBP.

These results are particularly interesting when viewed in the context of the success of Abraxane, an albumin-bound form of paclitaxel.[1–5] Abraxane is considered is one of the most impactful achievements in drug delivery over the last decade. Many more albumin-based approaches are currently under development or in clinical trials. Researchers recently reported a cancer vaccine using albumin as a carrier showing great promise in *in vivo* trials.[39] FBP-based approaches, discussed at length in this dissertation, present an interesting contrast to albumin-based approaches since FBP is present at far lower serum concentrations and is much more selective regarding cell uptake.

As demonstrated through this body of research, heterogeneity and serum protein interactions are two significant obstacles to clinical translation. Researchers may turn more towards protein-based therapies to mitigate these challenges. In addition, protein-based therapies help to avoid problems of immunogenicity, deleterious serum protein interactions, and biodegradability associated with synthetic targeted therapies.

Characterizing and understanding the role of nanoparticle distributions was a central theme of the research presented in this dissertation. This work not only built upon colleagues' earlier efforts on targeted drug delivery projects but also drew from methods and expertise

developed on tissue analysis projects. The examples discussed in the Introduction (Chapter 1, to be submitted) illustrate how this body of work leveraged 20+ years of the research team's institutional knowledge and expertise. The FA-conjugates themselves are the product of years of research and several doctoral degrees focused on identifying, characterizing, and controlling heterogeneous mixtures.[28,29,32–36,40,41] Our studies on FBPNP distributions depended on image analysis and statistical methods developed for research on heterogeneity in collagen structure.[42–49] The translation and application of all these techniques in combination was critical for yielding valuable insights on the role of FBP in biotrafficking pathways. The scientific understanding we developed allowed us to expand our efforts to examining the role of FBP in an *in vivo* tumor model, with remarkable preliminary results.

In addition to showcasing these specific scientific achievements, this dissertation aims to make a broader argument on heterogeneity and distributions in biological materials. The magnitude and role of heterogeneity in biological materials is often underappreciated. The ways in which analytical techniques or methods of data interpretation mask heterogeneity is not often considered. As a result, *in vivo* results do not match predictions from *in vitro* models, clinical research on mechanisms of disease or therapy is slowed, and clinical translation is hindered. In the new research presented in this dissertation, as well as the cases discussed in the Introductions, we show how explicit consideration of distributions was necessary for reaching key biological conclusions. We make the case here for widespread investment in molecular level analyses of biological materials and the development of methods to facilitate this research. Understanding molecular level distributions is critical for interpreting the interplay between structural variation and function.

6.2. References

(1) Kratz, F.; Elsadek, B. Clinical Impact of Serum Proteins on Drug Delivery. *J. Control. Release* **2012**, *161* (2), 429–445.

(2) Elsadek, B.; Kratz, F. Impact of Albumin on Drug Delivery — New Applications on the Horizon. *J. Control. Release* **2012**, *157* (1), 4–28.

(3) Kratz, F. Albumin as a Drug Carrier: Design of Prodrugs, Drug Conjugates and Nanoparticles. *J. Control. Release* **2008**, *132* (3), 171–183.

(4) Merlot, A. M.; Kalinowski, D. S.; Richardson, D. R. Unraveling the Mysteries of Serum Albumin - More than Just a Serum Protein. *Front. Physiol.* **2014**, *5*, 1–7.

(5) Larsen, M. T.; Kuhlmann, M.; Hvam, M. L.; Howard, K. A. Albumin-Based Drug Delivery: Harnessing Nature to Cure Disease. *Mol. Cell. Ther.* **2016**, *4*, 3.

(6) Pedersen, T.; Svendsen, I.; Hansen, S.; Holm, J.; Lyngbye, J. Aggregation of a Folate-Binding Protein from Cow's Milk. *Carlsberg Res. Commun.* **1980**, *45* (2), 161–166.

(7) Hansen, S. I.; Holm, J.; Lyngbye, J.; Pedersen, T. G.; Svendsen, I. Dependence of Aggregation and Ligand Affinity on the Concentration of the Folate-Binding Protein from Cow's Milk. *Arch. Biochem. Biophys.* **1983**, *226* (2), 636–642.

(8) Holm, J.; Schou, C.; Babol, L. N.; Lawaetz, A. J.; Bruun, S. W.; Hansen, M. Z.; Hansen, S. I. The Interrelationship between Ligand Binding and Self-Association of the Folate Binding Protein. The Role of Detergent?tryptophan Interaction. *Biochim. Biophys. Acta - Gen. Subj.* **2011**, *1810* (12), 1330–1339.

(9) Holm, J.; Lawaetz, A. J.; Hansen, S. I. Ligand Binding Induces a Sharp Decrease in Hydrophobicity of Folate Binding Protein Assessed by 1-Anilinonaphthalene-8-Sulphonate Which Suppresses Self-Association of the Hydrophobic Apo-Protein. *Biochem. Biophys. Res. Commun.* **2012**, *425* (1), 19–24.

(10) Christensen, U.; Holm, J.; Hansen, S. I. Stopped-Flow Kinetic Studies of the Interaction of Bovine Folate Binding Protein (FBP) and Folate. *Biosci. Rep.* **2006**, *26* (4), 291–299.

(11) Kaarsholm, N. C.; Kolstrup, A.-M.; Danielsen, S. E.; Holm, J.; Hansen, S. I. Ligand-Induced Conformation Change in Folate-Binding Protein. *Biochem. J.* **1993**, *292* (3), 921–925.

(12) Holm, J.; Babol, L. N.; Markova, N.; Lawaetz, A. J.; Hansen, S. I. The Interrelationship between Ligand Binding and Thermal Unfolding of the Folate Binding Protein. The Role of Self-Association and pH. *Biochim. Biophys. Acta - Proteins Proteomics* **2014**, *1844* (3), 512–519.

(13) Bruun, S. W.; Holm, J.; Hansen, S. I.; Jacobsen, S. Application of Near-Infrared and Fourier Transform Infrared Spectroscopy in the Characterization of Ligand-Induced

Conformation Changes in Folate Binding Protein Purified from Bovine Milk: Influence of Buffer Type and pH. *Appl. Spectrosc.* **2006**, *60* (7), 737–746.

(14) Bruun, S. W.; Holm, J.; Hansen, S. I.; Andersen, C. M.; Norgaard, L.; Nørgaard, L. A Chemometric Analysis of Ligand-Induced Changes in Intrinsic Fluorescence of Folate Binding Protein Indicates a Link between Altered Conformational Structure and Physico-Chemical Characteristics. *Appl. Spectrosc.* **2009**, *63* (12), 1315–1322.

(15) Bailey, L. B.; Gregory, J. F. Folate Metabolism and Requirements. *J. Nutr.* **1999**, *129* (4), 779–782.

(16) Kompis, I. M.; Islam, K.; Then, R. L. DNA and RNA Synthesis: Antifolates. *Chemical Reviews*. American Chemical Society 2005, pp 593–620.

(17) Chen, C.; Ke, J.; Zhou, X. E.; Yi, W.; Brunzelle, J. S.; Li, J.; Yong, E.-L.; Xu, H. E.; Melcher, K. Structural Basis for Molecular Recognition of Folic Acid by Folate Receptors. *Nature* **2013**, *500* (7463), 486–489.

(18) Wibowo, A. S.; Singh, M.; Reeder, K. M.; Carter, J. J.; Kovach, A. R.; Meng, W.; Ratnam, M.; Zhang, F.; Dann, C. E. Structures of Human Folate Receptors Reveal Biological Trafficking States and Diversity in Folate and Antifolate Recognition. *Proc. Natl. Acad. Sci.* **2013**, *110* (38), 15180–15188.

(19) Colman, N.; Hettiarachchy, N.; Herbert, V. Detection of a Milk Factor That Facilitates Folate Uptake by Intestinal Cells. *Science*. 1981, pp 1427–1429.

(20) Salter, D. N.; Blakeborough, P. Influence of Goat's-Milk Folate-Binding Protein on Transport of 5-Methyltetrahydrofolate in Neonatal-Goat Small Intestinal Brush-Border-Membrane Vesicles. *Br J Nutr* **1988**, *59* (3), 497–507.

(21) Mason, J. B.; Selhub, J. Folate-Binding Protein and the Absorption of Folic Acid in the Small Intestine of the Suckling Rat. *Am. J. Clin. Nutr.* **1988**, *48* (3), 620–625.

(22) Ford, J. E.; Scott, K. J.; Sansom, B. F.; Taylor, P. J. Some Observations on the Possible Nutritional Significance of Vitamin B12-and Folate-Binding Proteins in Milk. Absorption of [58Co]cyanocobalamin by Suckling Piglets. *Br. J. Nutr.* **1975**, *34* (3), 469–492.

(23) Rothberg, K. G.; Ying, Y. S.; Kolhouse, J. F.; Kamen, B. A.; Anderson, R. G. The Glycophospholipid-Linked Folate Receptor Internalizes Folate without Entering the Clathrin-Coated Pit Endocytic Pathway. *J. Cell Biol.* **1990**, *110* (3).

(24) Rothberg, K. G.; Ying, Y. S.; Kamen, B. A.; Anderson, R. G. Cholesterol Controls the Clustering of the Glycophospholipid-Anchored Membrane Receptor for 5-Methyltetrahydrofolate. *J. Cell Biol.* **1990**, *111* (6).

(25) Birn, H.; Zhai, X. Y.; Holm, J.; Hansen, S. I.; Jacobsen, C.; Christensen, E. I.; Moestrup, S. K. Megalin Binds and Mediates Cellular Internalization of Folate Binding Protein. *FEBS J.* **2005**, *272* (17), 4423–4430.

(26) Kur, E.; Mecklenburg, N.; Cabrera, R. M.; Willnow, T. E.; Hammes, A. LRP2 Mediates Folate Uptake in the Developing Neural Tube. *J. Cell Sci.* **2014**, *127* (10), 2261–2268.

(27) Merzel, R. L.; Chen, J.-J.; Marsh, E. N. G.; Holl, M. M. B. Folate Binding protein—Outlook for Drug Delivery Applications. *Chinese Chem. Lett.* **2015**, *26* (4), 426–430.

(28) van Dongen, M. A.; Silpe, J. E.; Dougherty, C. A.; Kanduluru, A. K.; Choi, S. K.; Orr, B. G.; Low, P. S.; Banaszak Holl, M. M. Avidity Mechanism of Dendrimer–Folic Acid Conjugates. *Mol. Pharm.* **2014**, *11* (5), 1696–1706.

(29) van Dongen, M. A.; Rattan, R.; Silpe, J.; Dougherty, C.; Michmerhuizen, N. L.; Van Winkle, M.; Huang, B.; Choi, S. K.; Sinniah, K.; Orr, B. G.; et al. Poly(amidoamine) Dendrimer–Methotrexate Conjugates: The Mechanism of Interaction with Folate Binding Protein. *Mol. Pharm.* **2014**, *11* (11), 4049–4058.

(30) Merzel, R. L.; Boutom, S. M.; Chen, J.; Frey, C.; Shedden, K.; Marsh, E. N. G.; Banaszak Holl, M. M. Folate Binding Protein: Therapeutic Natural Nanotechnology for Folic Acid, Methotrexate, and Leucovorin. *Nanoscale* **2017**, *9* (7), 2603–2615.

(31) Merzel, R. L.; Frey, C.; Chen, J.; Garn, R.; van Dongen, M.; Dougherty, C. A.; Kandaluru, A. K.; Low, P. S.; Marsh, E. N. G.; Banaszak Holl, M. M. Conjugation Dependent Interaction of Folic Acid with Folate Binding Protein. *Bioconjug. Chem.* **2017**, *28* (9), 2350–2360.

(32) van Dongen, M. A.; Desai, A.; Orr, B. G.; Baker, J. R.; Banaszak Holl, M. M.; Baker Jr, J. R.; Banaszak Holl, M. M. Quantitative Analysis of Generation and Branch Defects in G5 Poly(amidoamine) Dendrimer. *Polymer.* **2013**, *54* (16), 4126–4133.

(33) Dougherty, C. A.; Furgal, J. C.; van Dongen, M. A.; Goodson, T.; Banaszak Holl, M. M.; Manono, J.; DiMaggio, S. Isolation and Characterization of Precise Dye/Dendrimer Ratios. *Chem. – A Eur. J.* **2014**, *20* (16), 4638–4645.

(34) Dougherty, C. A.; Vaidyanathan, S.; Orr, B. G.; Banaszak Holl, M. M. Fluorophore:Dendrimer Ratio Impacts Cellular Uptake and Intracellular Fluorescence Lifetime. *Bioconjug. Chem.* **2015**, *26* (2), 304–315.

(35) Mullen, D. G.; Banaszak Holl, M. M. Heterogeneous Ligand–Nanoparticle Distributions: A Major Obstacle to Scientific Understanding and Commercial Translation. *Acc. Chem. Res.* **2011**, *44* (11), 1135–1145.

(36) Mullen, D. G.; Fang, M.; Desai, A.; Baker, J. R.; Orr, B. G.; Banaszak Holl, M. M. A Quantitative Assessment of Nanoparticle−Ligand Distributions: Implications for Targeted Drug and Imaging Delivery in Dendrimer Conjugates. *ACS Nano* **2010**, *4* (2), 657–670.

(37) Chen, J.; van Dongen, M. A.; Merzel, R. L.; Dougherty, C. A.; Orr, B. G.; Kanduluru, A. K.; Low, P. S.; Marsh, E. N. G.; Banaszak Holl, M. M. Substrate-Triggered Exosite Binding: Synergistic Dendrimer/Folic Acid Action for Achieving Specific, Tight-Binding to Folate Binding Protein. *Biomacromolecules* **2016**, *17* (3), 922–927.

(38) Merzel, R. L.; Chen, J.; Frey, C.; Jones, Alexis, K.; Vartanian, M.; Ward, B. B.; Banaszak Holl, M. M. Folate Binding Protein Inhibits Tumor Growth. *Submitted*.

(39) Zhu, G.; Lynn, G. M.; Jacobson, O.; Chen, K.; Liu, Y.; Zhang, H.; Ma, Y.; Zhang, F.; Tian, R.; Ni, Q.; et al. Albumin/vaccine Nanocomplexes That Assemble in Vivo for Combination Cancer Immunotherapy. *Nat. Commun.* **2017**, *8* (1), 1954.

(40) Mullen, D. G.; Desai, A.; van Dongen, M. A.; Barash, M.; Baker, J. R.; Banaszak Holl, M. M. Best Practices for Purification and Characterization of PAMAM Dendrimer. *Macromolecules* **2012**, *45* (12), 5316–5320.

(41) van Dongen, M. A.; Dougherty, C. A.; Banaszak Holl, M. M. Multivalent Polymers for Drug Delivery and Imaging: The Challenges of Conjugation. *Biomacromolecules* **2014**, *15* (9), 3215–3234.

(42) Erickson, B.; Fang, M.; Wallace, J. M.; Orr, B. G.; Les, C. M.; Banaszak Holl, M. M. Nanoscale Structure of Type I Collagen Fibrils: Quantitative Measurement of D-Spacing. *Biotechnol. J.* **2013**, *8* (1), 117–126.

(43) Wallace, J. M.; Chen, Q.; Fang, M.; Erickson, B.; Orr, B. G.; Banaszak Holl, M. M. Type I Collagen Exists as a Distribution of Nanoscale Morphologies in Teeth, Bones, and Tendons. *Langmuir* **2010**, *26* (10), 7349–7354.

(44) Wallace, J. M.; Erickson, B.; Les, C. M.; Orr, B. G.; Banaszak Holl, M. M. Distribution of Type I Collagen Morphologies in Bone: Relation to Estrogen Depletion. *Bone* **2010**, *46* (5), 1349–1354.

(45) Fang, M.; Liroff, K. G.; Turner, A. S.; Les, C. M.; Orr, B. G.; Holl, M. M. B. Estrogen Depletion Results in Nanoscale Morphology Changes in Dermal Collagen. *J. Invest. Dermatol.* **2012**, *132* (7), 1791–1797.

(46) Fang, M.; Goldstein, E. L.; Turner, A. S.; Les, C. M.; Orr, B. G.; Fisher, G. J.; Welch, K. B.; Rothman, E. D.; Banaszak Holl, M. M. Type I Collagen D-Spacing in Fibril Bundles of Dermis, Tendon, and Bone: Bridging between Nano- and Micro-Level Tissue Hierarchy. *ACS Nano* **2012**, *6* (11), 9503–9514.

(47) Fang, M.; Holl, M. M. B. Variation in Type I Collagen Fibril Nanomorphology: The Significance and Origin. *Bonekey Rep.* **2013**, *2*.

(48) Cauble, M. A.; Rothman, E.; Welch, K.; Fang, M.; Duong, L. T.; Pennypacker, B. L.; Orr, B. G.; Banaszak-Holl, M. M. Alteration of Type I Collagen Microstructure Induced by Estrogen Depletion Can Be Prevented with Drug Treatment. *Bonekey Rep.* **2015**, *4*, 697.

(49) Cauble, M. A.; Muckley, M. J.; Fang, M.; Fessler, J. A.; Welch, K.; Rothman, E. D.; Orr, B. G.; Duong, L. T.; Holl, M. M. B. Estrogen Depletion and Drug Treatment Alter the Microstructure of Type I Collagen in Bone. *Bone Reports* **2016**, *5*, 243–251.

Appendix A. Supplementary Information for Chapter 3: Folate binding protein: Therapeutic Natural Nanotechnology for Folic Acid, Methotrexate, and Leucovorin

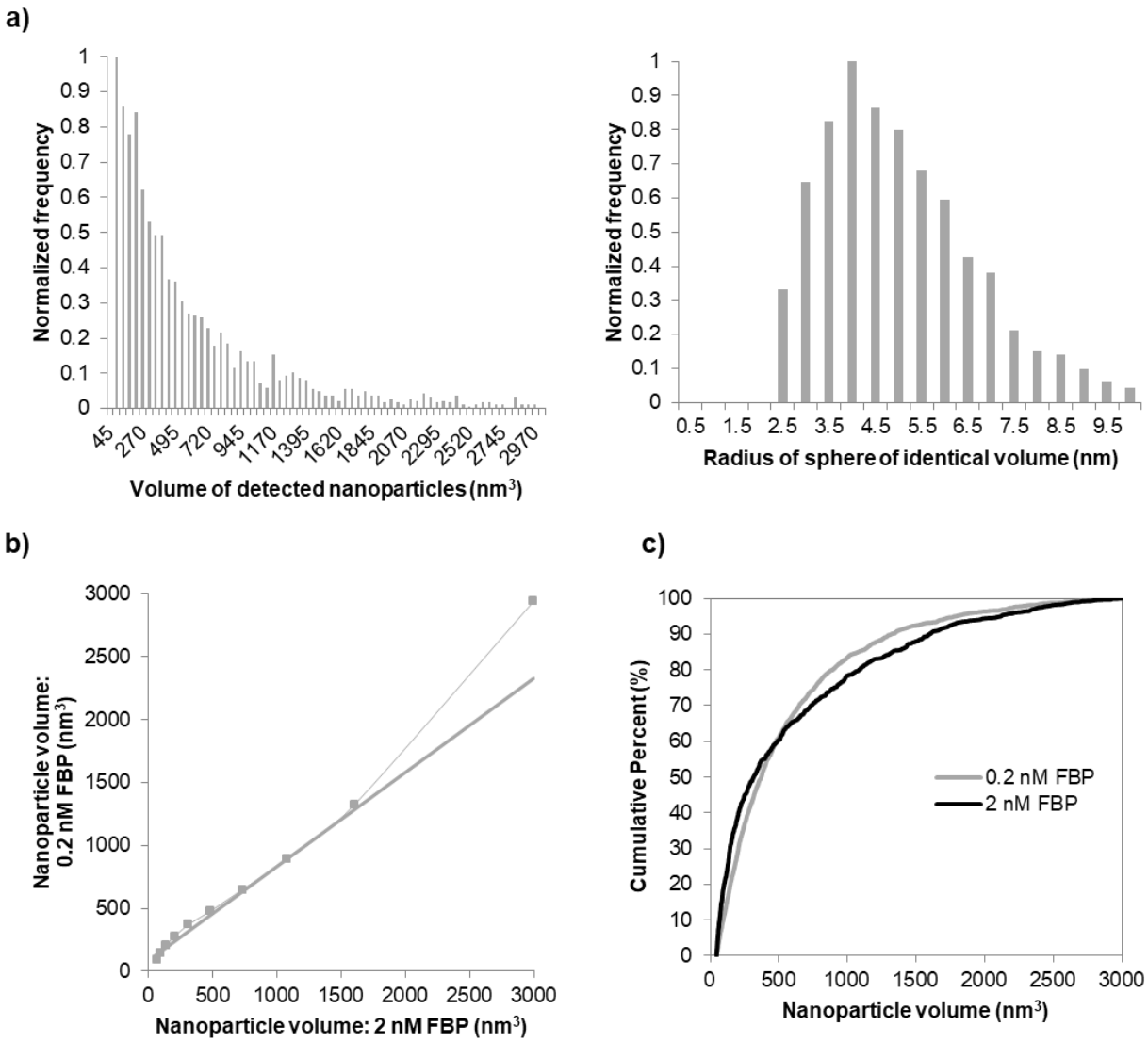

Figure A.1. a) Histograms; b) Q-Q plots; c) and CDF plots for the FBPNP formed from 0.2 nM FBP. The K-S test comparing FBPNP at 0.2 nM and 2 nM protein rejected the null hypothesis, indicating the two nanoparticle populations are statistically different.

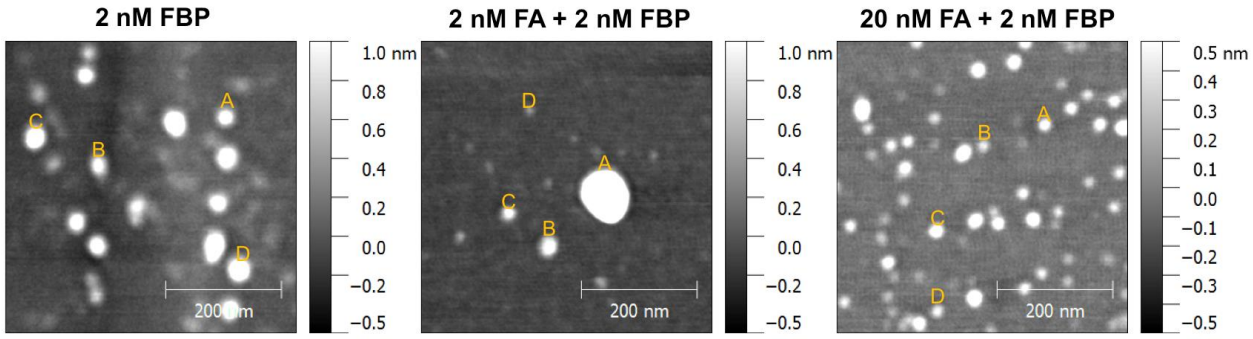

	Radius (nm)	#FBP
A	6.2	22
B	5.7	17
C	7.4	37
D	8.0	48

	Radius (nm)	# FBP
A	18.3	570
B	5.9	19
C	4.6	9
D	2.9	2

	Radius (nm)	# FBP
A	3.6	4
B	3.1	3
C	4.4	8
D	3.1	3

Figure A.2. Representative detailed frames of AFM images showing FBP nanoparticles. Idealized spherical radii and the number of FBP comprising each selected nanoparticle are provided.

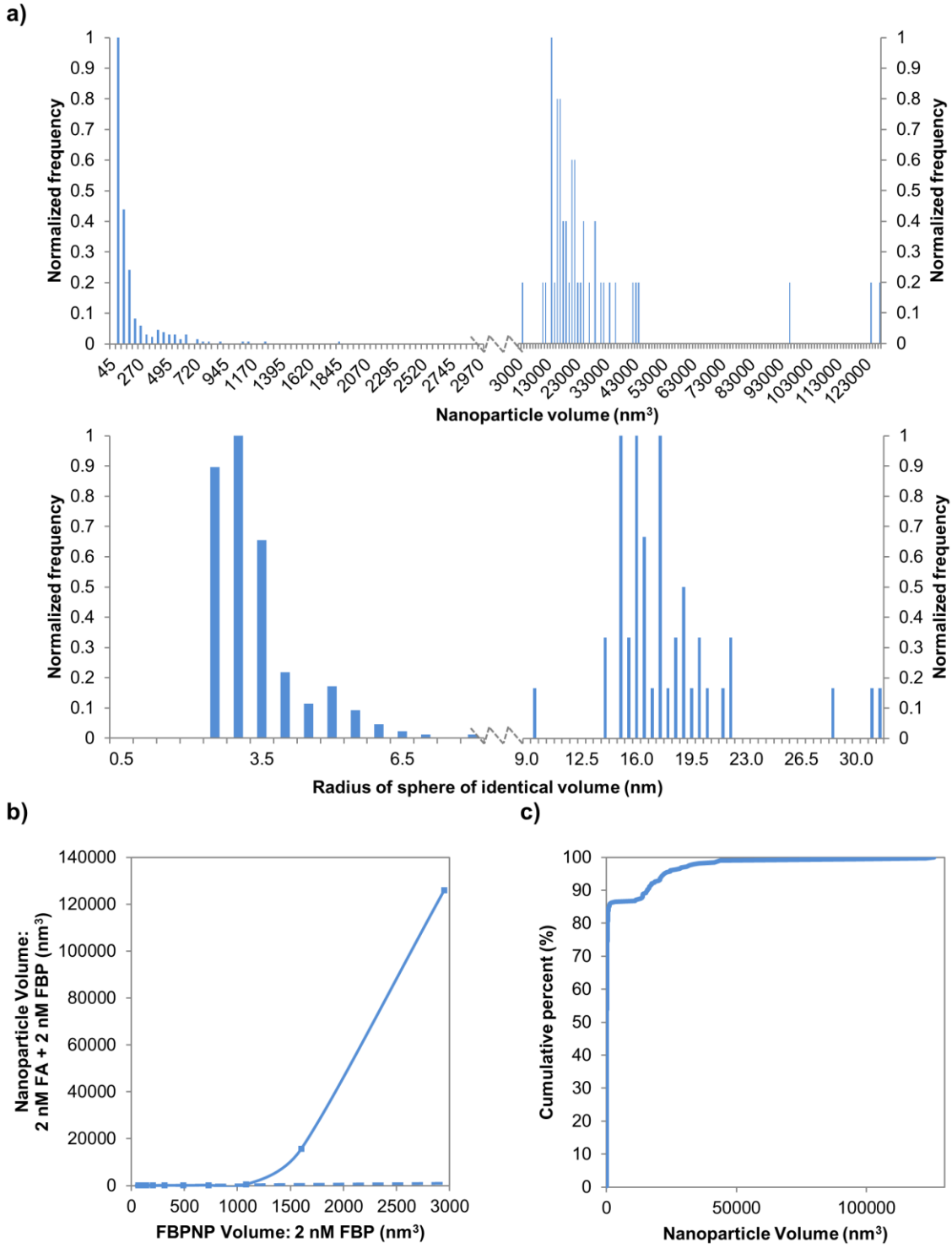

Figure A.3. Histograms, Q-Q plots, and CDF plots of the full data set of FBPNP formed from 2 nM FA + 2 nM FBP demonstrating the biomodal distribution of FBPNP volumes.

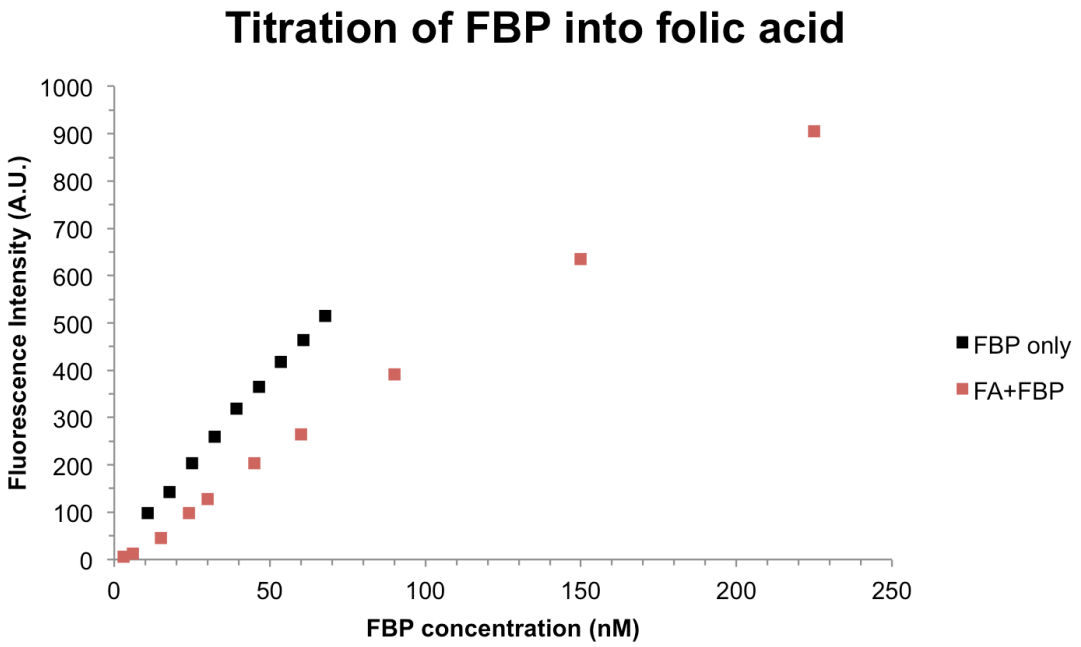

Figure A.4. Titration of FBP into FA (30 nM). Trytophan fluorescence was excited at 280 nm and emission detected at 340 nm. The flatter slope of the ligated FBP fluorescence is suggests asymmetrical aggregation of apo- and holo-FBP.

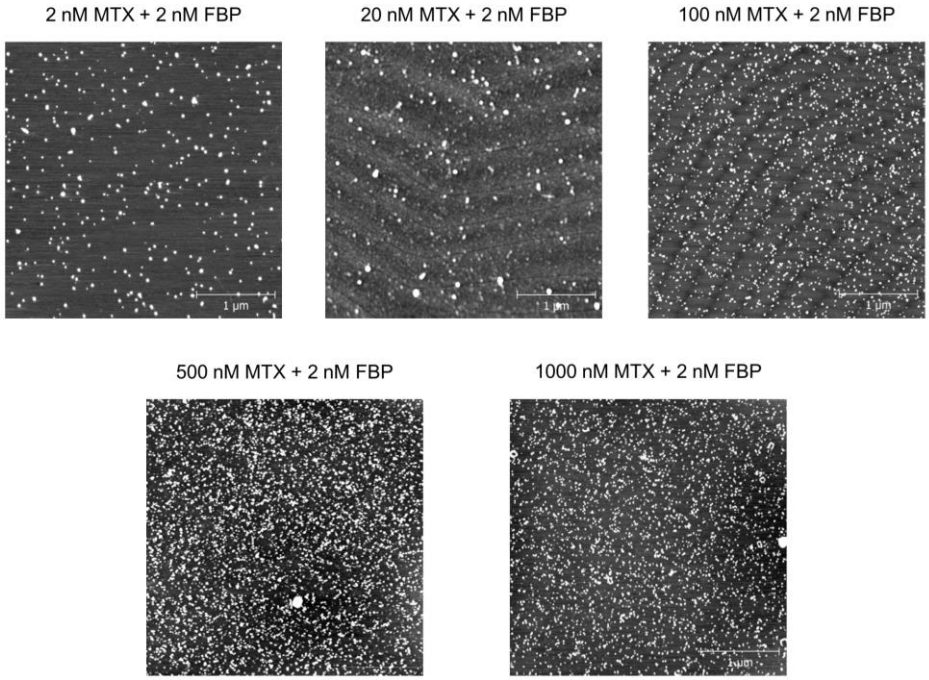

Figure A.5. AFM images of FBPNP formed from a range of MTX:FBP ratios. For all samples, the FBP concentration was held constant at 2 nM in 1x PBS. AFM images were captured by spin coating the solutions onto freshly-cleaved mica.

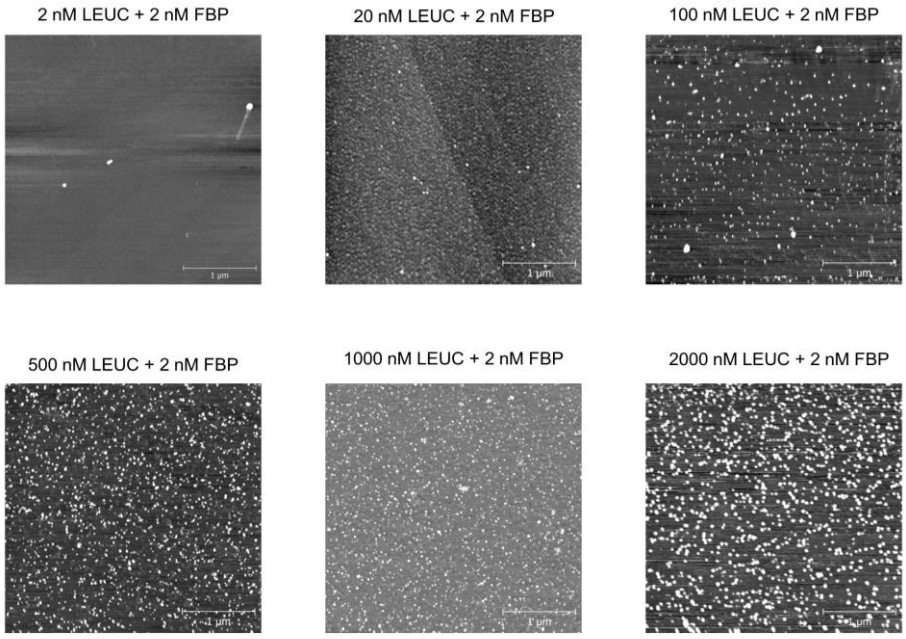

Figure A.6. AFM images of FBPNP formed from a range of LEUC:FBP ratios. For all samples, the FBP concentration was held constant at 2 nM in 1x PBS. AFM images were captured by spin coating the solutions onto freshly-cleaved mica.

Tango Plot

Thu May 07 23:18:48 CEST 2015

Provided by :
Centre de Regulacio Genomica
Serrano group

Beta aggregation

pH = 7.4
Temperature = 298.15
Ionic Strength = 0.02
Nterm = No Protection
Cterm = No Protection

Peptide :

MAWQMTQLLLLALVAAAWGAQAPRTPRARTDLLNVCMDAKHHKAEPGPED
SLHEQCSPWRKNACCSVNTSIEAHKDISYLYRFNWDHCGKMEPACKRHFI
QDTCLYECSPNLGPWIREVNQRWRKERVLGVPLCKEDCQSWWEDCRTSYT
CKSNWHKGWNWTSGYNQCPVKAACHRFDFYFPTPAALCNEIWSHSYKVSN
YSRGSGRCIQMWFDPFQGNPNEEVARFYAENPTSGSTPQGI

Plot :

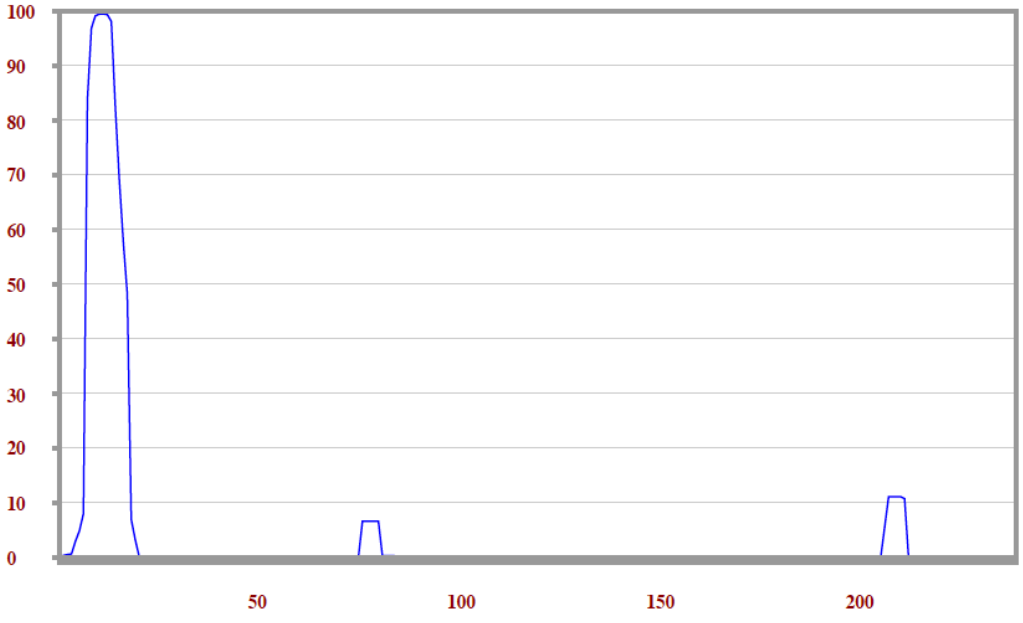

Thanks for using TANGO

Page : 1

Figure A.7. TANGO output for bovine apo-FBP (P02702). The N-terminus 8-18 LLLLALVAAAW sequence has ~99% aggregation tendency at 10 μM (the lowest concentration with which the code is compatible).

Tango Plot

Thu May 07 23:28:35 CEST 2015

Provided by :
Centre de Regulacio Genomica
Serrano group

Beta aggregation

pH = 7
Temperature = 298.15
Ionic Strength = 0.02
Nterm = No Protection
Cterm = No Protection

Peptide :

MAQRMTTQLLLLLVWVAVVGEAQTRIAWARTELLNVCMNAKHHKEKPGPE
DKLHEQCRPWRKNACCSTNTSQEAHKDVSYLYRFNWNHCGEMAPACKRHF
IQDTCLYECSPNLGPWIQQVDQSWRKERVLNVPLCKEDCEQWWEDCRTSY
TCKSNWHKGWNWTSGFNKCAVGAACQPFHFYFPTPTVLCNEIWTHSYKVS
NYSRGSGRCIQMWFDPAQGNPNEEVARFYAAAMSGAGPWAAWPFLLSLAL

Plot :

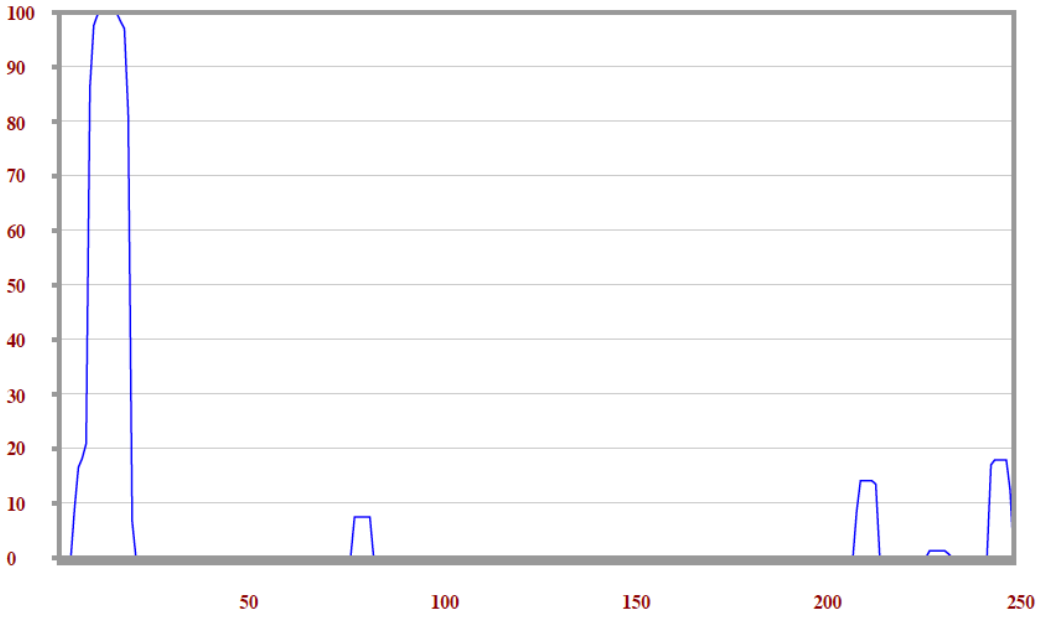

Thanks for using TANGO

Page : 1

Figure A.8. TANGO output for human apo-hFRα(P02702)+FA. The N-terminus 9-19 LLLLVWVAVV sequence has ~99% aggregation tendency at 10 μM (the lowest concentration with which the code is compatible).

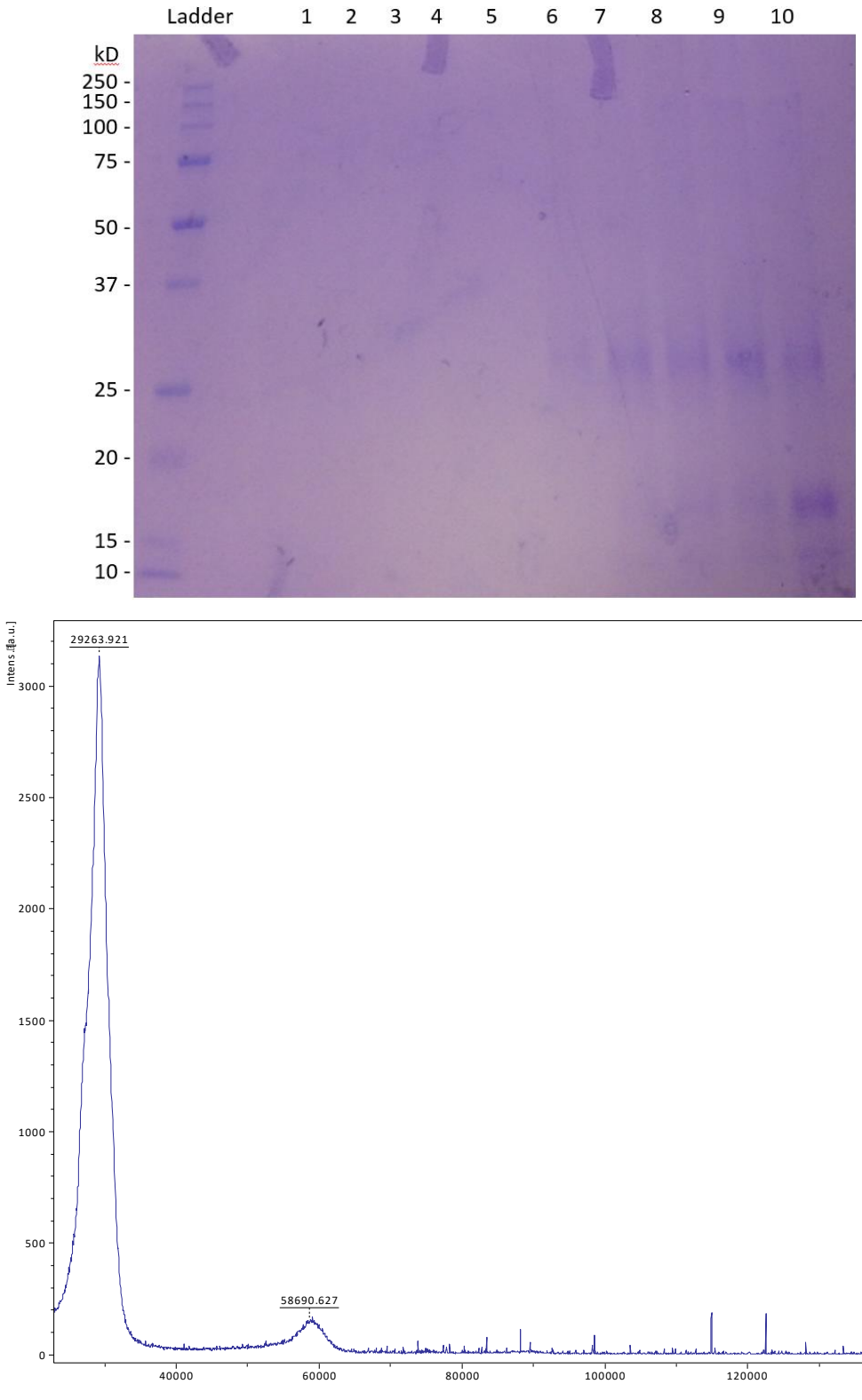

Figure A.9. SDS-PAGE and MALDI of FBP. The protein were collected by fractions and the ~29kDa fractions were pooled together. The FBP exhibited a molecular weight distribution around ~29kDa because of glycosylation at residue 68N and 160N.

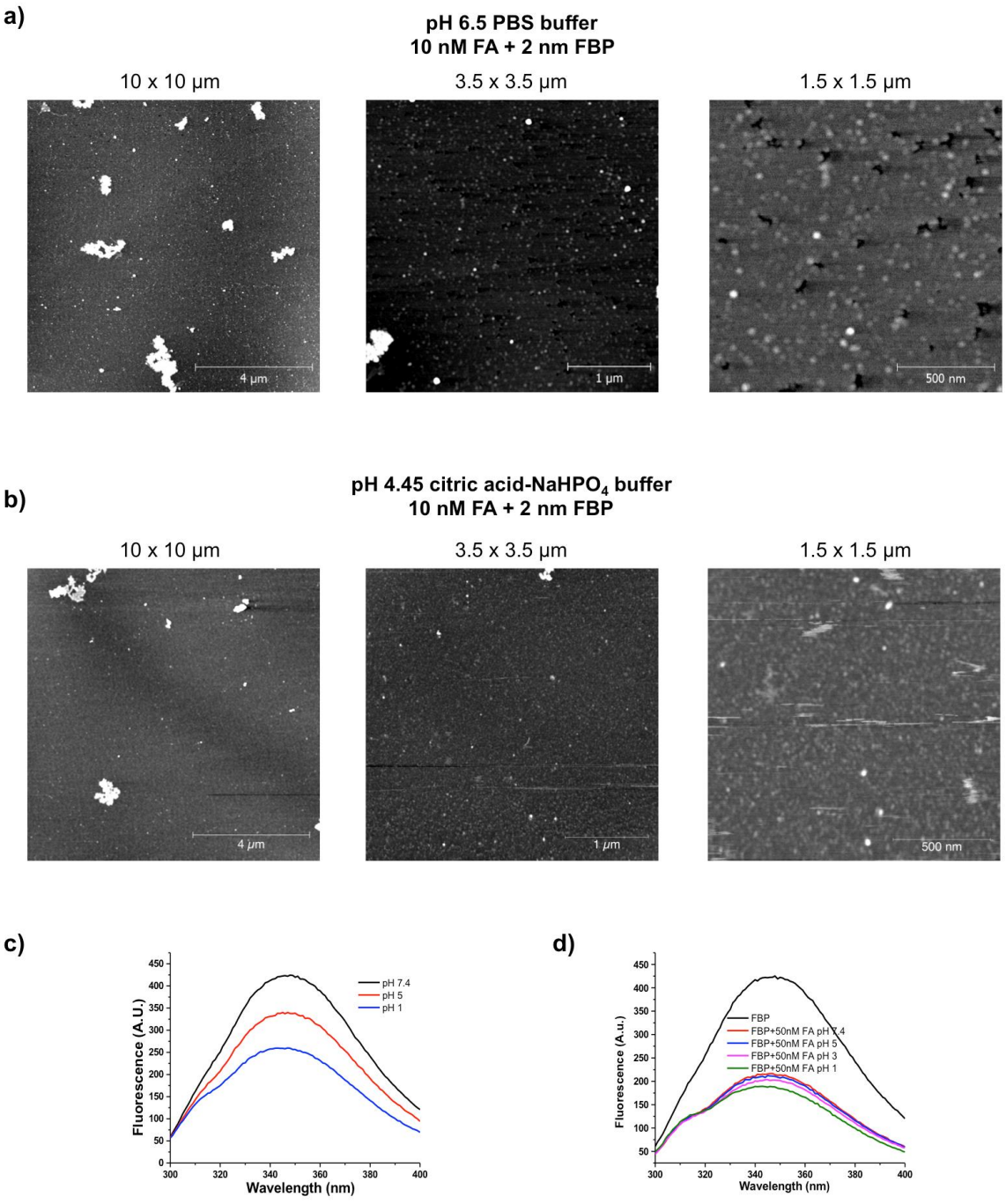

Figure A.10. AFM images of 10 nM FA + 2 nM FBP at pH 6.5; b) AFM images of 10 nM FA + 2 nM FBP at pH 4.45. Images in both (a) and (b) show substantially less nanoparticle formation as compared to FA+FBP solution at pH 7.4; c) Tryptophan fluorescence of FBP over a range of pH values ([FBP] = 58 nM); d) Tryptophan fluorescence of FBP (58 nM) in the presence of FA (50 nM). Excitation: 280 nM; Emission: 340 nM

Appendix B. Supplementary Information for Chapter 4: Conjugation Dependent Interaction of Folic Acid with Folate Binding Protein

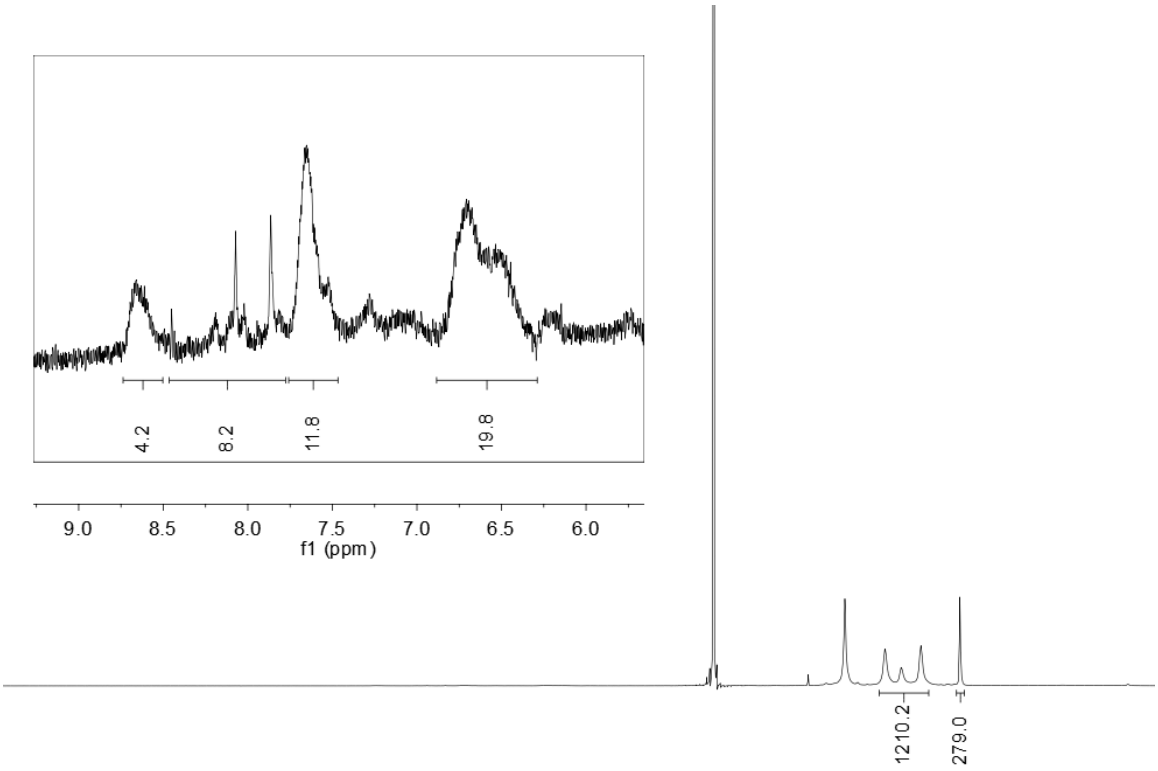

Figure B.1. ^{1}H NMR spectrum (D_2O) of $G5_{Ac}$-$FA_{4(avg)}$-$FITC_2$ (G5Ac-$FA_{4(avg)}$). The singlet at 1.97 ppm corresponds to the terminal acetyl groups on the dendrimer. The broad singlet at 8.7 corresponds to 1 FA proton, indicating an average of ~4 FA per dendrimer. The broad signal with a max at 6.7 ppm includes 2 FA protons and 5 FITC, leading to an average of ~2 FITC per dendrimer.

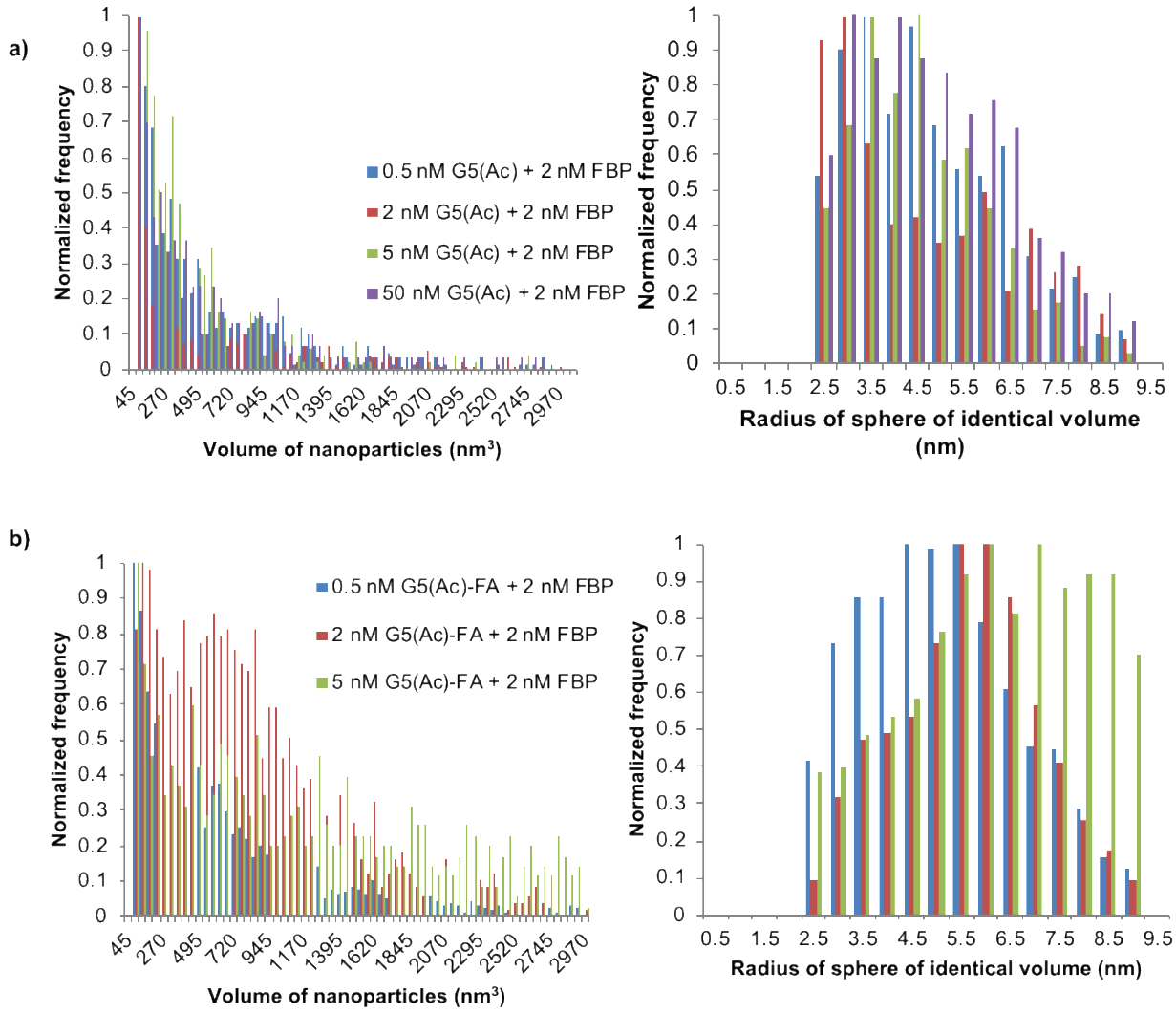

Figure A.2. a) Histograms showing the volume (left) and extrapolated radii (right) distributions of FBP nanoparticles generated with G5Ac; b) Histograms showing the volume (left) and extrapolated radii (right) distributions of FBP nanoparticles generated with G5Ac-$FA_{4(avg)}$.

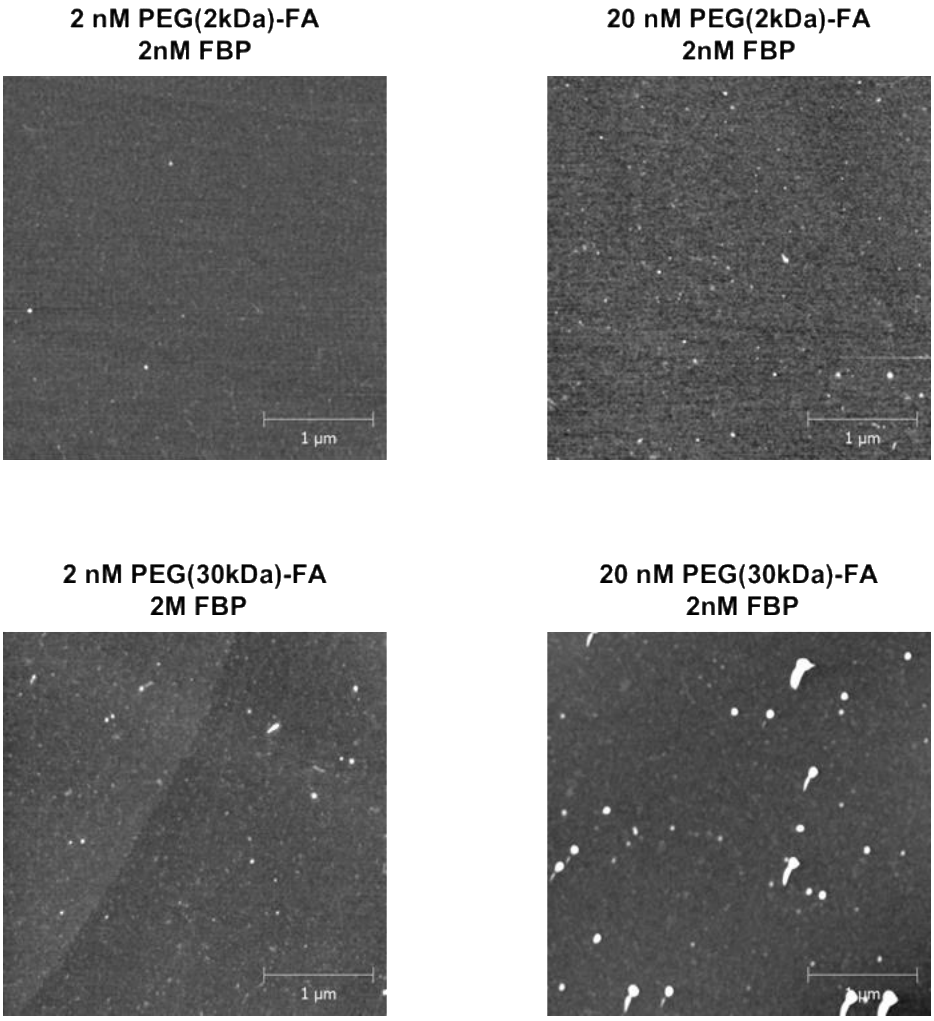

Figure A.3. AFM images (3.5x3.5 µm) of mixtures of FBP + PEG-FA of varying polymer molecular weights at different concentrations. In all cases, PEG-FA was added to FBP (2 nM in 1x PBS). AFM images were captured by spin coating the solutions onto freshly-cleaved mica. The lack of nanoparticles indicates that PEG-FA disrupted already existing apo-FBPNP. Higher concentrations of PEG-FA were attempted, but multilayers of polymer were observed. This phenomenon is already evident in the PEG(30kDa)-FA samples.